MOLECULAR CHARACTERIZATION OF DISSOLVED ORGANIC MATTER IN SÃO PAULO, BRAZIL WET DEPOSITION BY ULTRA-HIGH RESOLUTION MASS SPECTROMETRY

A Thesis

by

JACKSON SEYMORE

BS, University of North Carolina at Chapel Hill, 2020

Submitted in Partial Fulfillment of the Requirements for the Degree of

MASTER OF SCIENCE

in

CHEMISTRY

Texas A&M University-Corpus Christi
Corpus Christi, Texas

May 2022

May 2022

MOLECULAR CHARACTERIZATION OF DISSOLVED ORGANIC MATTER IN SÃO PAULO, BRAZIL WET DEPOSITION BY ULTRA-HIGH RESOLUTION MASS SPECTROMETRY

A Thesis

by

JACKSON SEYMORE

This thesis meets the standards for scope and quality of
Texas A&M University-Corpus Christi and is hereby approved.

J. D. Felix, PhD
Chair

H. Abdulla, PhD
Committee Member

J. Conkle, PhD
Committee Member

May 2022

ABSTRACT

Rainwater dissolved organic matter (DOM) is a complex mixture of organic compounds, the composition of which remains to a large extent unknown. This is despite its central role in a host of fundamentally important atmospheric processes (e.g. aerosol hygroscopicity, light absorption, etc.). The molecular composition of DOM has been used to infer emission sources and investigate atmospheric reactions that produce secondary organic aerosols (SOA), which comprise the main contributor of uncharacterized compounds in rainwater organics. This work illustrates the molecular composition of DOM in rainwater collected from February 2020 to June 2021 (n = 32 of rain samples) in Ribeirão Preto, SP (21.166 S, 47.845 W) using complimentary methods of traditional ion chromatography cooperatively with Orbitrap mass spectrometry and novel statistical analysis. This approach provides a detailed, ultra-high resolution, high-throughput method for future rainwater DOM investigations which is demonstrated here with direct-injection, positive mode electrospray ionization. Using this method, 41,383 total molecular formulas in 32 samples were identified over the mass range m/z^+ range of 80 to 800; among them 2,788 molecular formulas were unique. DOM character in São Paulo rainwater is revealed to be largely influenced by organic nitrogen, as 2,397 of the unique formulas identified contained nitrogen. This represents 86.0% of the total variety of organic compounds identified, with many of these likely peptides or amino acid derivatives. These findings also show that in terms of variety and number the general proportions of elemental formula classes remain relatively consistent over many samples, but the composition of the individual classes varies as function of its constituent emission sources. Recent pandemic related influences on anthropogenic activity as well as biomass burning in the São Paulo region of Brazil are seen through variations in rainwater DOM characteristics. Rainwater collected prior to the COVID-19 pandemic's

emergence in Brazil is distinct from reduced anthropogenic activity rainwater in both DOM character—seen in the increase in primary compounds and direct amino acid contribution, wider range of O:C ratios, and the absence of atmospheric NO_x related CHON oligomers—and major ion content—marked by a reduction in sulfate, nitrate, potassium, and formate. Clustering analysis shows that these distinctions are mostly driven by changes in anthropogenic reactive nitrogen emissions as well as in part to seasonal influence. This research highlights the potential for public policy to reduce the emission of air pollutants and other biologically relevant anthropogenic emissions, particularly through reducing traffic loading and expanding remote working.

DEDICATION

This master's thesis is dedicated to Dr. Adele Hite, who has been a key foundation to my academic journey and a beloved aunt.

ACKNOWLEDGEMENTS

Many thanks to the contributors to this work, Dr. J. David Felix, Dr. Hussain Abdulla, Daniela Bergmann, Dr. Lucia Campos, and Jacques Florencio.

TABLE OF CONTENTS

Page

LIST OF FIGURES

Page

LIST OF TABLES

Page

CHAPTER I. INTRODUCTION

Atmospheric OM—also referred to as aerosols—is a major component of both marine and continental rainwater[1,2] that influences climate, air quality, and ecosystem health[3–5] and is generated by a variety of anthropogenic and biogenic emission sources. The molecular composition of atmospheric OM results from its emission source and aging processes.[6] Its molecular composition will, in part, determine its impacts on properties such as light absorption,[7] aerosol hygroscopicity,[8,9] and bioavailability upon deposition.[10,11] These properties define the role atmospheric OM plays in regulating climate through direct and indirect effect in both radiative forcing and cloud seeding,[4,5,12,13] as well as its role in nutrient loading.[14,15] Certain aerosols can supply nutrients that stimulate net ecosystem growth or, alternatively, toxins that suppress a biogeochemical cycle.[5] Acidic aerosols (such as sulfates or nitrates) deposit over terrestrial ecosystems as acid rain and enhance the leaching of nutrients from the system.[16]

While atmospheric OM influences many natural systems, its role in air quality and public health is often the most visible. In the form of particulate matter (PM) and volatile organic compounds (VOCs)—the dominant forms of OM—it is an environmental factor that is associated with increased respiratory morbidity and mortality.[17–19] PM is responsible for 3.7-4.8 million premature deaths worldwide.[20] Of these deaths, 92% occur in low and middle income countries[17,21,22] and 2.8 million of these deaths are due to biomass burning for wood cookstoves.[23] VOCs have complex risk factors, supporting ozone production[24] and posing individual toxic and carcinogenic risks.[25] High mass concentrations of PM and VOCs are common indications of poor air quality and smog events.[26,27] The currently understood driving forces of PM toxicity are size fraction, mass concentration, and composition/oxidative potential.[28–30] While the EPA regulates PM based on mass concentration,[31] recent studies using

in vitro exposure techniques now suggest that PM mass concentration is not the causal factor in health risks and that overall PM toxicity differs from the toxicity of its individual components.[32] *In vitro* exposure techniques in tandem with chemical and biological characterization have begun to identify specific constituents of PM most relevant to overall toxicity.[28,33,34] Current research has demonstrated that secondary processing of aerosols, namely photochemical changes, result in differential *in vitro* genomic responses, suggesting an increase in overall toxicity.[19,35–37] For example, secondary organic aerosols (SOA) from isoprene photooxidation are demonstrated to significantly increase known inflammatory biomarkers IL-8 and COX-2 mRNA levels in human bronchial epithelial cells (BEAS- 2B).[38]

The many primary sources (emitted directly into the atmosphere) of atmospheric OM can be categorized as biogenic (emitted by natural systems) or anthropogenic (emitted by human activity). Biogenic primary sources are related to emissions of VOCs from vegetation, mechanically suspended biological particles (pollen, plant debris, soil, dust, bacteria, and viruses), forest fires, emissions from marine environments (sea-air gas exchange and bubble bursting action suspending OM in the sea surface microlayer), volcanoes, etc. Anthropogenic primary sources include: combustion and production of fossil and biofuels (motor vehicle exhaust, electric generation units), biomass burning, domestic heating and cooking, tire and asphalt wear, solvent use, emissions from agriculture (such as pesticides), and natural gas exploration.[14] Globally, primary sources are mostly biogenic in origin (80%) and are dominated by isoprene and monoterpene emissions from vegetation.[39,40]

At least half of global primary emissions of atmospheric OM are chemically transformed in the atmosphere to create SOA.[12,41] These reactions generally follow one of two pathways: degradation of large molecules by oxidation or generation of higher weight molecules through

oligomerization. Both of these pathways are mediated by oxidants and/or solar radiation.[42] Secondary processing of organic aerosols have seen increasing attention and study in the past decade, notably in relation to climate effects. Secondary processing bolsters OM's role as cloud condensation nuclei, incorporating OM into cloud droplets and aiding its subsequent removal through precipitation.[41] Precipitation removes organic compounds from atmospheric circulation with efficiency and is a major process by which balance between sources and sink of atmospheric organics is achieved.[43] This dissolved organic matter (DOM) has been sparsely characterized and used to investigate atmospheric reactions that produce SOA, which comprise the main contributor of uncharacterized compounds in rainwater OM.[1,2]

Rainwater DOM is a complex heterogeneous mixture of organic compounds, the composition of which is considered less than 50% chemically characterized.[1,2] Identifying the composition of organic species in atmospheric waters has been held back largely by the difficulty of analyzing species present in very low abundances in a complex matrix of thousands of unique compounds. Significant progress has been made to identify the composition of complex DOM in organic aerosols and rainwater DOM using Fourier transform ion cyclotron resonance mass spectrometry (FT-ICR MS),[44–47] however these methods have a low throughput and the resultant studies are limited in sample size (the highest being seven samples[45]). These methods also involve preconcentration usually through solid-phase extraction (SPE), which contribute to analyte loss particularly for higher oxygen content and more polar species.[48–50] Alternative high resolution mass analyzers in the Fourier transform family such as the Orbitrap have started to become part of routine analysis in numerous areas of research.[51,52] Orbitrap has been used to characterize riverine DOM and ambient aerosols,[53–55] and its high resolution, mass accuracy, and ability to be used in combination with other mass selection technologies make it an ideal

candidate for complex analysis and has begun to garner global attention for its application in studying environmental systems. At present however, no studies using Orbitrap MS to characterize rainwater DOM nor any high-resolution chemical characterization of DOM in South American rainwater have been published. Currently only 9–14% of the water soluble organic compounds (WSOC) have been identified in any chemical characterization study of South American aerosols.[56] In this present work, direct injection Orbitrap mass spectrometry was used on rainwater samples collected in Brazil to further the study on rainwater DOM and as a representation of WSOC in South American airsheds.

Primary emission sources of atmospheric OM are zonally and seasonally variable.[14] To that effect, the Brazilian wet season occurs during the months of October to March whereas the dry season occurs during the months of April to September. During dry seasons, wildfires and slash-and-burn agriculture makes Brazil susceptible to biomass burning influence and subsequent air quality issues.[57] Starting August 2019, the Amazon rainforest has seen significant increase in both area of effect and number of forest fires, mostly related to deforestation. Smoke from these fires have been observed via satellite to travel 2,700 km from the Amazon rainforest to the city of São Paulo.[58] These large forest fires have undoubtedly influenced OM input into the airshed.

The COVID-19 pandemic has triggered a variety of responses in Brazil from federal, state and local governments, impacting on politics, education, the environment, and the economy.[59] The profound impact of the pandemic response accelerated deforestation and decreased travel and industrial activity.[60] It is unknown how these processes influence OM input and cycling into the São Paulo airshed, but it appears likely that these influences will decrease biogenic VOCs and anthropogenic emissions. Preliminary studies into the São Paulo airshed during the COVID-19 pandemic have observed drastic reductions on NO (up to −77.3%), NO_2

(up to −54.3%), and CO (up to −64.8%) concentrations in the urban area compared to the five-year monthly mean and to the four-week mean before the partial lockdown. As an effect, an increase of 30% in ozone concentrations was observed in urban areas highly influenced by vehicle traffic.[61]

In this study, a series of continental rainfall samples were collected in a typical urban and agricultural region, Ribeirão Preto, São Paulo, to study the influence of pandemic policies, biomass burning, and social isolation on the molecular composition and chemical character of DOM. This study covers the period before partial lockdown orders were issued (February 26 to March 24, 2020) through to March 2021. High-resolution Orbitrap mass spectrometry was used to characterize the specific molecular composition of rainwater DOM during this period, which was then analyzed alongside inorganic ion and select organic acid content. Potential compounds of interest along with possible emission signatures were identified using powerful statistical techniques such as principal component analysis, volcano plotting, and positive matrix factorization. Conclusions drawn from the analysis of these samples further the discussion around the role of organic nitrogen in the water-soluble fraction of organic aerosols.

CHAPTER II. METHODS

2.1 Study Site and Description

Ribeirão Preto, São Paulo, Brazil

The state of São Paulo, Brazil is in the southeast Brazil subtropical region bordering the Atlantic Ocean. The state has an area of 248 x 108 km^2.[15] São Paulo is the largest state in Brazil, with a population of 45,919,049 people, and a total of 29,057,749 vehicles. Its capital, São Paulo, is the largest city in Latin America, with a population of 12,252,023 people, and an urbanization rate of 99.1%.[62] São Paulo has important agriculture and industrial economic sectors as well as defined wet and dry seasons.[15] The agro-industries, metallurgical, food, and agriculture industries are contributors to emissions. Biomass burning as part of slash-and-burn practices is performed during sugar cane harvesting which is a large source of reduced nitrogen and of gases and aerosols containing oxidized nitrogen.[15] During the winter there is less precipitation than the summer, resulting in more biomass burning during the winter. In rural areas of the state, sugar mills are common.

The city of Ribeirão Preto shown in Figure 1 is a municipality located in the northeast region of the state (21°09'58.64 S, 47°50'42.960 W). The central, northern, and western regions of the state's economy is based on agro-industries: sugar/alcohol, orange, livestock and meat packaging. The southern regions of the state rely more heavily on metallurgical and food industries and agriculture industry (i.e. tea and banana) for its region's economy. Because of its location, the city of Ribeirão Preto economy is based primarily on agro-industries. The distance from the city to the South Atlantic Ocean is about 338 kilometers and hosts an estimated 700,000 citizens. Furthermore, its position geographically puts Ribeirão Preto free from influence by the Atlantic – as indicated by air mass projections being almost entirely landlocked, with few

samples originating from the Atlantic Ocean. This city was chosen for sampling due to ongoing collaborations between the research group at Texas A&M University – Corpus Christi and the group at the University of São Paulo Ribeirão Preto.

In response to the global COVID-19 pandemic, partial lockdown was ordered by the São Paulo state government on March 24th, 2020,[63] which closed many public spaces like shopping malls, restaurants, fitness centers, elementary, middle and high schools, and universities. Supermarkets and drugstores continued operating with restrictions concerning person-to-person distance and public transportation continued with reduced hours. Since partial lockdown was first ordered, estimated social isolation varied from 54% (March 24th), achieving a minimum of 47% (April 9th) and a maximum of 59% (several dates), with an average of 54%.[63] It is important to highlight that while industrial activity was not ordered to lockdown, many industries saw reduced operation which in part is related to decreasing demand.[61] Publicly available mobility data from registered cell phone activity indicates that the average activity deviation in Ribeirão Preto of retail, transit, and workplace areas leaves baseline on March 14, 2020 reaching a seven-day average minimum of -54.8% on March 27th and then gradually increases for the rest of the year.[64] The seven-day average of this deviation first returns to baseline on December 17, 2020. In this study, sample groupings contrasting different levels of anthropogenic activity conditions use the publicly available mobility data to distinguish the sample cohorts. This data and details are provided in the Appendix. The sample groupings are divided into (1) reference, before March 14th, whereafter average activity deviation falls below baseline and doesn't return; (2) reduced activity, after March 14th to December 17th where seven-day average of activity deviation is below baseline; and (3) post return to baseline, after December 17, 2020 where seven-day average of activity first returns to baseline.

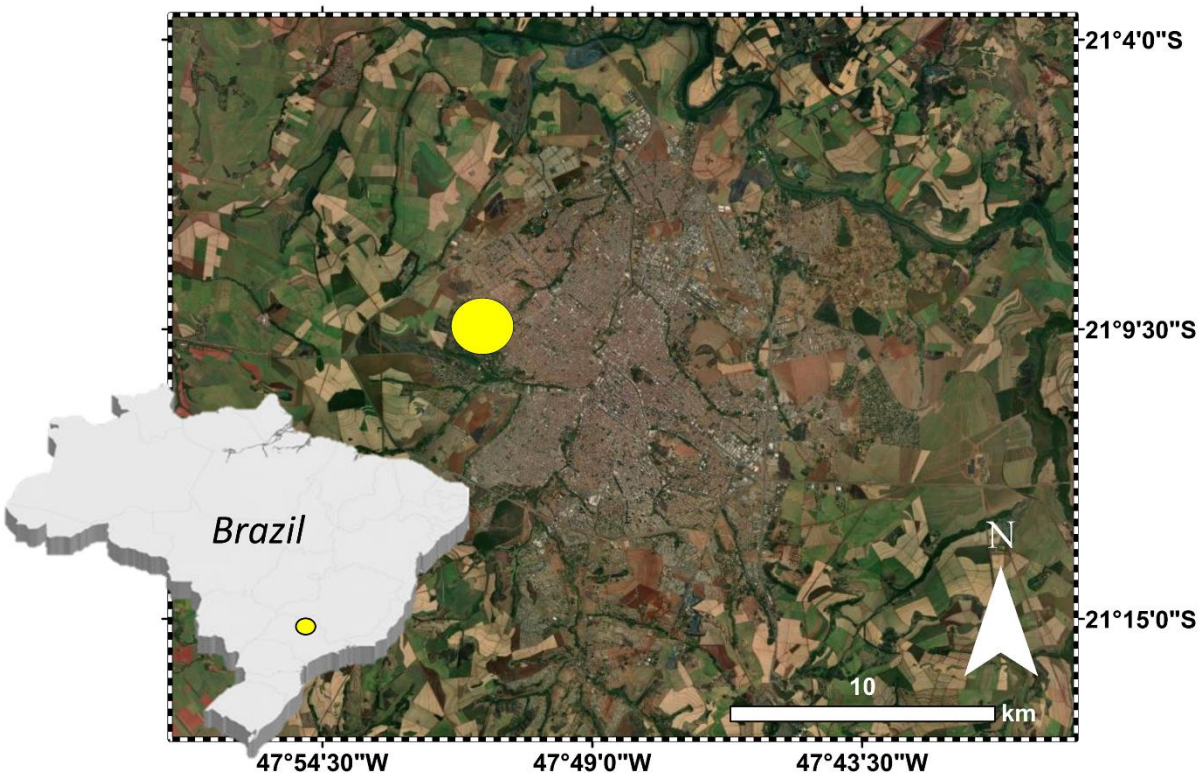

Figure 1. Location of the city of Ribeirão Preto, São Paulo, Brazil

2.2 Sample Collection

Rain samples (n = 32) were collected using an automatic wet-only collector on an event-basis from 2/26/2020 through 5/2021 in Ribeirão Preto, São Paulo, Brazil (21°09’58.64 S, 47°50’42.960 W). Samples were collected in previously cleaned high density polyethylene bottles and were retrieved from the field immediately after the event or during the following morning (when the rain event occurred at night). New sets of clean sampler funnels and flasks were installed after each rain event. Further description can be found in Coelho et. al. 2011.[65] After collection, each sample was filtered with a 0.2 µm quartz fiber filter to isolate DOM from

PM. Samples were then stored at 0°C until analysis to preserve the chemical composition of rainwater samples. Samples were shipped from USP-RP to TAMU-CC in coolers containing freezer packs.

2.3 Back trajectory

The NOAA's Hybrid Single-Particle Lagrangian Integrated Trajectory (HYSPLIT) online transport model was used to examine the air mass back trajectory from the São Paulo sampling location. Backward trajectories were run starting at altitudes 200 m, 500 m, and 700 m with a duration of 48 hours prior to sample collection at 21°09'58.64 S, 47°50'42.96 W. These parameters default parameters were used for mixing layer heights and estimated releasing height for this region based on parameters used by prior studies on rainwater DOM.[66] Model Vertical Velocity was used for the vertical motion calculation method.

2.4 Ultrahigh-Resolution Mass Spectrometer (UHRMS) analysis

Sample analysis was performed with an UHRMS (Orbitrap Fusion Tribrid Mass Spectrometer (OT-FT-MS); Thermo Fisher Scientific, Waltham, Massachusetts, USA) coupled to a UPLC system (Vanquish Ultra Pressure Liquid Chromatography). Analytes were separated using a 1.7 μm ACQUITY UPLC BEH C_{18} reversed-phase column by Waters (130Å, 1.7 μm, 2.1 mm × 150 mm) with mobile phases consisting of a linear gradient of acetonitrile:formic acid and Milli-Q water:formic acid. The gradient started at 5% formic acid for 2 min (including a 7-min prerun equilibrium), increasing to 65% formic acid over 20 min, holding at 65% acetonitrile for 1 min, and then increasing to 100% formic acid over 3 min. The spray voltage of the ESI source was +3.2 kV, to produce ions in positive mode. The injection volume of each sample was 20 μL and blank samples were also analyzed for background subtraction.

2.5 Inorganic Ion and DON/DOC Quantitation

Inorganic ions along with DOC and dissolved organic nitrogen (DON) were quantitated using the same method described in Crispim et. al. 2018. Inorganic nitrogen species (NO_3^-,NO_2^-, and NH_4^+) were analyzed using suppressed ion chromatography with conductivity detection (Model 881 Compact IC pro; Metrohm, Brazil). The anion analysis employed a Metrosep A Supp 5 column (Metrohm) and an eluent composed of sodium carbonate (3.2 mmol L^{-1}) and sodium bicarbonate (1.1 mmol L^{-1}). A solution of sulfuric acid (100 mmol L^{-1}) was used as the regenerant for chemical suppression. The cation analysis was performed using a Metrosep C4 column (150×4.0 mm, Metrohm) and an eluent composed of nitric acid (1.7 mmol L^{-1}) and dipicolinic acid (0.7 mmol L^{-1}). Ion chromatography standard solutions were used to construct the analytical curves. The limits of detection (LODs) were estimated visually by decreasing the concentration of each standard until the signal reached a value approximately 3 times higher than the noise.[67,68]

2.6 Data Processing

The obtained LC-MS spectrums were processed with Compound Discoverer software (version: 3.2.0.421). Molecular formula assignments were made using Molecular Formula Calculator (v.1.2.3) and an in-house python code. It should be noted that the compositional elemental of these formulas was constrained as $C_{5\sim100}H_{4\sim200}O_{0\sim50}N_{0\sim10}S_{0\sim3}P_{0\sim3}$ and that the allowed m/z tolerance was 2 ppm. Several indicators were adopted to illustrate the characters of OM subgroups including elemental ratios, double bond equivalent (DBE), Aromaticity index (AI), and Kendrick mass defect (KMD). Their specific calculation and utilization are as follows.

2.7 Van Krevelen Analysis

Van Krevelen (VK) analysis was used to show the H:C and O:C molar ratios for each sample formula to describe the general overall composition or organic mixture composition.[69] The area within the diagram further characterize the atmospheric OM distinct classes.[46]

2.8 Homologous Series Analysis

To identify compounds of a homologous series that have different numbers of specific base units, Kendrick mass (KM) analysis was used.[69] To determine the Kendrick mass, the measured IUPAC mass is normalized to 14.000u instead of the IUPAC 14.01565. Subtracting the nominal mass from KM will produce the Kendrick mass defect (KMD).[47] When the KMD is plotted as a function of the nominal mass these series of oligomers fall on a horizontal line separated by 14 Da, differing chemically by a methylene unit. This makes identifying compounds of different classes visually simpler as they are displaced vertically.

2.9 Double Bond Equivalence

The double bond equivalence (DBE) was calculated in order to determine the characterized ions using the following formula (1). DBE = number of rings plus double bonds to carbon.[47] DBE cannot be a negative integer.[45]

$$DBE = c - \frac{1}{2}h + \frac{1}{2}(n + p) + 1 \quad (1)$$

Where elemental composition is $C_cH_hO_oN_nP_pS_s$

2.10 Aromaticity index

Aromaticity index (AI), based on Koch and Dittmar 2006, was assigned to each molecular formula. The following formula (2) will be classified as AI<0.5 non-aromatic, AI>0.5 aromatic and AI≥0.67 condensed aromatic.[47]

$$AI = \frac{DBE_{AI}}{C_{AI}} = \frac{1+\frac{1}{2}(2c-h-2o-2s)}{c-o-n-s-p} \quad (2)$$

2.11 Volcano Plot

To identify statistically relevant changes in the rainwater DOM dataset, volcano plots were created by plotting significance against fold-change (FC) on the y and x axes respectively. These plots are common in omic experiments such as genomics, proteomics, and metabolomics where the most meaningful changes need to be identified from a set of thousands of replicate data points between two conditions.[70] The x axis is the log of the FC between the two conditions while significance ($-\log_{10}$ of p-value from an ANOVA or t-test) is on the y-axis. For all plots, p-value was set to 0.05 and FC was set to 1. The log of the FC is used so that changes in both directions appear equidistant from the center. Plotting points in this way results in two regions of interest in the plot: the top of the plot far to either the left or right side. These points represent values that display large magnitude FC (being far to the left or right) as well as high statistical significance (being towards the top). Compounds with significant p-values and FC meeting the upper or lower FC threshold are specific to that group of samples or can be said to be characteristic of that sample group. It follows that these statistically distinct compounds can be isolated to explore how sample groups differ based on compound class and structure. The volcano plots produced were created using Compound Discoverer software (version: 3.2.0.421).

2.12 Principal Component Analysis

Principal component analysis (PCA) was used to characterize both the ion species and organics measured in the rainwater. A full description of this statistical technique can be found in Jolliffe (2002).[71] Ion PCA was performed using Matlab software (version R2020b) while organic matter PCA was performed using Compound Discoverer software (version: 3.2.0.421). Formulas present in only one sample and formulas present in all samples were removed to avoid biasing the PCA toward rare formulas and to eliminate formulas that do not contribute to the sample variance.[44]

2.13 Positive Matrix Factorization

Positive Matrix Factorization (PMF) analysis was performed on the ion concentrations data using the EPA PMF 5.0 model.[72] PMF was used as a multivariate factor analysis tool to identify source apportionment of species and can be briefly described by its foundational equation (3):

$$X_{ij} = \sum_{K=1}^{p} g_{ik} f_{kj} + e_{ij} \quad (3)$$

where X_{ij} is a data matrix of i by j dimensions, p is the number of factors, g_{ik} is the contribution of the k^{th} factor to the i^{th} sample, f_{kj} is the fraction of the k^{th} factor arising from congener j and e_{ij} is the residual for each sample/species. Samples with missing values were excluded from the data matrix before PMF was performed. The model was run 20 times for all eligible samples with a random seed of 80 and then run 20 times again excluding outliers with a random seed of 23. The five factor models were chosen for analysis after comparison with three, four, and six factor models on the basis of residual size, mapping bootstrap factors to base factors, and species regression accuracy. The details of the model can be found in the EPA PMF 5.0 user manual and

associated materials.[72] The calculation of data uncertainties is illustrated in the supplementary materials.

CHAPTER III. RESULTS AND DISCUSSION

3.1 Organic Characterization

This analysis assigned 41,383 total mass features in 32 samples with 2,788 of these molecular formulas being unique. This is specifically an underestimate of the actual number of compounds because for each elemental composition there are multiple structural isomers possible, with the number of isomers increasing as molecular weight increases. In addition, the single ionization mode means species that do not readily ionize in positive ESI are not detected; this may include species such as, for example, nitrooxy- or nitrooxy-organosulfates. The omission of a preconcentration step may also put DOM constituents in particularly trace concentrations below detection limits. This does however prevent the loss of particularly volatile components or components lost during extraction; it is known that methods such as SPE contribute to analyte loss for higher oxygen content and more polar species up to 70% loss by mass.[48–50]

Table 1 provides a breakdown of the number of molecular formulas and their atomic characteristics per species subclass and its percent abundance relative to the total number of unique formulas in all samples. The most prominent species are CHON and CHONP, together making up 53.8% of unique formulas identified followed by CHONS with 17.6%. The other N containing species CHN, CHNS, and CHONSP then represent 14.6% of the total unique formulas. The remaining 14.0% are CHO, CHOP, CHOS species with a few CHS and CH formulas. No CHOPS species were identified within detection limits in any sample. Overall, species containing a nitrogen atom represent 86.0% of the organic species identified in this study. These findings differ from studies on total atmospheric organics in aerosol content, which show 36.6% atomic content for nitrogen containing species in mixed source aerosols and, at

highest, only 53.3% for biomass burning aerosols.[44] This prominence of N containing species is in part due to ion source bias, since this study used only positive ion mode in its MS analysis. This does corroborate with other UHRMS studies using positive ion mode to focus on characterizing rainwater DON which report nearly 2455 N containing formulas as compared to the 2397 presented here.[45] However, this does still suggest that true rainwater DOM character content is strongly influenced if not dominated by DON. Other rainwater DOM UHRMS studies using negative ion mode have reported only a total of 552 unique molecular species,[2] of which at least 15% are N containing formulas. To add the identified species from such a negative ion mode study to this would still imply the majority of characterized DOM are N containing (~74%, or ~71% assuming all N containing formulas are duplicates). This of course makes many specious assumptions, such as that (1) duplicate formulas do not exist, (2) the union of both ion modes represents characterization for all DOM constituents, (3) extraction loss is minimal and unbiased in all studies, and (4) the datasets are congruent. Regardless, it is possible that the large portion of N containing species seen here are species typically lost during extraction and preconcentration. This method of looking at chemical species highlights the variety of compounds present, rather than the total mass or amount, so while other species may be more abundant, N containing species present the highest variety of unique compounds in this analysis. In this method, variety will tend to influence how chemical character is judged more than abundance. To illustrate, by concentration the samples in this study show DON/DOC ratios that range from 0.1% to 16.9%, averaging 5.8%, while the total N:C ratio of all unique formulas assigned is 20%.

	n Formulas	Atomic Content (%)	H/C	O/C	O/N	O/S	N/C	DBE
CHN	262	9.40	1.70 ± 0.52	0.00	0.00	-	0.14 ± 0.13	2.82 ± 2.55
CHNS	94	3.37	1.72 ± 0.51	0.00	0.00	0.00	0.18 ± 0.07	4.44 ± 2.67
CHO	173	6.21	1.38 ± 0.64	0.30 ± 0.11	-	-	0.00	4.49 ± 3.35
CHON	716	25.68	2.00 ± 0.28	0.19 ± 0.11	1.73 ± 1.8	-	0.19 ± 0.14	2.23 ± 1.95
CHONP	784	28.12	2.42 ± 0.14	0.23 ± 0.10	0.74 ± 0.30	-	0.32 ± 0.05	0.04 ± 1.49
CHONS	490	17.58	2.11 ± 0.20	0.24 ± 0.22	1.53 ± 2.75	2.98 ± 2.79	0.23 ± 0.11	2.14 ± 1.80
CHONSP	51	1.83	2.16 ± 0.18	0.70 ± 0.33	6.30 ± 5.57	8.75 ± 4.54	0.20 ± 0.12	1.85 ± 1.38
CHOP	34	1.22	2.21 ± 0.09	0.39 ± 0.03	-	-	0.00	0.38 ± 0.69
CHOS	176	6.31	1.87 ± 0.11	0.65 ± 0.11	-	5.68 ± 2.34	0.00	1.90 ± 1.10
CHS	5	0.18	1.38 ± 0.02	0.00	-	0.00	0.00	6.70 ± 0.45
CH	3	0.11	1.59 ± 0.10	0.00	-	-	0.00	2.50 ± 0.00
All	2788	100.0	2.06 ± 0.42	0.23 ± 0.2	1.21 ± 2.03	3.56 ± 3.40	0.20 ± 0.14	1.82 ± 2.38

Table 1. Total unique formulas and atomic content of all species positively identified from all samples (n = 32).

However, there are various other potential explanations for what drives ON's disproportionately large influence on DOM chemical character. Such explanations could be that ON emissions are large relative to other organic emissions (i.e. N containing species are high input into this system, likely biomass burning related), ON emissions have more variety relative to other organic emissions (i.e. emissions of N containing species are diverse), that N containing species have higher water solubility than other organics (i.e. rainwater scours ON preferentially to other organics), or that atmospheric nitrogen chemistry—particularly that involving NO_x and NH_3—adds diversity to DOM (i.e. species have many pathways to chemically incorporate nitrogen into their structure once in atmosphere). The findings here concerning the water soluble organic nitrogen (WSON) fraction are generally consistent with other studies that demonstrate

the important role of ON as a ubiquitous and significant component of both rainwater and aerosol chemistry.[45,73] These findings may also suggest that other studies that miss this high N content may inaccurately infer certain properties about rainwater DOM, namely underestimating its potential bioavailability. Many studies have demonstrated the high bioavailability of rainwater DOM relative to other matrices, such as streams, rivers, and estuaries, and those that use molecular indicators for bioavailability, e.g. N:C ratio, very well may be underestimates.[74–78] Furthermore, the findings here may begin to explain the drivers of rainwater DOM's high bioavailability molecularly. Many general explanations are often attributed to inputs of labile DOM, namely fresh terrestrial plants,[79,80] marine phytoplankton,[81] and combustion sources,[82] but few consider photochemical transformations of organic compounds in atmosphere, particularly those involving atmospheric NO_x and NH_3.

The relative abundances of each class of fomulas are not static over time. Figure 2 illustrates this by graphing the percent abundance of each formula class for each sample. The proportions of each class remain relatively stable over the whole sample set with no immediately recognizable trends. The largest variations are associated with the CHON and CHONP classes which can deviate as much as 20% with notable variations in CHO, CHN, and CHONS which can deviate as much as 8%, 9%, and 12% respectively. CHS only appears in samples n23 through n26, reaching only as high as 1.2% abundance. Backtrajectories for n23 though n26 do not show any marine influence nor any strong similarity in backtrajectory. Inorganic data indicates n23 and n24 have the same primary factor influence however no inorganic ion data is available for n25 and 26. In the organic PCA, these four samples are clustered in Q1 with the most positive PC 1 and PC 2 values. Within the groupings of anthropogenic activity (shown in the supplemental material Figure A2), no strong trends or deviations are observed between

groups. The largest deviation is associated with CHON with a maximum difference of 4.6% with the next highest of 2.6% for CHN. Simplifying down to only observing the percent of formulas containing N, containing S, or containing P does not indicate any apparent trends or differences between groupings. For all formulas, 86.0% contain N, 29.3% contain S, and 31.2% contain P with standard deviations among all samples of 2.5%, 3.3%, and 4.4% respectively. The maximum deviations for these metrics are 11.2%, 13.0%, and 20.6%. This shows that the largest variations are among P containing species, mostly driven by deviations in CHONP. Since CHON is the formula class with the largest maximum deviation while N containing species hold the lowest deviations overall, this indicates that changes in CHON abundance are compensated by changes in other N containing species. Simple Pearson correlations between percent containing N, containing S, and containing P show a slight negative correlation between %N containing and %S containing of $r = -0.24$ ($p = 0.19$) and a positive correlation between %S containing and %P containing of $r = 0.33$ ($p = 0.07$), with no significant correlation between %N containing and %P containing ($r = 0.04$, $p = 0.84$). This could suggest that N containing species and S containing species may have stronger differences in emission origins while S containing species and P containing species may be more related in origin. It could also imply that chemical exchange in the atmosphere is competative among N containing species and S containing species. Concerning the anthropogenic activity groupings, the maximum deviations between the groupings are 0.9% for N containing, 2.0% for S containing, and 2.8% for P containing. With each of these being below the standard deviations, it appears there is no significant difference between the Reference, Reduced activity, and Post-baseline groups in regards to percent containing N, containing S, or containing P species.

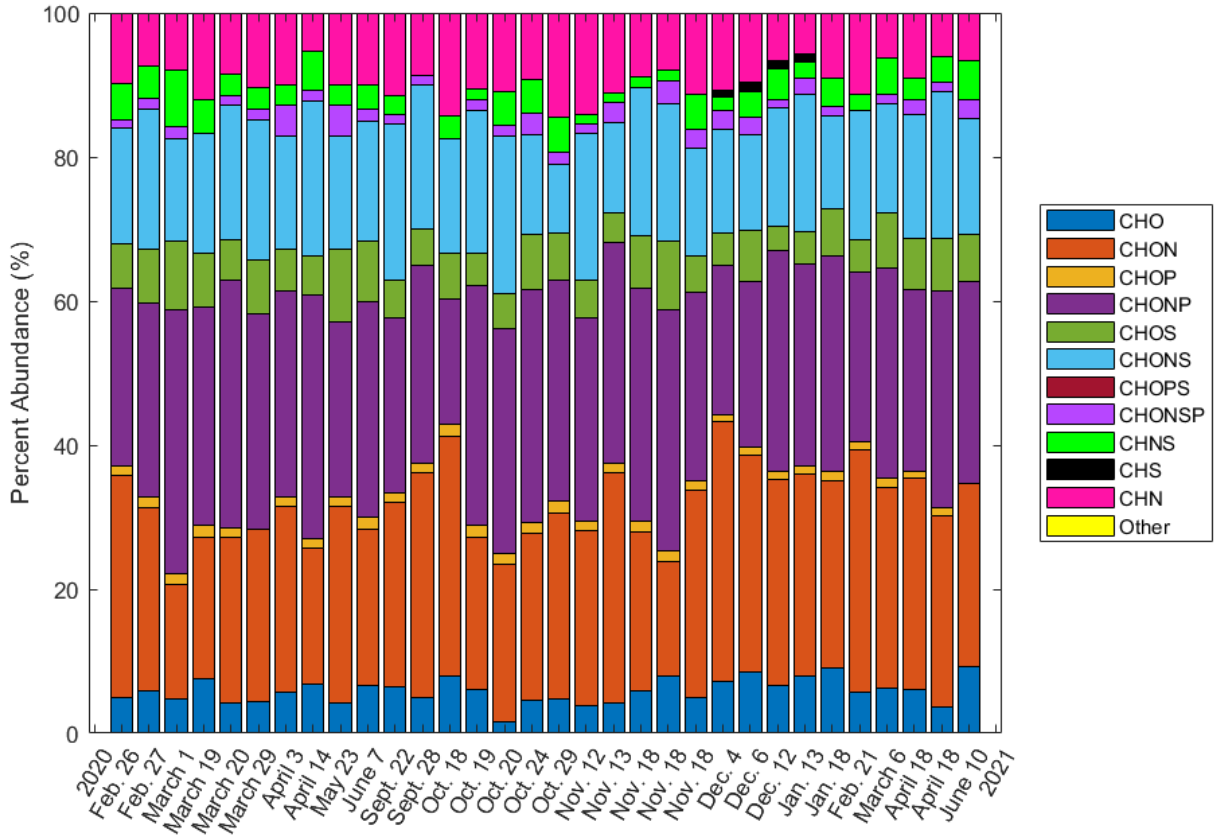

Figure 2. Percent abundance of formula class detected in each sample in order of collection.

Highlighted in the Van Krevelen diagram in Figure 3, the majority of identified compounds are in the O:C ratio range of 0 to 0.4, particularly among CHON, CHONP, CHO species. Sulfur containing species, such as CHONS, CHONPS, CHOPS, and CHOS inhabit a wider range of O:C ratios and are the primary species in higher oxidation ranges, likely related to the oxygen dense organsulfate functional group. Conversely, the H:C ratio range of the CHO species is much wider than the other organic species, sitting between 0.5 and 2.5. Of the N containing species, CHN and CHS species have the lowest H:C ratio (1.71 ± 0.52 and 1.72 ± 0.51 respectively) while out of all oxygen containing classes CHON, CHONP, and CHONS have

the lowest O:C ratios (Table 1). While CHONP is localized rather tightly in the 2 to 2.5 range of H:C ratios with an average of 2.42 ± 0.14 (Table 1), indicating mostly phospholipids, CHON compounds range between 1.3 and 2.4 with an average of 2.00 ± 0.28 strongly indicating a variety of BVOCs, amino acids, and peptides. Amino acids are a commonly measured component of WSON as they are highly reactive, easily oxidized in the atmosphere, and can have a catalytic role in condensation reactions.[83] Indeed, the presence of valine, glycine, glutamine, glutamate, phenylalanine, and proline were directly confirmed with fragment ion spectral matching, along with serine, leucine, glycine, glutamine, glutamate, and phenylalanine derivatives. While the direct contribution of amino acids typically range from only 2-25% of total WSON,[84,85] their true contribution to total WSON is likely higher as the presence of certain amino acid derivatives are already confirmed, CHON class compounds are the dominate fraction of WSON, and there are regular patterns in CHON mass difference (seen in the Kendrick analysis in Figure 8) indicating the presence of reaction product oligomers. This is congruent with other studies that suggest amino acids contribute more to total WSON than just the free amino acid content.[45,84]

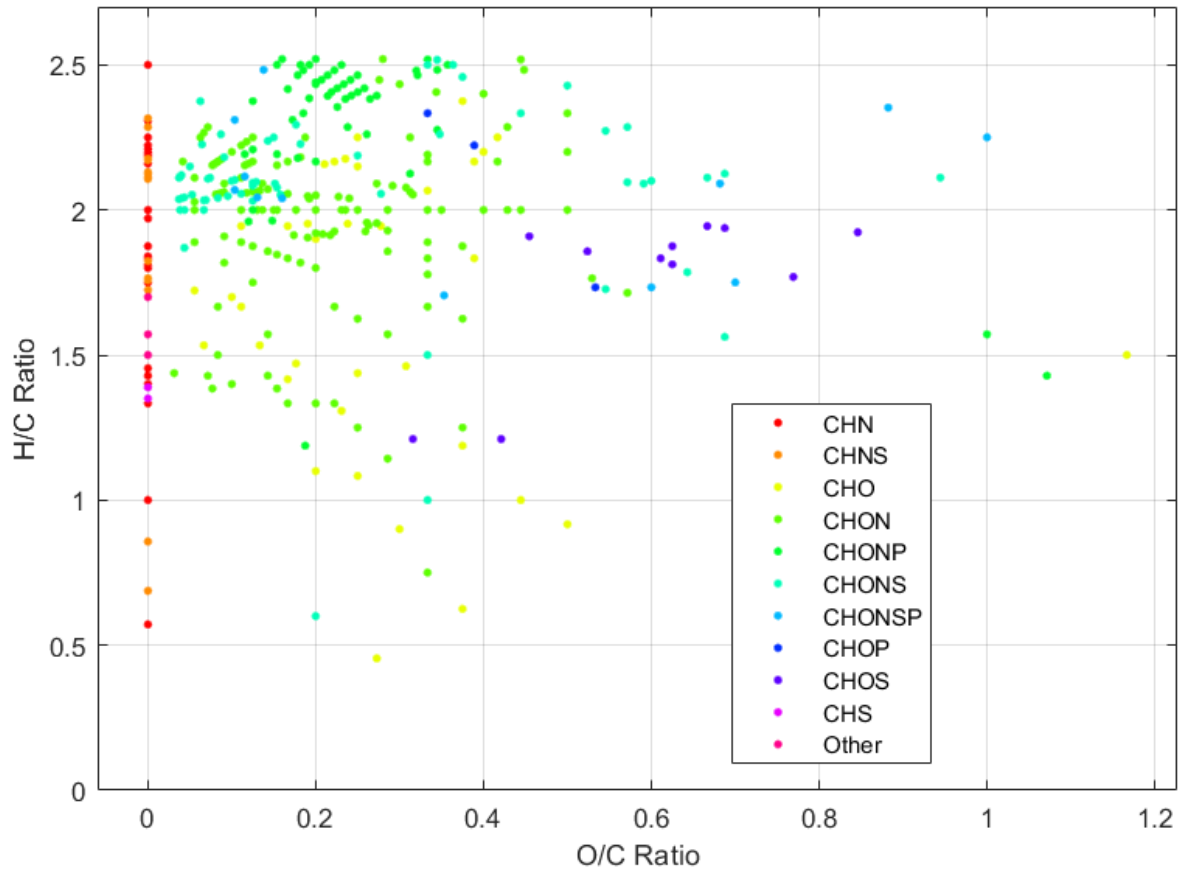

Figure 3. Van Krevelen Diagram of all unique organic species positively identified from all samples. (n = 32).

The presence of aliphatic S containing species, that is CHOS and CHONS with O:C ratios between 0.3 and 1.2 and H:C ratios between 1.3 and 2.0, are indicative of oxidized anthropogenic urban/vehicular emissions.[44] However, other species also indicative of oxidized anthropogenic urban/vehicular emissions such as CHO and CHON formulas with O:C ratios between 0.35 and 0.85 are not present. This could indicate that either these species are not present in the airshed or that more oxidized CHO and CHON compounds have reduced solubility in water, thus not appearing in the WSOC fraction. That however is contrary to other work that has shown that secondary formation via aqueous reactions in the anthropogenic environment with higher NO_x concentrations produce water soluble carbonyls with high O:C ratios.[86] It is

more likely that these oxidized species are simply not ionized in positive mode ESI, and therefore not detected.

None of the S containing free amino acids methionine, cysteine, homocysteine, or taurine were detected in these samples. However, CHONS compounds dominate the S containing compound classes (which are 29.3% of all formulas), representing 60% of all S containing formulas. This lends itself to the strong possibility that S containing amino acids derivatives are still strong contributors to the organic S content. Free methionine has been detected in marine rainwater studies and likely undergoes secondary reactions to alter the C, O, and N content of the molecule.[45] These reactions retain the thioether bond leading to a variety of CHONS compounds analogous to other known amino acid reactions. The failure to detect S containing free amino acids here doesn't necessarily indicate that S containing amino acids do not contribute to the organic S content, but that they may only contribute through peptides or secondary products of the free amino acids. The CHOS and CHONSP classes have the highest O:C ratio of all compound classes (0.65 ± 0.11 and 0.70 ± 0.33 respectively) while all P containing classes have O:C ratios higher than the total average O:C ratio. These higher O:C ratios indicate it's more likely that the majority of CHOS and P containing species are derived from secondary reactions involving inorganic S and P rather than from primary emission of organic S and organic P.[87]

On the whole, with an average H:C ratio of 2.06 ± 0.42 and O:C ratio of 0.23 ± 0.20, this study shows DOM that is more hydrogenated, less oxidized than bulk aerosol OM studies[44] and marine related rainwater DON studies also using positive mode ESI.[45] Comparing atomic ratio per sample, shown in Figure 4, indicates that both Reference and Post-baseline samples occupy a narrow range of H:C and O:C ratios, while Reduced activity sample have a much broader range of H:C and O:C ratios. This could indicate a strong reduction in the primary species that weight

the ratios in the Reference and Post-baseline groups. Alternately grouping the samples by season (in Figure 5), it can be seen that the dry season samples occupy slightly higher O:C ratios than the wet season samples, likely indicating the presence of more oxidized species in the dry season. This is congruent with higher proportions of biomass burning related compounds, which tend to be highly oxidized. Average atomic ratios for other heteroatoms do not show similar relationships for these same groupings (presented in Figures A4-A6).

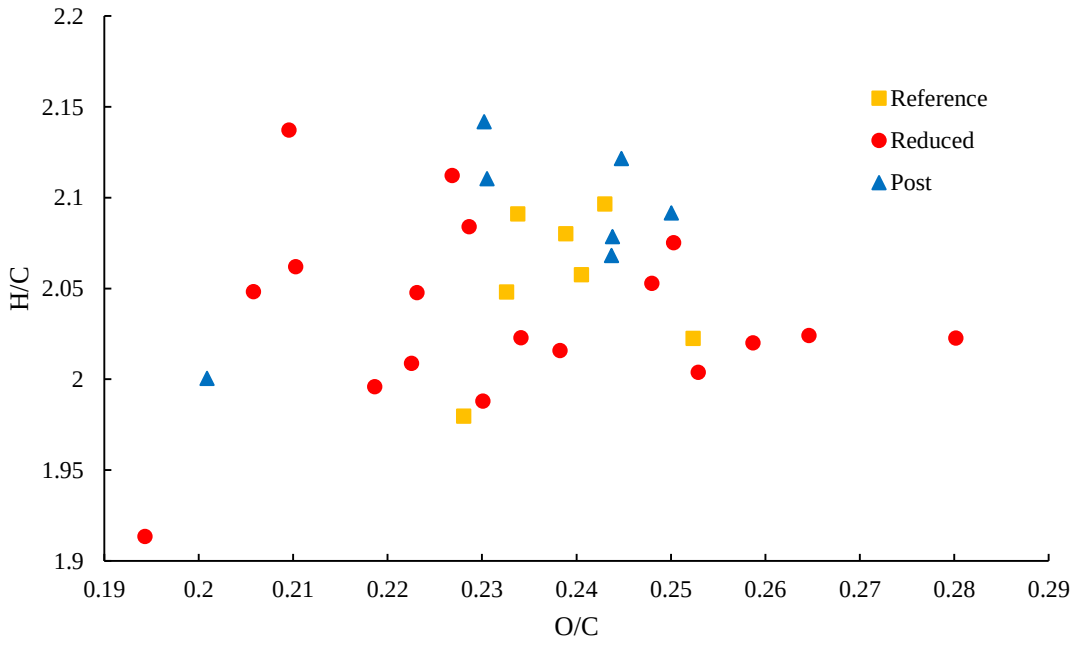

Figure 4. Van Krevelen Diagram of each sample's average atomic ratio labeled by activity group. (n = 32).

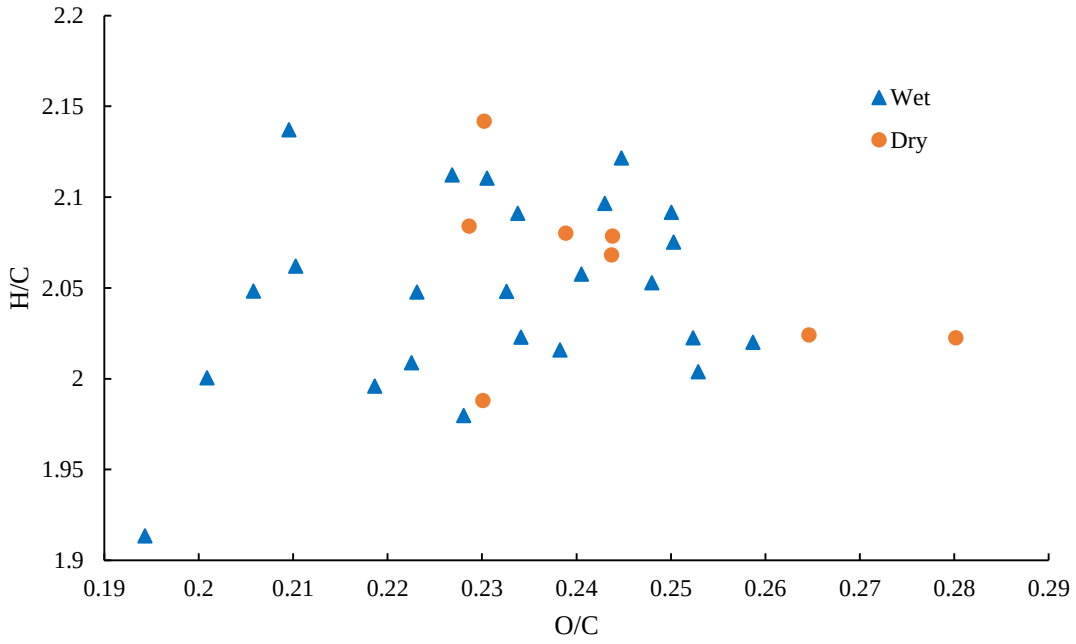

Figure 5. Van Krevelen Diagram of each sample's average atomic ratio labeled by season. (n = 32).

3.2 Organic PCA

PCA was utilized to describe the differences in the overall chemical character of the organic species present between samples. In the initial PCA, PC1 and PC2 described 19.6% and 11.8% of the variance, respectively. The PCA shown in Figure 6 manages to roughly distinguish samples from different levels of anthropogenic activity, placing six out of the seven Reference period samples in quadrant four (Q4), generally locating Reduced period samples around zero in PC 2 in a wide range of PC 1 values, and clustering Post-baseline samples with positive PC 2 values and PC 1 values near the Q1 and Q2 boundary, leaning towards Q1. This grouping contrasts samples at different levels of anthropogenic activity to demonstrate a change in DOM chemical character as a response to pandemic related trends in anthropogenic activity. Looking at the samples ordinally, the Reference period samples tend to be more negative in PC 2 and positive in PC 1 moving from Q4 to Q3 and Q2 as their PC 1 values decrease and their PC 2

values increase. These samples, n20 to n29, cover February to May 2020. However, the samples in the Reduced period with PC 2 values closest to zero also have a wider range of PC 1 values than samples with more extreme PC 2 scores. These samples encompass the range of n30 to n41, collected between June to November 2020. The Post-baseline samples tend to be the highest PC 2 valued samples with generally positive PC 1 scores. These samples, n42 to n51, go from December 2020 to June 2021.

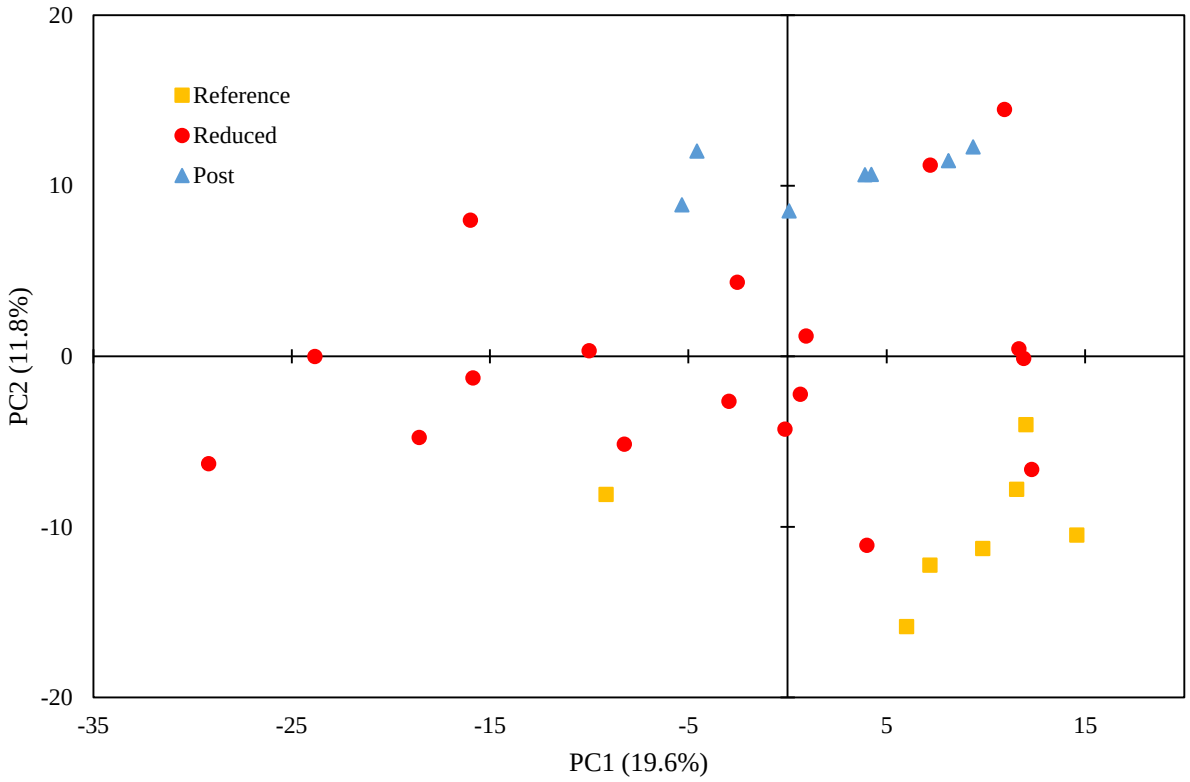

Figure 6. Organic Character PCA plot of all samples, labeled by activity deviation group.

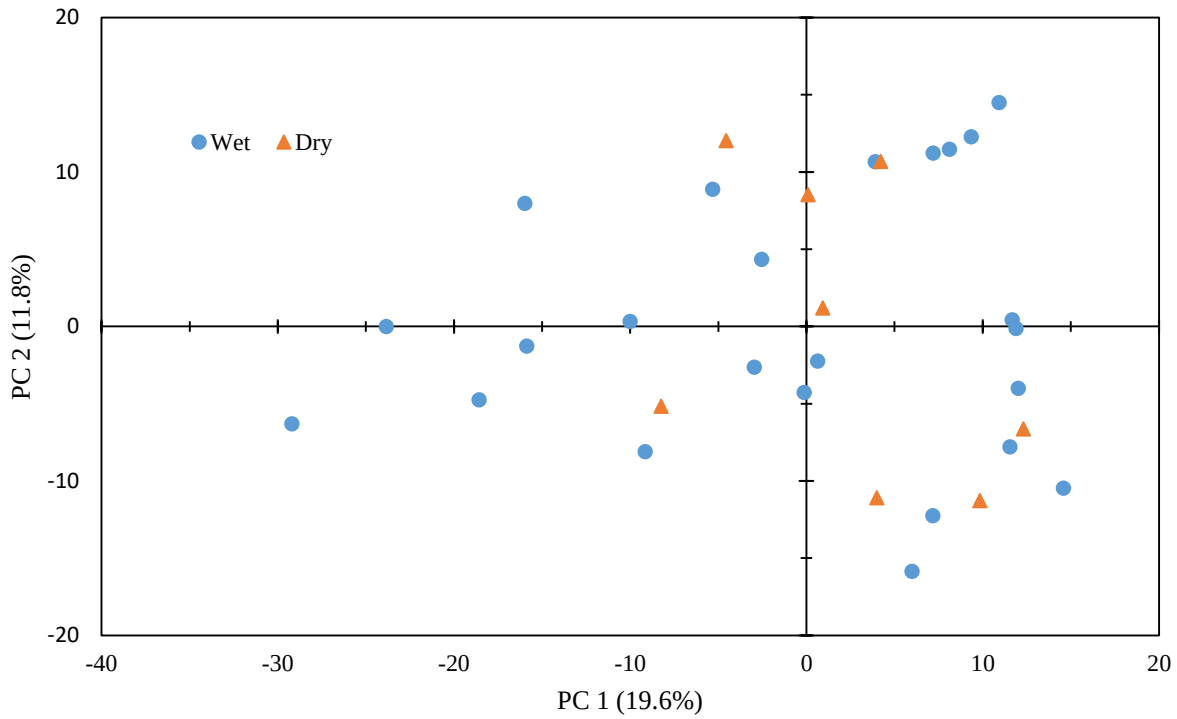

Figure 7. Organic Character PCA plot of all samples, labeled by if the sample was collected in either the wet season (orange) or the dry season (blue).

Comparing the activity deviation grouping in Figure 6 to Figure 7, grouped by wet or dry season, it can be seen that the two seasons cannot be significantly distinguished from each other, indicating that Figure 6's clustering is likely not seasonally derived or at least not primarily, as the inorganic ion PCAs could be. Performing this same analysis for air mass back trajectory using HYSPLIT (Figure A3), provides a similar result with no particular relationship arising from spatial distribution. As long range backtrajectory is not a primary driver of clustering, this suggests that long range transport is not a large influence relative to local emissions, as also suggested by other studies in this region.[65,88] Isotopic studies also illustrate that local emissions tend to be influential in determining rainwater DOC, with residence time on the order of days.[66]

In order to probe what species drive the differences in chemical character, identifying the species that weigh in the PCA loadings plot is a viable option. However, a statistically more

rigorous method is found in volcano plotting, discussed further on. Alternately, looking at how specific classes or related compounds are represented in the PCA loadings plot may reveal their relevance to overall organic character. The Kendrick analysis in Figure 8 identifies a series of related oligomers which when highlighted in the PCA loadings plot in Figure 7, all weight positively in PC 1 and evenly balanced in PC 2. This indicates that samples placed in Q1 or Q4 of the organic character PCA likely contain some or all of these oligomers. These samples, largely the Reference group and samples nearing the December Post-baseline crossing, could represent a higher level of nitrogen input, likely related to agricultural or anthropogenic sources. The oligomers of interest were all assigned a CHON formula with a mass tolerance < 1ppm, which supports the notion that these are related SOA compounds. It is known that heterogeneous multiphase chemical transformations are a pathway for anthropogenic related alkaloids to undergo oligomerization and incorporation into the WSOC fraction of SOA.[55,86,89–91] However, further study and structural analysis is needed to make more definitive assertions towards the origins and possible secondary processing of these specific oligomers.

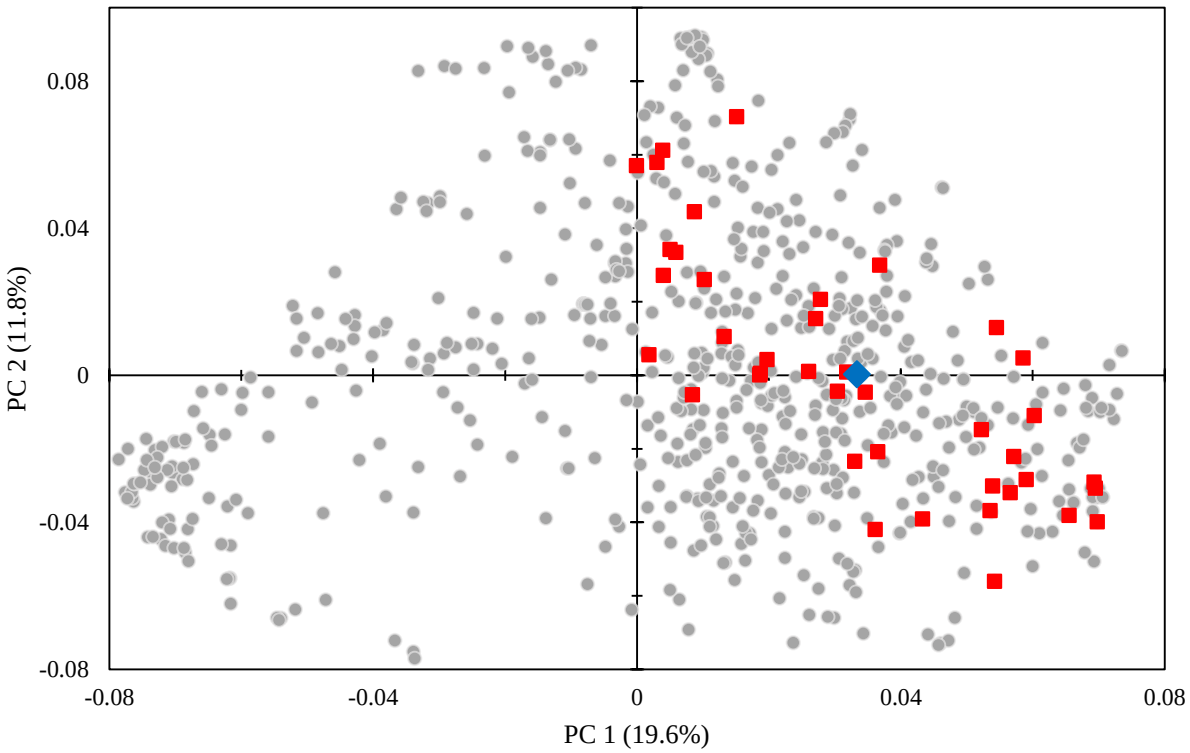

Figure 8. Organic Character PCA loading plot of all species used to calculate each sample's PCA score in Figure 6. Highlighted in red squares are related oligomers also highlighted in the following Kendrick plot. The blue diamond is their average weighting.

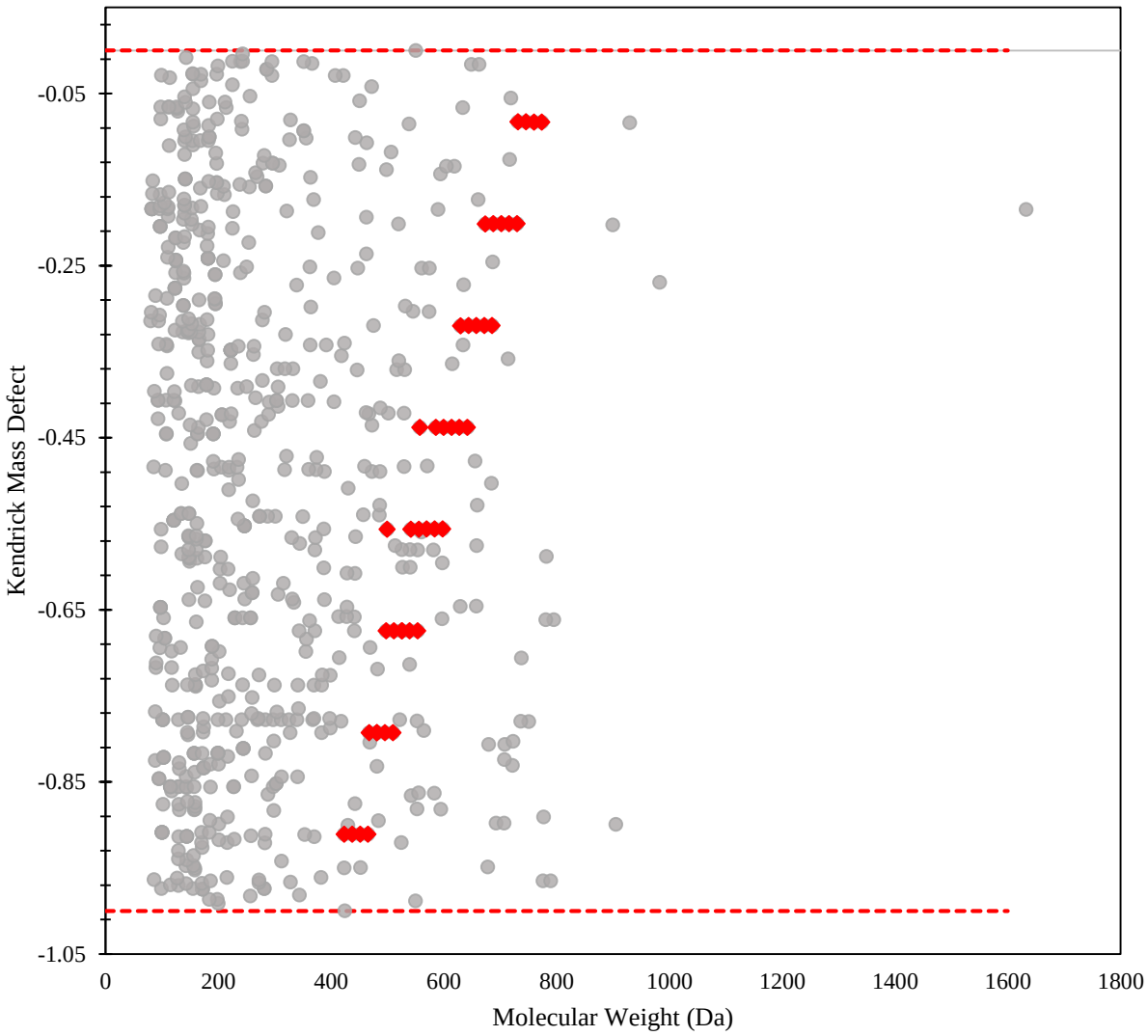

Figure 9. Kendrick mass defect plot all organic species positively identified. Highlighted in red are related oligomers also highlighted in the previous PCA loadings plot in Figure 7.

3.3 Volcano Plot

Volcano plots were used to identify statistically relevant changes in the rainwater DOM dataset between different groupings of samples. The first pairing in Figure 10, contrasting Reference and Reduced activity samples, found 57 up-regulated compounds (i.e. significant to Reference period samples) and 127 down-regulated compounds (i.e. significant to Reduced activity samples), presented in full in Tables A1 and A2. The up-regulated species are

compounds such as choline, linoleamide, chloropicrin, and what appear to be mostly CHON and CHONP compounds whose structures could not be resolved. Many of these compounds appear to be biosynthetic related,[92,93] however many can be agriculture or industrially related, particularly noted by the presence of chlorinated species confirmed with fragment ion analysis. The down-regulated compounds appear to be a variety of molecules, particularly BVOCs, some of which contain aromatic rings, others are amino acids such as phenylalanine, serine, norvaline, or amino acid derived like tyramine or biosynthetic such as the carnitine derivatives and many that cannot be structurally resolved. Altogether they do not point to a specific emissions relationship, though individually they are likely biosynthetic or biomass burning related. The significance of direct amino acid contribution to the Reduced period samples may be a strong indicator of the increased proportion of primary species in these samples. This suggests that either these samples were influenced more directly by primary emissions or overall atmospheric secondary processing decreased with decreasing anthropogenic activity. Other research has begun to demonstrate that the atmospheric oxidation capacity and the formation potential of SOA increases with increasing air pollution,[94,95] however both the Rio de Janeiro and São Paulo regions both saw an increase in ozone concentration of nearly 30% during the Reduced period due to NO_x reduction in VOC controlled ozone conditions.[61,96] Typically an increase in ozone would also suggest an increase in secondary processing of VOCs due to its strong oxidative potential, however that would neglect the changes in the overall oxidation capacity of the airshed, which these results would suggest decreased during the Reduced period.

Combustion related emissions, likely biomass burning are likely the sources for the aromatic and condensed species identified here such as thioquinox, phenethylamine, and pyridoxal. Although traditionally defined to be water insoluble, it has been shown that many

combustion derived aromatic and condensed compounds that fit the definition of black carbon (BC) do appear in the WSOM fraction of atmospheric organics[44] and aquatic DOM.[97] Indeed, BC is recognized to exist on a spectrum of solubility and recent studies have demonstrated that the oxidation of BC can increase its solubility,[98,99] supporting the idea that secondary processing may enhance the incorporation of combustion products into the WSOC fraction of OA. These aromatic and condensed aromatic compounds have higher potential for absorbing light than more saturated molecules,[7] highlighting their importance in climate systems.

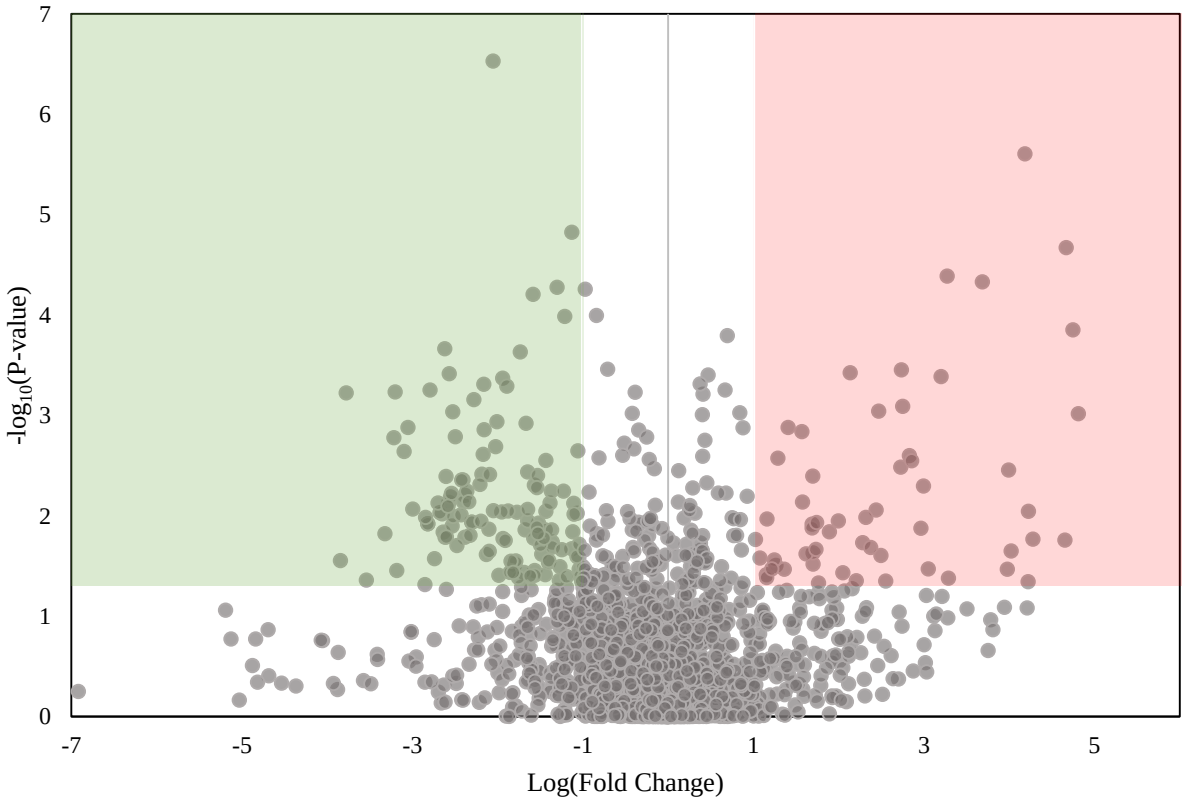

Figure 10. Volcano plot of Reference group samples against Reduced activity group samples. Up-regulated compounds are located in the red region (Reference group significant compounds) while down-regulated compounds are located in the green region (Reduced group significant compounds).

The second pairing in Figure 11 contrasts Reference and Post-baseline activity samples. This analysis found 221 down-regulated compounds (i.e. significant to Post-baseline period samples) and 86 up-regulated compounds (i.e. significant to Reference period samples), presented in full in Tables A3 and A4. The up-regulated compounds are largely the same or similar to the up-regulated compounds in the prior volcano analysis contrasting the Reference and Reduced groups, with 45 out of the 57 compounds in the previously up-regulated—Reference significant compounds—being up-regulated compounds here. However, the additional up-regulated compounds here are more biosynthetic related and amino acid related such as leucine and carnitine. The down-regulated compounds here have a few overlapping species with the prior down-regulated compounds, namely thioquinox and phenethylamine, which are the aromatic containing species previously discussed to be more biomass burning related. This indicates that the Reduced and Post-baseline groups are likely similar in biomass burning influence, which is corroborated by their similarity in season. The Reference and Post-baseline groups differ most in season and not in their activity. To that effect, the most notable down-regulated compounds are carbamates, palmitates, and some glycerol and sorbitol related compounds. Carbamates are notably involved in photosynthetic CO_2 capture[100] while palmitates are natural biosynthetic products of a wide variety of tropical plants, particularly the *Pandanaceae* family and many domesticated crops such as *Vitis vinifera* (the common grape), *Aloe vera*, and, most importantly, palm oil.[101,102] The glycerol and sorbitol species are also likely photosynthetically related, being rather notable biomolecules. These particular compounds may be seasonal indicators of photosynthetic activity in this region and may prove useful as BVOC indicators in future work.

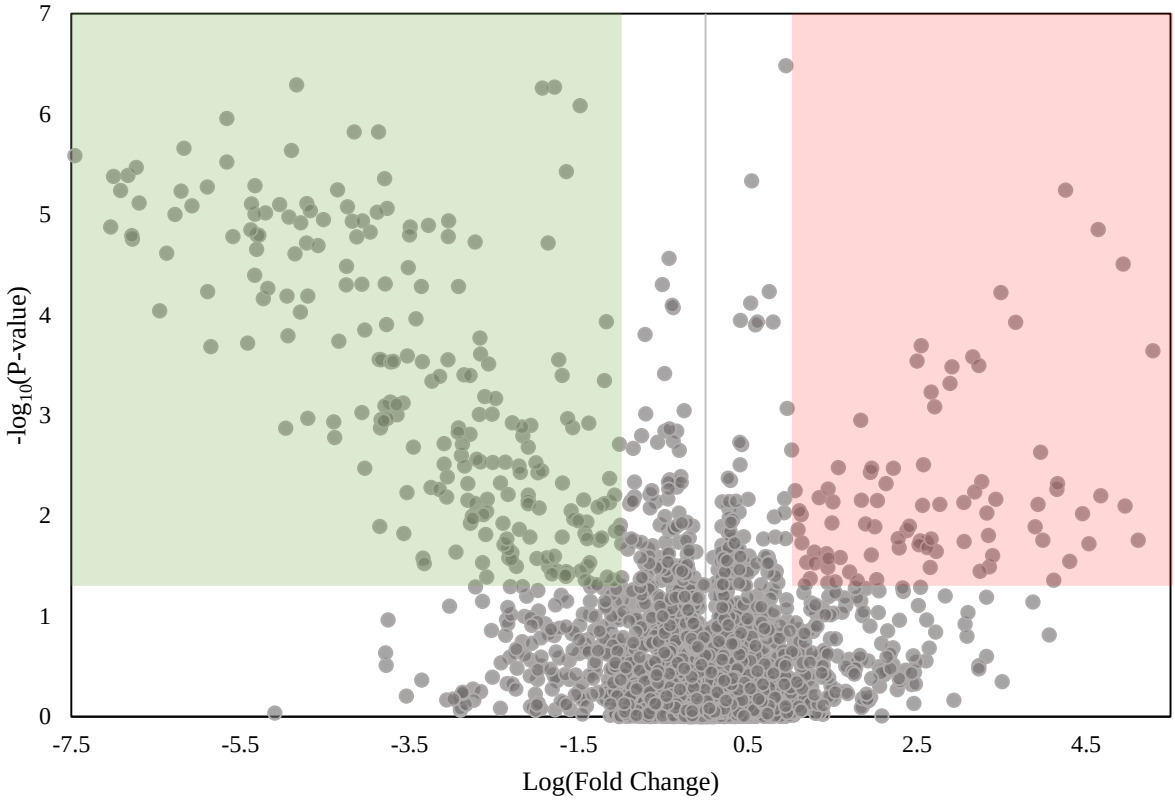

Figure 11. Volcano plot of Reference group samples against Post-baseline group samples. Up-regulated compounds are located in the red region (Reference group significant compounds) while down-regulated compounds are located in the green region (Post-baseline group significant compounds).

The last volcano plot analysis pairing contrasts Post-baseline and Reduced activity samples in Figure 12. This analysis found 24 down-regulated compounds (i.e. significant to Reduced period samples) and 135 up-regulated compounds (i.e. significant to Post-baseline period samples), presented in full in Tables A5 and A6. The up-regulated compounds have many overlapping species with the down-regulated compounds in the previous volcano analysis contrasting the Reference and Post-baseline samples, particularly the palmitates, sorbitol, and glycerol species. The carbamates notably are mostly missing, indicating that many of them likely appear both in the Reduced and Post-baseline samples. This may suggest the palmitates, sorbitol, and glycerol species may be more prevalent or only present during a specific seasonal transition

or timeframe that is not covered in the Reduced group while the carbamates are more ubiquitous. Most of the down-regulated species are strikingly simple biomolecules and amino acids, namely norleucine, leucine, l-threo-3-Phenylserine, norvaline, and carnitine derivatives. This again suggests that there is an increase in the proportion of primary species in the Reduced samples, likely indicating that overall atmospheric secondary processing for these primary species decreased with decreasing anthropogenic activity. It also indicates conversely that as anthropogenic activity came closer to returning to baseline, the proportion of these primary species decreased and their secondary processing increased. In this analysis, there is a higher variety and number of up-regulated compounds. This larger diversity could indicate a larger variety of emission sources, a higher input of specific sources that have a higher chemical diversity, or the enhancement of secondary processes, which often promotes chemical diversity.[41] However, basing this assertion solely on the number and variety of up or down-regulated species identified is a rather specious claim when considering the statistical basis of volcano plot analysis.

Volcano plots are traditionally used in proteomic, genomic, and metabolomics studies and this is one of its first applications in environmental systems. Volcano plotting selects significant and relevant compounds based on their p-value and fold change, and adjusting the tolerance for each of those parameters will drastically alter the number of selected compounds and not proportionally. This means that the number and variety of selected compounds may have more to do with the parameters of the analysis and less with true variety of species in the sample groups. For instance, raising the p-value threshold from 0.05 to 0.04 in the first volcano plot analysis in Figure 10 would eliminate 11% of the significant up-regulated compounds while only eliminating 4% of the significant down-regulated compounds. Adjusting further to 0.01 would

eliminate 60% and 51% of selected significant up and down-regulated compounds respectively. Indeed, even with consistent parameters volcano plots have come under scrutiny for a high type I error rate, leading to an inflation of false discoveries.[103] While remedies for these issues have begun to be applied and the technique itself is a strong statistical tool, it is important to remember that features identified through this analysis are not conclusive nor comprehensive but merely statistically strong indicators of relevant components. Further study and considerations are required to sufficiently begin adopting volcano plotting techniques for use outside of their traditional fields.

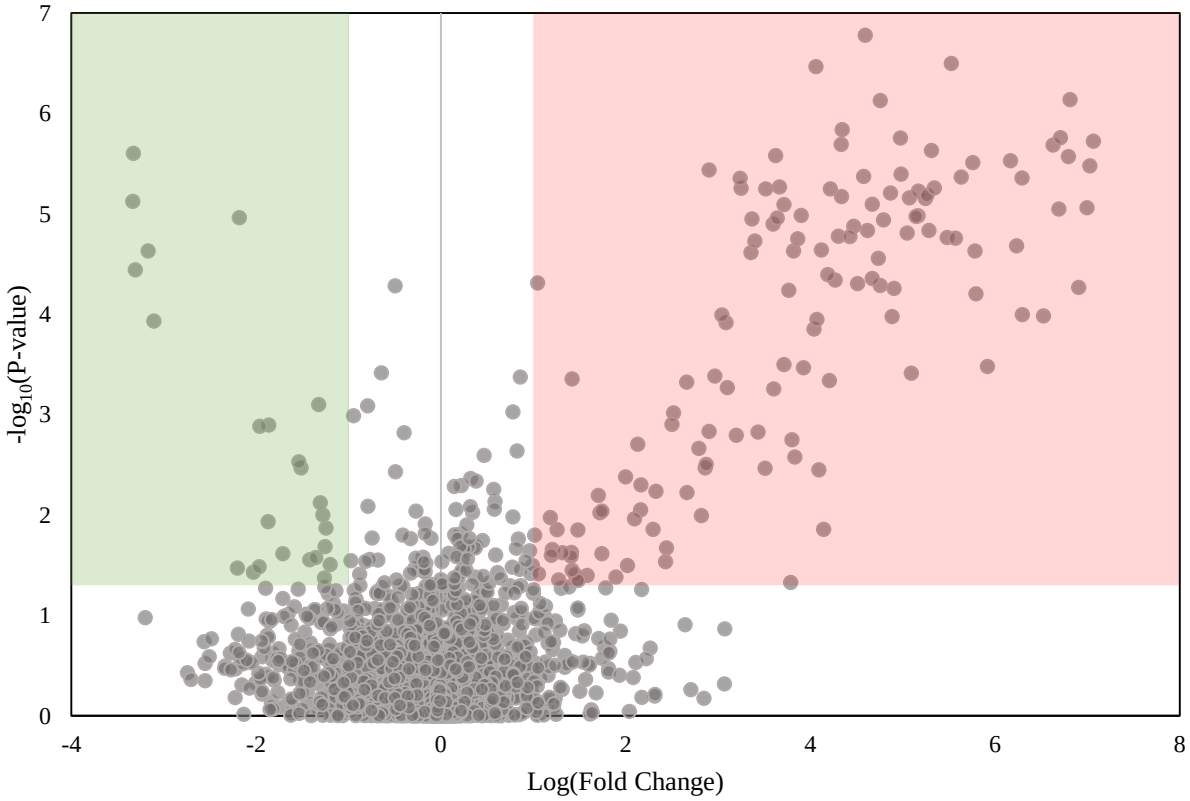

Figure 12. Volcano plot of Post-baseline group samples against Reduced activity group samples. Up-regulated compounds are located in the red region (Post-baseline group significant compounds) while down-regulated compounds are located in the green region (Reduced group significant compounds).

3.4 Inorganic Ion PCA

PCA was also utilized to describe the differences in the inorganic species present between samples. In the unaltered PCA, PC 1 represents 51.7% of the variance in the sample set, indicating it can explain about half of the variance in the ion concentrations, while PC 2 and 3 only explain 19.1% and 12.2% respectively. The PCA as presented in Figure 13 strongly identifies three outlier samples, n3, n11, n12 in the ion PCA that lie outside the main cluster around the origin, each with at least one PCA score that is greater than three standard deviations from the mean. These outlying samples score positive along PC 1, indicating that they are influenced by species that weight positively in the component factors for PC 1, such as Ca^{2+} and Mg^{2+} as seen in the component factor loadings in Figure 15. The component loadings show that PC 1 weights reactive nitrogen species positively as well as PO_4^{2-} and DOC, suggesting high PC 1 scores indicate those samples are likely agriculturally influenced. For organic acids, PC 1 favors acetate, glycolate, and oxalate over formate, possibly indicating that higher scored PC 1 samples may represent less oxidative processing.

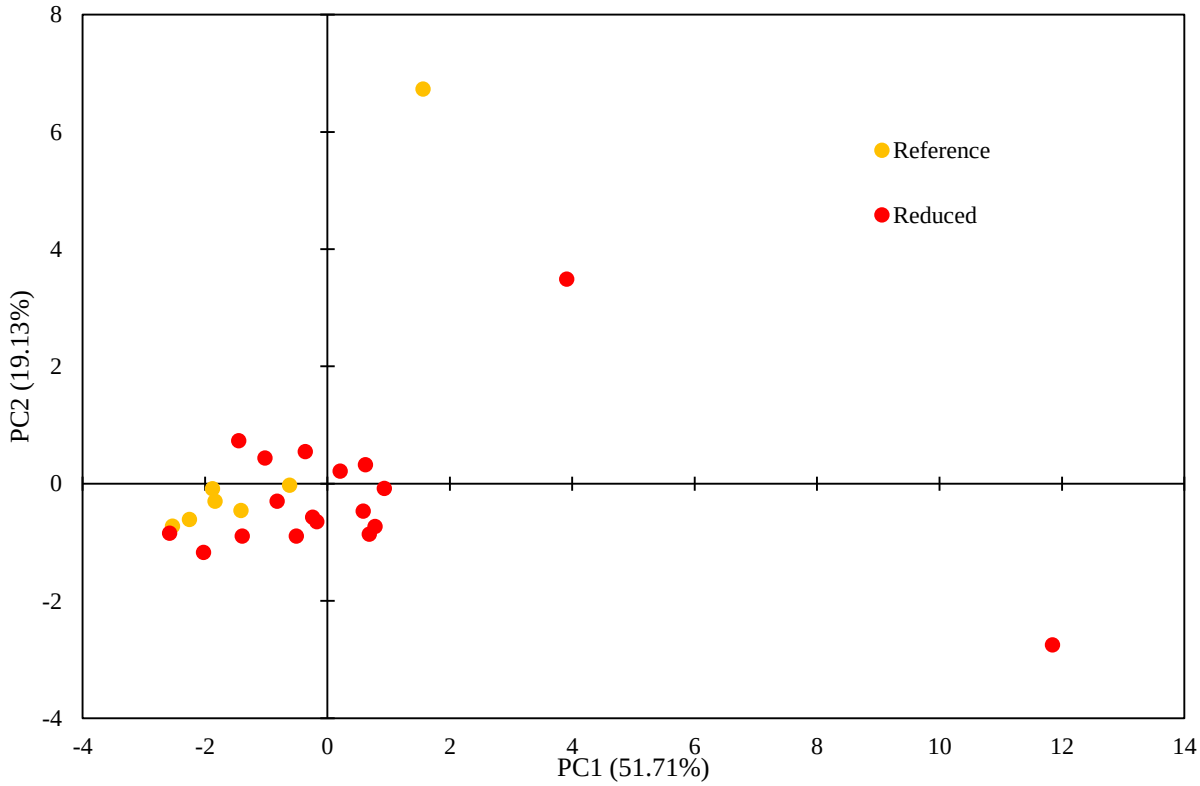

Figure 13. Ion PCA plot of PC 1 (51.7%) against PC 2 (19.1%)

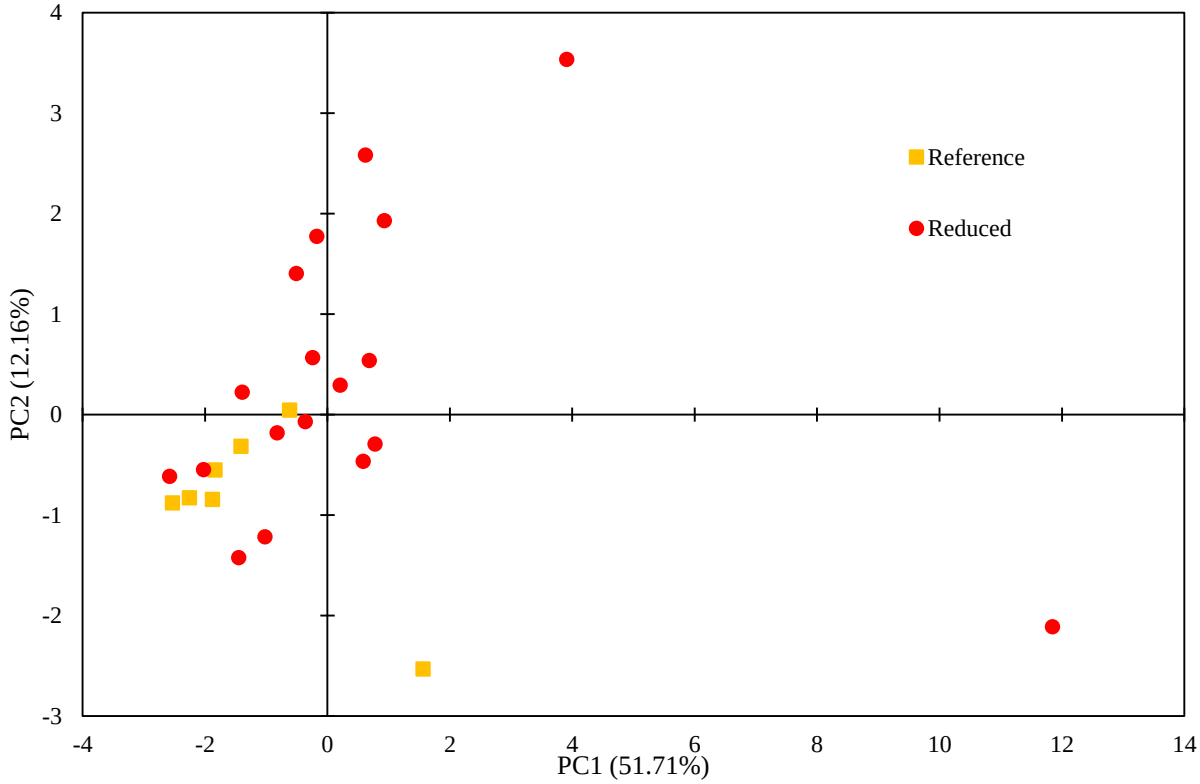

Figure 14. Ion PCA plot of PC 1 (51.7%) against PC 3 (12.2%)

N12 scores very high in PC 1 and negatively in both PC 2 and PC 3, quite possibly due to its high concentration of NO_3^- and organic acids, specifically glycolate, formate, and oxalate. n11 scores high in all three PCs, likely due to its high NH_4^+, Ca^{2+}, acetate, formate, and SO_4^{2-}. n3 however scores only barely higher in PC 1 than the main cluster of samples, while it has the highest PC 2 score and lowest PC 3 score. This could be attributed to its high concentrations of Na^+, K^+, Ca^{2+} and Mg^{2+}. PC 2 weights NO_3^- and Na^+ most positively with K^+ and Ca^{2+} weighted most negatively. PC 2 also favors formate over acetate and oxalate, suggesting that higher PC 2 scores indicate more oxidative processing but less biomass burning influence. PC 3 weights NH_4^+, acetate, formate, and Cl^- most positively while weighting strongly against DOC.

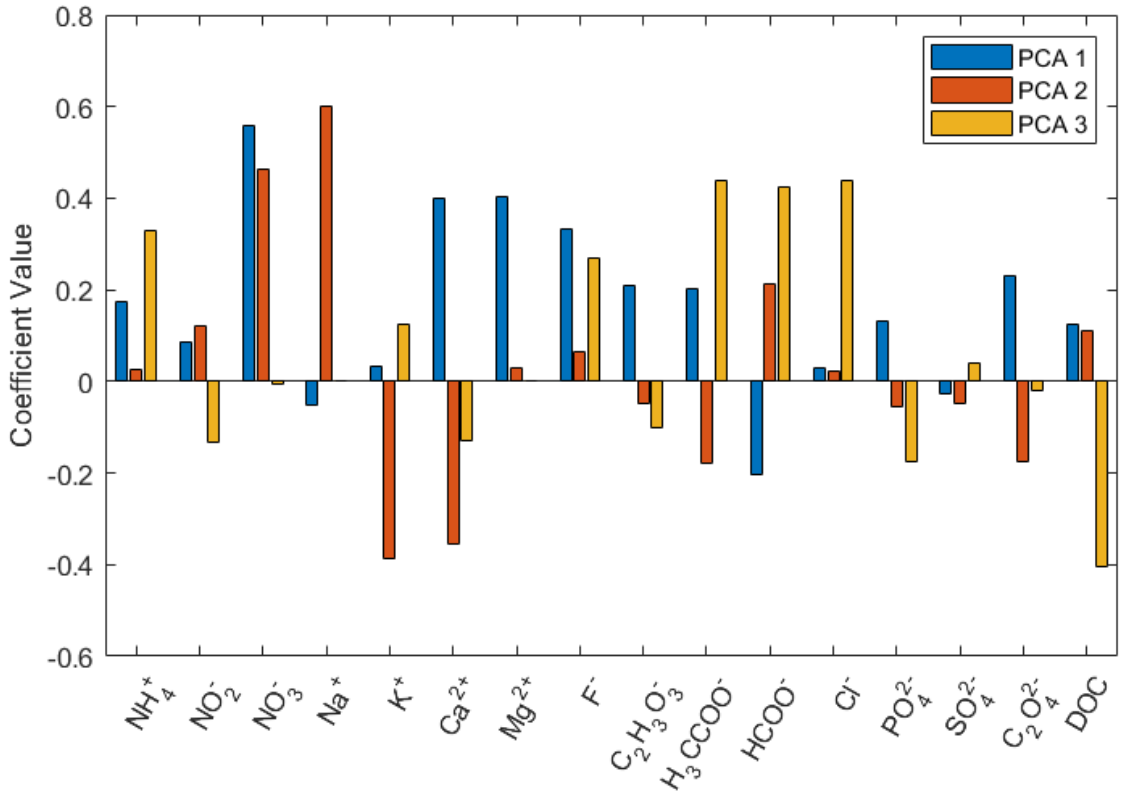

Figure 15. Component Factor loadings for major ions and DOC (n = 25)

Adjusting the PCA by removing the strongly outlying samples shows a more balanced PCA than the unaltered PCA, displayed in Figure 16 compared to Figures 13 and 15. However, this trimmed PCA does not strictly cluster samples into discrete groups that can easily be distinguished. Since n3, n11, n12 are thought to be heavily influenced by biomass burning or agriculturally related soil resuspension, removing these samples from the PCA leaves samples that are either more subtly related to these emission sources or related to vehicles, industry, biogenic emissions. The component loadings as shown in Figure 17 indicate how each species is weighted in the PCA. Both PC 1 and 2 weight reactive nitrogen species positively, suggesting samples in quadrant I (Q1) have agricultural influence. PC 1 and 2 both weight Na^+ and Ca^{2+} negatively but differ on K^+ and Mg^{2+}, with PC 1 weighting them positively and PC 2 weighting them negatively. This might place samples with biomass burning influence in quadrant IV (Q4). PC 2 weights SO_4^{2-} very positively while PC 1 weights DOC very positively. As for organic acids, glycolate weights positively and oxalate weight negatively in both PC 1 and 2, while acetate weights negatively in PC 2 and formate weights positively in PC 1.

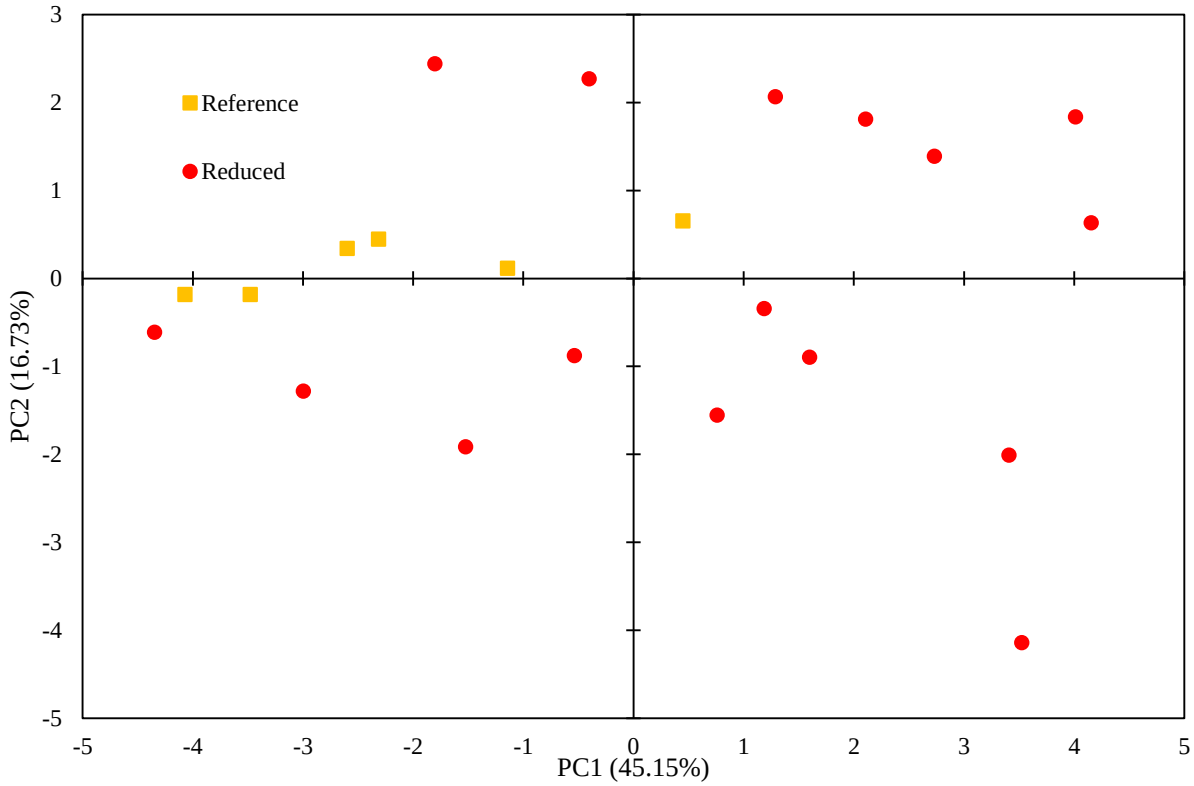

Figure 16. Ion PCA plot of PCA 1 (45.2%) against PCA 2 (16.7%) with outliers removed (n = 22)

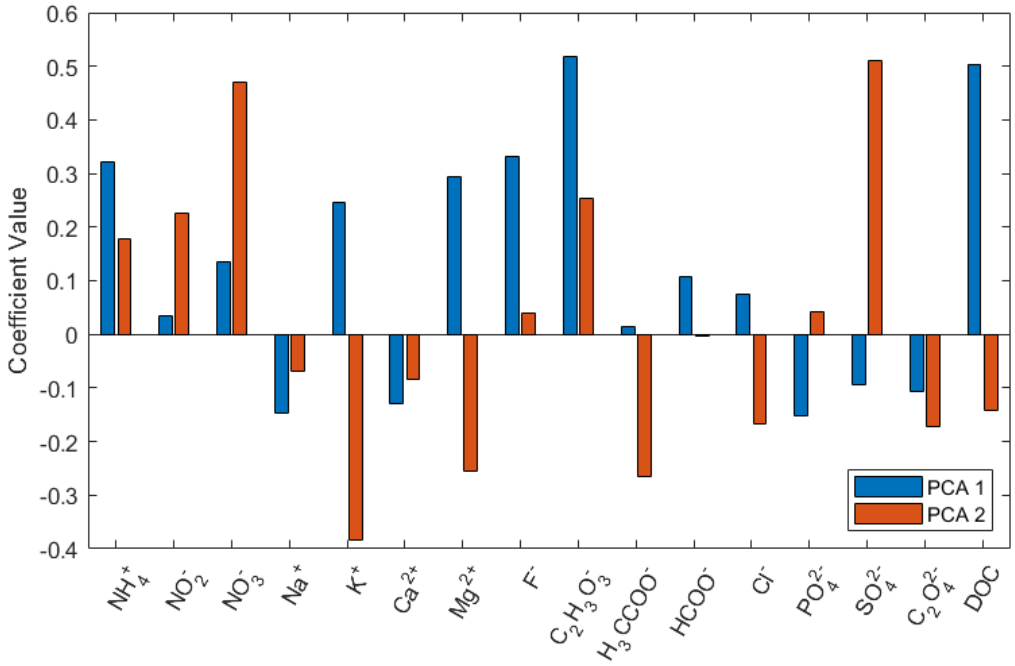

Figure 17. Component Factor loadings for major ions and DOC (n = 22) with outliers removed

Alternatively labelling the PC plot with information from other analysis reveals how effectively the ion PCA differentiates or clusters the samples presented. In Figure 16, the Reference period samples cluster tightly on the PC 2 axis but have more variance within PC 1. This suggests that the Reference period samples are rather similar in regards to PC 2. Figure 18(a) shows that dry season samples tend to cluster near the top of the PCA plot with similar PC 2 scores but may vary more along PC 1. This might suggest that the differences of the Reference samples relative to the Reduced group may be due in part to the season the samples were collected. More ion data is required to better understand the extent of this influence.

Figure 18(c) indicates how the organic character PCA and ion PCA compare in their clustering. Samples with organic PCA scores in Q4 show clustering in quadrant II (Q2) of the ion PCA. These samples comprise the Reference group, indicating that the Reference samples are distinct from Reduced activity samples in both ion composition and organic matter character. Because other organic character PCA groups don't show as strong clustering as the Q4 group in Figure 18(c), this could suggest that organic matter character and ion composition for these samples may not be as strongly related to each other in Reduced activity samples. Conversely, this suggests that organic matter character and ion composition are related in Reference group samples, indicating strong similarity in either emission source or secondary production.

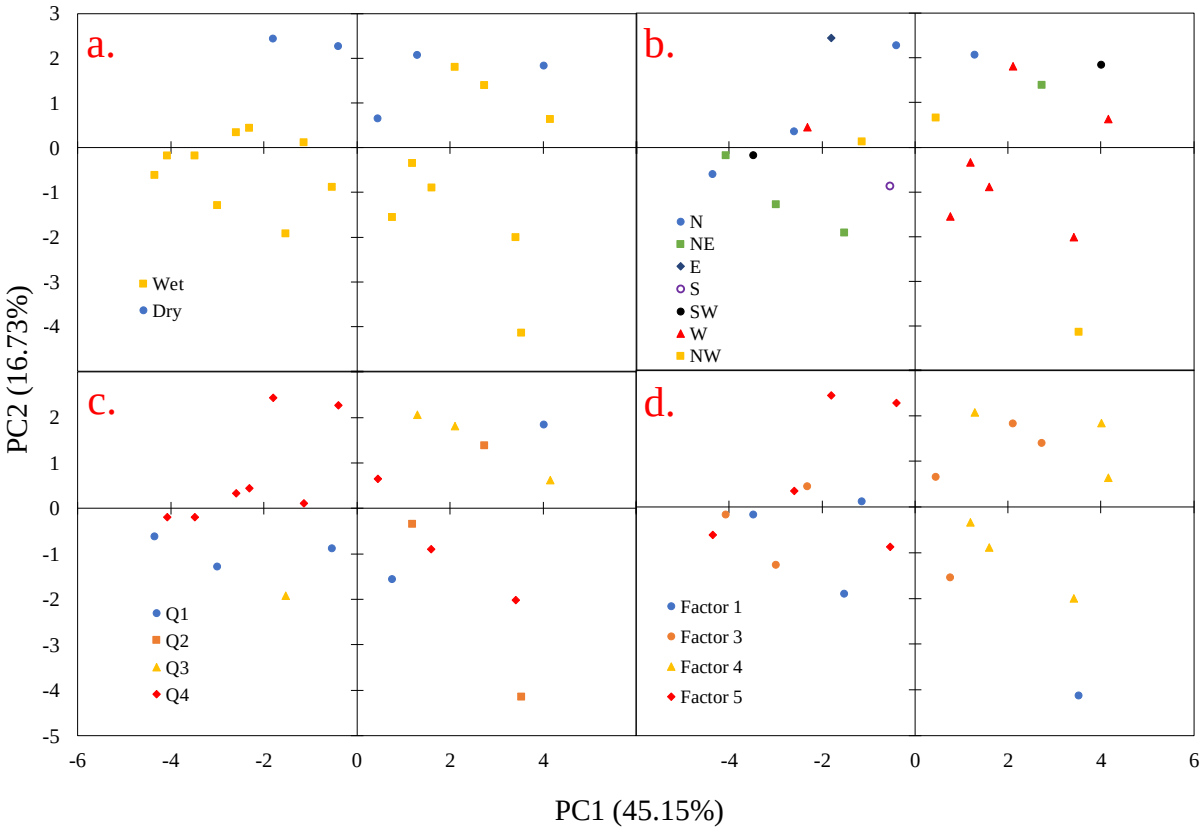

Figure 18. Inorganic Ion PCA plots of PCA 1 (45.2%) against PCA 2 (16.7%) with outliers removed (n = 22) labeled by groupings of (a) season, (b) HYSPLIT backtrajectory, (c) quadrant the sample is located in the organic PCA plot, (d) primary PMF factor contributor from the combined five factor PMF model. Factor 2 was not the primary factor contributor for any sample in this figure, but was the primary factor contributor for n11 and n12 which were removed in the base PCA.

3.5 Combined PCA

Incorporating organic character parameters into the PCA model further expounds on the characteristics of the arising clusters. Figure 19 shows the PCA clustering plot arising from the union of inorganic ion and DOM characteristic data. This plot clusters Reference sample very tightly on PC 2 with wider variation in PC 1. These Reference period samples all present positive PC 2 values with mostly negative PC 1 values, thus located in Q2. The Reduced activity samples then inhabit a wide range of various regions of the PCA, with the samples closest to the return to Post-baseline date appearing close to the Reference cluster in Q2. Looking at the drivers of

clustering, exhibited in the PCA loadings plot in Figure 20, parameters located closely to one another are generally believed to be related parameters in terms of emission source. Mg^{2+} and K^+ are very close to DBE in Q1, indicating that these species are most likely related through biomass burning. O:C and O:N are both collocated at the top of the plot, indicated that more oxidized species appear close to the top of the PCA plots via strong PC 1 values. Since most Reduced samples in Figure 19 fall below zero in PC 1, this may indicate that the Reduced samples are mostly less oxidized than the Reference period samples as well as indicate that the Reduced samples located far in Q1 are biomass burning related. The location of Na^+ closer to the top of the loadings plot suggest that the presence of Na^+ in this system is related to biomass burning rather than marine influence, as seen in other studies that correlate its presence to marine influence with Cl^-. All the quantitated organic acids and reactive nitrogen species, along with F^- and Cl^- as well as DOC and DON, appear rather closely in Q4. This may suggest that these parameters are related through anthropogenic activity. Because the organic acid constituents are considered part of the DOC fraction, it is not surprising that they are closely weighted in the PCA. Their relation to NO_3^- and DON are more revealing in that it suggests that reactive nitrogen, organic nitrogen, and organic acids are moderately linked in emission source. Indeed, recent studies have also highlighted organic acids as notable anthropogenic emissions contributors.[95] Both H:C and N:C appear in Q3, suggesting that less oxidized species and more nitrogenated species are placed towards the bottom of the PCA. These atomic ratios though, as previously discussed, are rather stable in all samples and they can simply be considered as balancing parameters in the PCA. Balancing these ratios, the distribution of parameters in the RHS cluster is more relevant to understanding the drivers of the PCA clustering. Following that reactive nitrogen species and DON are centrally located, compounds that incorporate

atmospheric NO_x would be located towards the center left of the PCA. These drivers indicate that the Reference period samples all have similar levels of oxidation and are likely influenced by chemical exchange with atmospheric reactive nitrogen, which is not present in most Reduced activity samples. The decrease in anthropogenic emissions, particularly vehicle-related NO_x, is the most probable driver in the reduction of these NO_x influenced characteristics. Conversely, the NO_x influenced characteristics in the Reference period samples are indicative of the larger influence of vehicle-related NO_x and other anthropogenic emissions during this period.

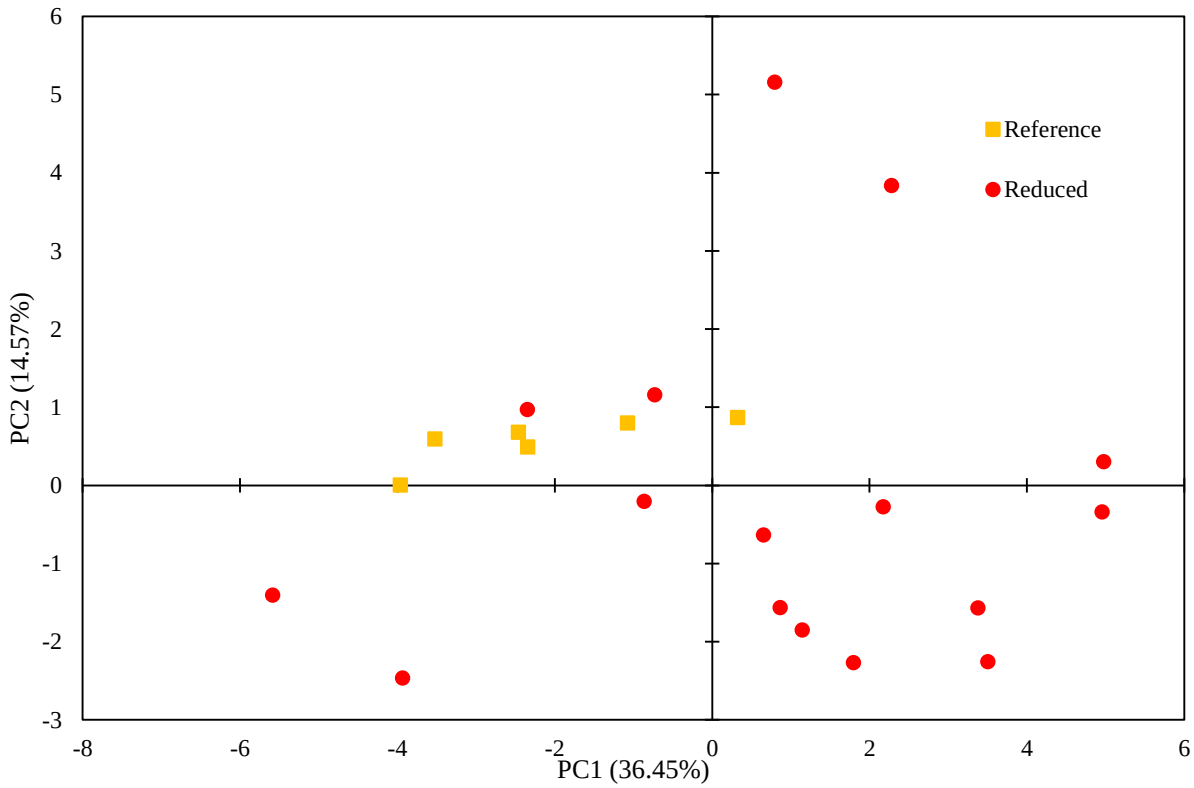

Figure 19. Combined Inorganic and Organic PCA plot of PCA 1 (36.5%) against PCA 2 (14.6%) with outliers removed (n = 22)

Performing a simple Pearson correlation calculation of all parameters also indicates (shown in Table A7) that parameters like NO_3^-, K^+, F^-, Cl^-, PO_4^{3-}, and the organic acids are

positively correlated to DBE in the DOM fraction and to each other rather strongly. Inversely, H:C is negatively correlated to all these parameters and to DBE. The strongest correlation that O:C has with any other parameter are with the other oxygen ratios, O:N and O:S. It appears that O:C ratio does not have simple direct relationships with other parameters. It does however negatively correlate with NO_3^-, K^+, F^-, Cl^-, PO_4^{3-}, and the organic acids slightly. Ions such as Na^+, Ca^{2+}, Mg^{2+}, and K^+ are strongly correlated to each other, likely indicating these parameters are related through mechanical suspension of soils. SO_4^{2-} strongly correlates with NH_4^+ and NO_3^- as well as the organic acids. It also slightly correlates to DBE, suggesting that it is not marine related but more likely a combustion product.

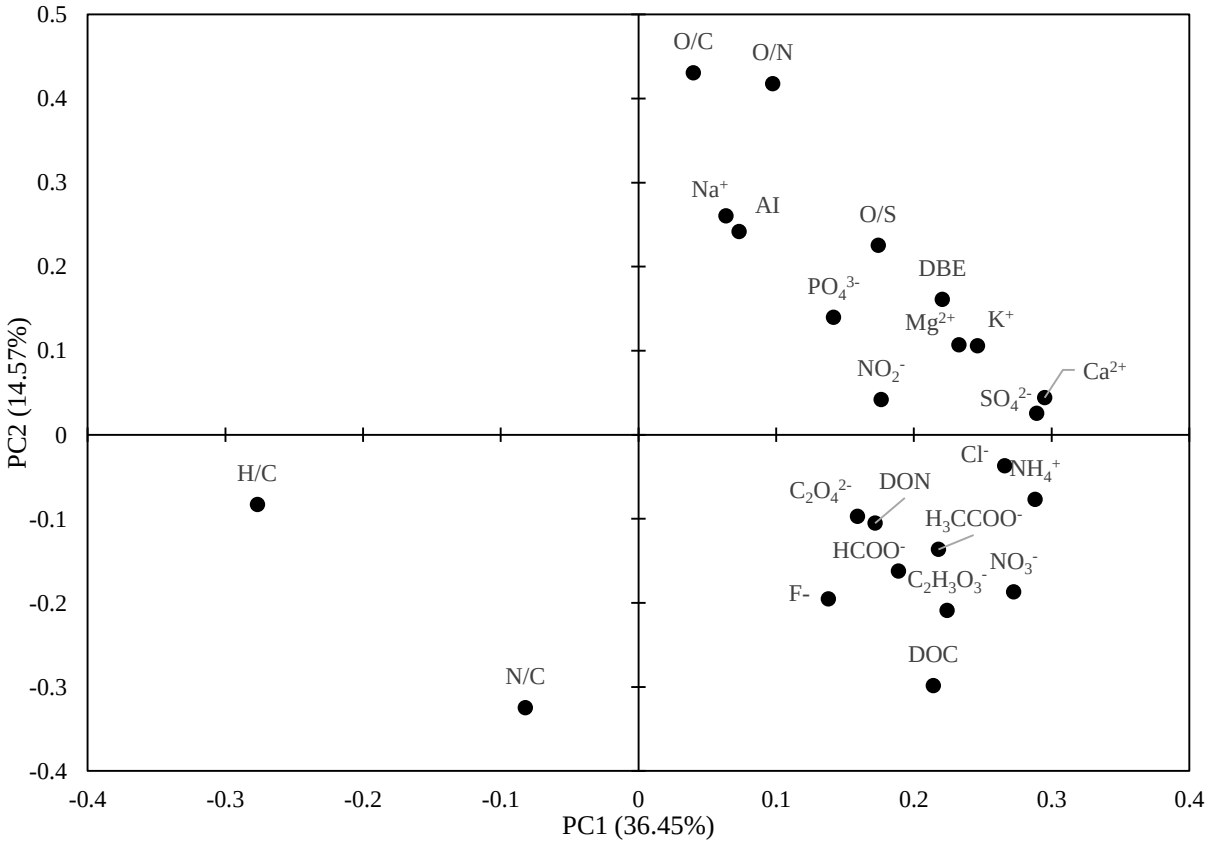

Figure 20. Combined Inorganic and Organic PCA loadings plot of PCA 1 (36.5%) against PCA 2 (14.6%) with outliers removed (n = 22)

3.6 Positive Matrix Factorization

As previously discussed, because the distance from the observation site to the South Atlantic Ocean is about 338 kilometers, its position geographically puts Ribeirão Preto virtually free from influence by the Atlantic. Confirming this, all previous analysis in this study have pointed to typical marine indicators like Cl^-, SO_4^{2-}, and Na^+ as being combustion or soil suspension in origin. Thus, marine emissions are eliminated as a potential source of emissions.

Since most of the energy produced in Brazil is from hydroelectric power; coal, petroleum, and natural gas burning power plants can also be ruled out as a significant source of emissions. This leaves agriculture, soil resuspension, vehicles, industry, biogenic emissions, and biomass burning as the remaining major potential sources of emissions for Ribeirão Preto.

The factor profiles for all inorganic species and quantitated organic acids are presented in Figure 21 and in Figure 22 where outliers are removed. Concerning the base PMF factor profiles for all samples with inorganic ion data available, most species are associated with either three or four factors, with only PO_4^{3-} and $C_2O_4^{2-}$ associated with two factors. NO_2^-, Ca^{2+}, and Cl^- are the only species associated with all five factors. Based on the prominence of Na^+, Ca^{2+}, Mg^{2+}, formate and SO_4^{2-} in the factor 5 profile, the factor can be assigned as some combination of soil resuspension and industrial activity. Factor 5 also shows a K^+/Ca^{2+} ratio of 0.524, which is most similar ratio to the one found by Coelho et. al. 2011 (0.0126) for resuspended soil dust.[65] The K^+/Ca^{2+} ratios for factors 1, 2, 3, and 4 are 0.686, 1.009, 6.890, 0.603 respectively, suggesting either factor 2 or 3 could be influenced by agricultural activity or sugar cane smoke based on their elevated K^+/Ca^{2+} ratio, similar to the relationship found by Coelho et. al. 2011 (1.19). The prominence of both NH_4^+ and PO_4^{3-} lends credence to assigning factor 4 as agricultural emissions, while the dominance of both NH_4^+ and NO_3^- in factor 1 suggest more vehicle

emission influence. Indeed, factor 1 has the lowest $HCOO^-/H_3CCOO^-$ ratio with 0.515, supporting the notion it may represent direct vehicle emissions or anthropogenic nitrogen inputs. Biomass burning, biogenic emissions and direct vehicular emissions tend to favor emission of acetic acid relative to formic acid.[104] With $HCOO^-/H_3CCOO^-$ ratios being 0.515, 0.881, 1.185, undefined, and 0.000 for factors 1, 2, 3, 4, and 5 respectively, it is plausible that factors 1, 2, or 5 are related to biomass burning, biogenic emissions or direct vehicular emissions. Other studies have demonstrated that direct traffic formate:acetate ratios tend to be closer to 0.25 and increases in that ratio may be related to photochemical production of formate by H_2CO oxidation.[105] This would indicate the factors here, even if they do represent vehicle emissions, are likely more oxidized than direct traffic emissions. Following that, factor 3 is likely to be biomass burning based on the dominance of NO_2^- and the $HCOO^-/H_3CCOO^-$ ratio favoring acetate, however PO_4^{3-} is not a contributor to this factor profile which is typically associated with agricultural emissions.

Overall, assigning emission sources for each factor in the base inorganic ion and organic acid PMF model is inconclusive. However, it does suggest that factor 5 may represent resuspended soil influence, factor 3 or 4 may be agriculturally influenced, factor 2 could be biomass burning, and factor 1 may be oxidized vehicle or urban emissions.

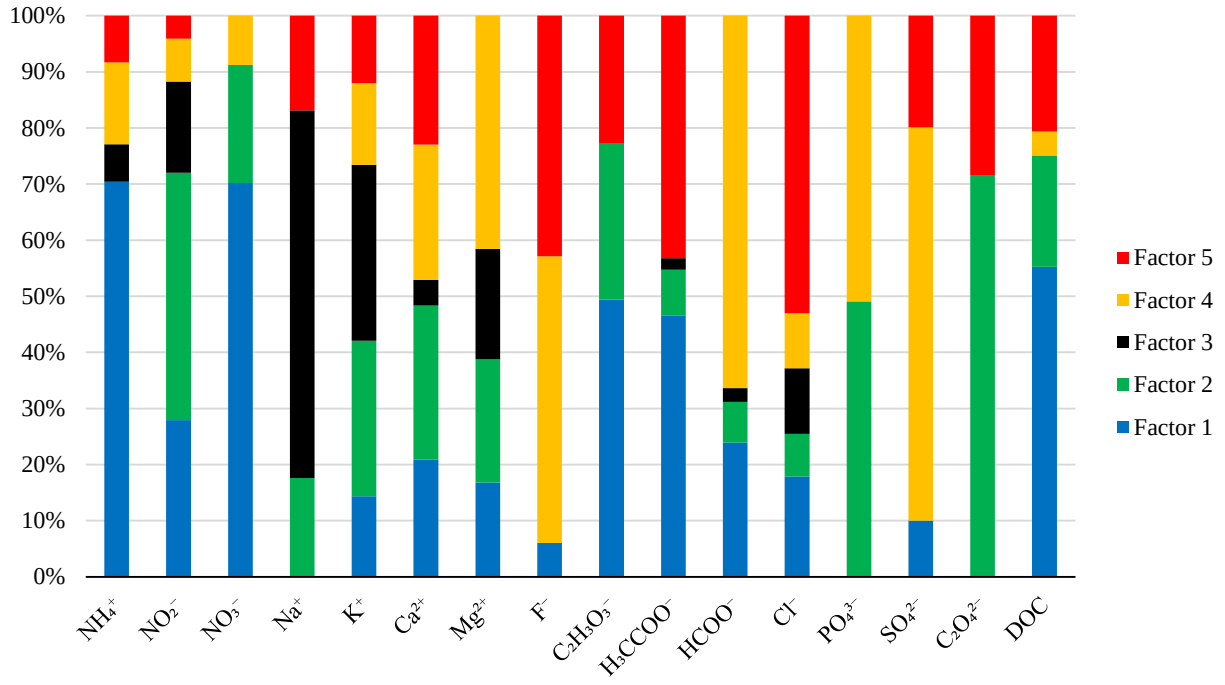

Figure 21. Factor Profiles of All Ion Species

Factor Profiles (percent of species sum) from Base Run #13 in the five factor PMF model of ion concentrations. (n = 24)

Simplifying by removing outliers in the base PMF model, specifically n4, n11, n12, and n13, may help reduce the uncertainty in assigning emission sources to the factor profiles. The n11, n12, and n13 outlier samples are believed to be biomass burning or agriculturally related due to their elevated DOC, formate, and K^+ concentrations while n4 may be more related to soil resuspension due to its high Ca^{2+}, Cl^- and Na^+ concentrations in addition to its high K^+ concentration. Removing these samples may help discern the other emissions source assignments drowned out by their strong signal in the model.

For the factor profiles present in Figure 22 representing the PMF model with outliers removed, most species did not decrease the number of associated factors compared to the base model. Instead, most species are associated with four factors with only NH_4^+, NO_2^-, and $HCOO^-$ being associated with three factors. PO_4^{3-} is still only associated with two factors, factors 2 and 4.

Factor 1 can be likely thought of as soil resuspension due to its Na^+, Ca^{2+}, Mg^{2+}, and SO_4^{2-} prevalence. This factor has only formate present and not acetate in its profile and its K^+/Ca^{2+} ratio is the lowest of any of the K^+ containing factors. Factor 2 is likely agriculturally related due to the prevalence of nitrogen species, K^+, PO_4^{3-}, and DOC. Factor 2 also has a formate:acetate ratio of 0.000 and a K^+/Ca^{2+} of 6.170, indicating it favors acetate and has the highest K^+/Ca^{2+} of all factors. Factor 3 and 4 are difficult to constrain. Both F^- and Cl^- are prominent in their profiles along with notable portions of the organic acids. Both have low formate:acetate ratios however factor 3 has a K^+/Ca^{2+} ratio of 0.0817 while factor 4 is 0.000. This may suggest they are related to industrial or anthropogenic activity, but their assignments are generally inconclusive. Factor 5 is likely same vehicle or urban emission signature as factor 1 in the base PMF model, as can be seen by the proportions of the nitrogen species and organic acids.

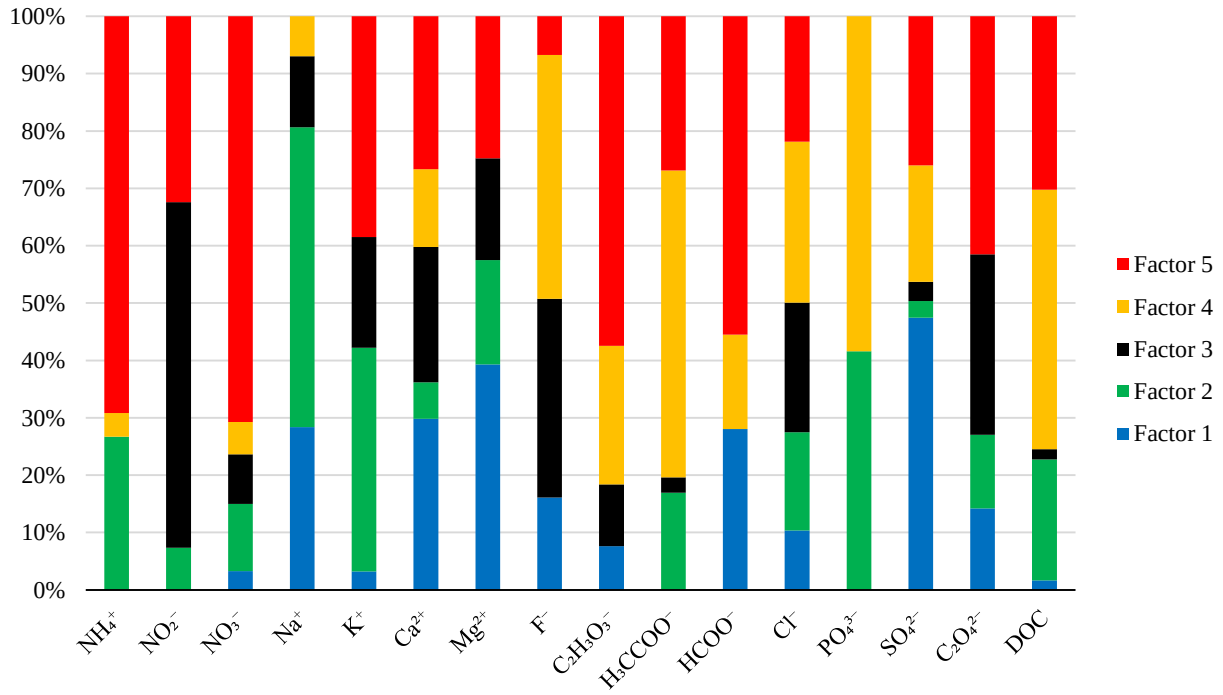

Figure 22. Factor Profiles of All Ion Species excluding Outliers

Factor Profiles (percent of species sum) from Base Run #3 in the five factor PMF model of ion concentrations, excluding outlier samples. (n = 20)

3.7 Combined PMF

Bringing DOM characteristics into the model may elaborate on the potential DOM characteristics associated with the factor profiles. The combined PMF factor profiles presented in Figure 23 are mostly similar to the base model PMF concerning only the inorganic ion species and organic acids. Factor 1 is most similar to factor 5 in the base model while factor 2 is to factor 4 in the base model, factor 3 is to factor 2 in the base model, factor 4 is to factor 1 in the base model, and factor 5 is to factor 3 in the base model. Their factor profile analysis earlier in the base model discussion is applicable here.

The organic parameters have little variation to them. Relative to the standard deviations of the inorganic species, the organic parameters have much larger deviations and are not the drivers of the model. For instance, the maximum relative standard deviation for any inorganic species is 5%, while the average relative standard deviation for the organic parameters is over 100% simply due to the wide diversity of organic species in the DOM fraction. The nature of these organic parameters are simply not highly compatible with the way PMF models function. To then try to infer emissions properties from their representation in any factor profile would lead to invalid assertions. For example, factor 2 is not represented in any organic parameter, which would imply that factor 2's corresponding emission signature lacks DOM, which can easily be dismissed by observing that DOC is present in factor 2's profile. However, information that can still be gleaned from this combined PMF model is that atomic ratios and DBE alone are not enough to profile emission signatures. The model also implies that factor 4 may contain the most oxidized and aromatic DOM constituents, as its profile has the largest representation in the oxygen ratios and AI. This would corroborate the idea that factor 4 represents combustion products from vehicle and urban emissions, but would also imply that factor 1 (possibly

representing resuspended soils) is more oxidized and aromatic than factor 5 and factor 3 (possibly representing agricultural influence and biomass burning respectively).

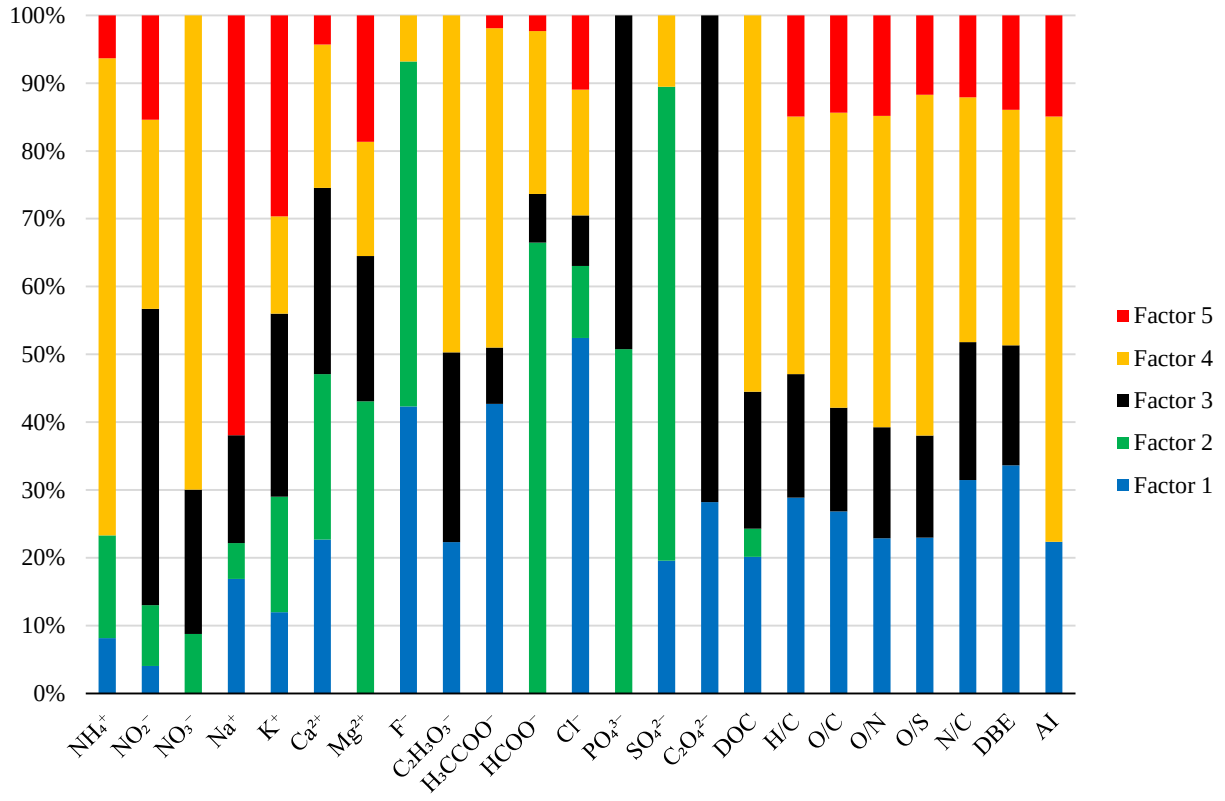

Figure 23. Combined PMF Factor Profiles of all parameters.

Factor Profiles (percent of species sum) from Base Run #14 in the five factor PMF model of inorganic, organic acid concentrations, and DOM characteristics. (n = 24)

CHAPTER IV. CONCLUSIONS AND IMPLICATIONS

Demonstrating the use of electrospray ionization ultrahigh-resolution Orbitrap mass spectrometry (ESI-UHRMS) for atmospheric organic characterization, the molecular characterization of DOM in continental Brazilian rainwater provides insight into the variability of atmospheric WSOC and WSON. Rainwater DOM shows significant variety in its chemical composition which can inform source apportionment and displays its dynamic role in many environmental processes. This form of analysis presents a high throughput method that supports the study of biologically relevant organics in the atmosphere which are meaningful to public health and ecosystems.

WSON represents a significant part of overall chemical character in the analyzed continental rainwater DOM, suggesting that true rainwater DOM character content is strongly influenced if not dominated by DON. Nitrogen containing species represent 86.0% of the organic compounds identified, many of these likely peptides or amino acid derivatives. While direct contribution of amino acids typically ranges from only 2-25% of total WSON,[84,85] their true contribution to total WSON is likely higher. Further exploration focusing on their secondary contributors could very well elucidate and constraint the upper bound of their contribution. Other studies that miss this large contribution of WSON may vastly underestimate the bioavailability of rainwater DOM.

The general proportions of classes of molecules as well as the proportions of them that contain specific heteroatoms remain relatively stable over the many samples presented. The average atomic ratios may differ sample to sample, indicating changes in the variety and atomic ratios of compounds within specific classes, but the proportions of the classes remain relatively

stable. Averaging along the different groupings of samples yields no significant differences between these class proportions.

This continental rainwater OM shows distinct evidence indicative of secondary processing and oxidized anthropogenic urban/vehicular emissions, however missing some key components shown in other studies such as CHO and CHON formulas with O:C ratios between 0.35 and 0.85.[44] Kendrick analysis identifies a series of related CHON oligomers, which are known markers of oxidized anthropogenic emissions. These oligomers play a strong role in distinguishing organic character in clustering analysis. The samples distinguished by these oligomers are largely prepandemic and samples collected towards the beginning of 2021, concerning the Reference and Post-baseline groups, thus markedly absent from samples collected in the months following the height of social isolation measures, April to November 2020. This change in the presence of these oligomers is likely in response to a strong reduction in ambient NO_x concentrations, which is corroborated in concurrent air quality monitoring studies.[61] The incorporation of this reactive nitrogen into DOM alters its properties and is a potential explanation for rainwater DOM's high bioavailability relative to other matrices.

Volcano plotting suggests that while despite an increase in average ambient ozone concentration, the proportion of primary species present, namely direct amino acid contributors and other biosynthetic compounds, increased with less secondary processing during the Reduced period. Condensed and aromatic compounds became more common going into the Reduced and Post-baseline periods and are likely biomass burning related species that became more prevalent as wildfire season progressed. Typical BC compounds were not found, but more water-soluble potential secondary products of BC were present. Possible indicators for seasonal BVOCs in this region may have been identified in carbamates and palmitates, however the novelty of volcano

plot analysis in environmental study and its high rate of false positives—also called type I errors—gives cause for concern and further consideration.

Further contrasting the chemical character of samples before and after the institution of partial lockdown orders, PCA analysis shows that Reference period rainwater is distinct from Reduced activity rainwater in both DOM character and major inorganic ion content. However, these distinctions are lost approaching the Post-baseline period. Reference period and Post-baseline DOM is distinguished by a higher variety of unique compounds and the CHON oligomers previously discussed while ion content is distinguished by a reduction in sulfate, nitrate, potassium, and formate in Reduced activity samples. The influences of seasonality on these effects are difficult to constrain and likely a contributor to inorganic variation. More data regarding the inorganic species is necessary to clarify this relationship. HYSPLIT analysis indicates no strong spatial influence on DOM character nor inorganic ion content, indicating that local emissions prevail over long-range transport. Other studies in this region have suggested the same.[65,88] Analyzing both organic and inorganic content in tandem reveals the relationships among inorganic and organic character parameters. Reactive nitrogen, organic nitrogen, and organic acids appear close in PCA loadings indicating that they are moderately linked in emission source. Attempting to do the same using PMF is misleading as bulk organic characteristic parameters such as atomic ratios and DBE tend to be incompatible with how the PMF analysis functions. Parameters such as NO_3^-, K^+, F^-, Cl^-, PO_4^{3-}, and the organic acids are positively correlated to DBE in the DOM fraction and to each other rather strongly. Inversely, H:C is negatively correlated to all these parameters and to DBE. While O:C ratio does negatively correlate with NO_3^-, K^+, F^-, Cl^-, PO_4^{3-}, and the organic acids slightly, it does not have simple direct relationships with other parameters.

While the consequences of pandemic related public policies are multifaceted and complex in effect, this work highlights the potential for public policy to reduce the emission of air pollutants and other biologically relevant anthropogenic emissions, particularly through reducing traffic loading and expanding remote working. Investigating both the organic and inorganic constituents of rainwater chemical character provides a fuller picture of the important components that indicate emission profiles and contributions. Orbitrap ESI-UHRMS and traditional IC methods provide a complementary set of data that can be thoroughly deconstructed through powerful statistical tools such as PCA, volcano plotting, and PMF. These methods demonstrate a high-throughput method with minimal sample prep that lay the groundwork for building a more comprehensive inventory of atmospheric OM as well as constraining the influences of emission sources.

REFERENCES

(1) Willey, J. D.; Kieber, R. J.; Eyman, M. S.; Avery, G. B.; Willey, D.; Kieber, R. J.; Eyman, M. S.; Brooks, G.; Jr, A. Rainwater Dissolved Organic Carbon: Concentrations and Global Flux. *Global Biogeochem. Cycles* **2000**, *14* (1), 139–148. https://doi.org/10.1029/1999GB900036.

(2) Altieri, K. E.; Turpin, B. J.; Seitzinger, S. P. Oligomers, Organosulfates, and Nitrooxy Organosulfates in Rainwater Identified by Ultra-High Resolution Electrospray Ionization FT-ICR Mass Spectrometry. *Atmos. Chem. Phys.* **2009**, *9* (7), 2533–2542. https://doi.org/10.5194/acp-9-2533-2009.

(3) Pillar-Little, E. A.; Guzman, M. I. An Overview of Dynamic Heterogeneous Oxidations in the Troposphere. *Environ. - MDPI* **2018**, *5* (9), 1–23. https://doi.org/10.3390/environments5090104.

(4) Liu, Z.; Yim, S. H. L.; Wang, C.; Lau, N. C. The Impact of the Aerosol Direct Radiative Forcing on Deep Convection and Air Quality in the Pearl River Delta Region. *Geophys. Res. Lett.* **2018**, *45* (9), 4410–4418. https://doi.org/10.1029/2018GL077517.

(5) Mahowald, N. Aerosol Indirect Effect on Biogeochemical Cycles and Climate. *Science (80-.).* **2011**, *334* (6057), 794–796. https://doi.org/10.1126/science.1207374.

(6) Jimenez, J. L.; Canagaratna, M. R.; Donahue, N. M.; Prevot, A. S. H.; Zhang, Q.; Kroll, J. H.; DeCarlo, P. F.; Allan, J. D.; Coe, H.; Ng, N. L.; et al. Evolution of Organic Aerosols in the Atmosphere. *Science (80-.).* **2009**, *326* (5959), 1525–1529. https://doi.org/10.1126/science.1180353.

(7) Andreae, M. O.; Gelencsér, A. Black Carbon or Brown Carbon? The Nature of Light-Absorbing Carbonaceous Aerosols. *Atmos. Chem. Phys.* **2006**, *6* (10), 3131–3148.

https://doi.org/10.5194/acp-6-3131-2006.

(8) Cerully, K. M.; Bougiatioti, A.; Hite, J. R.; Guo, H.; Xu, L.; Ng, N. L.; Weber, R.; Nenes, A. On the Link between Hygroscopicity, Volatility, and Oxidation State of Ambient and Water-Soluble Aerosols in the Southeastern United States. *Atmos. Chem. Phys.* **2015**, *15* (15), 8679–8694. https://doi.org/10.5194/acp-15-8679-2015.

(9) Chan, M. N.; Choi, M. Y.; Ng, N. L.; Chan, C. K. Hygroscopicity of Water-Soluble Organic Compounds in Atmospheric Aerosols: Amino Acids and Biomass Burning Derived Organic Species. *Environ. Sci. Technol.* **2005**, *39* (6), 1555–1562. https://doi.org/10.1021/es049584l.

(10) Wozniak, A. S.; Shelley, R. U.; Sleighter, R. L.; Abdulla, H. A. N.; Morton, P. L.; Landing, W. M.; Hatcher, P. G. Relationships among Aerosol Water Soluble Organic Matter, Iron and Aluminum in European, North African, and Marine Air Masses from the 2010 US GEOTRACES Cruise. *Mar. Chem.* **2013**, *154*, 24–33. https://doi.org/10.1016/j.marchem.2013.04.011.

(11) Wozniak, A. S.; Shelley, R. U.; McElhenie, S. D.; Landing, W. M.; Hatcher, P. G. Aerosol Water Soluble Organic Matter Characteristics over the North Atlantic Ocean: Implications for Iron-Binding Ligands and Iron Solubility. *Mar. Chem.* **2015**, *173*, 162–172. https://doi.org/10.1016/j.marchem.2014.11.002.

(12) Kanakidou, M.; Seinfeld, J. H.; Pandis, S. N.; Barnes, I.; Dentener, F. J.; Facchini, M. C.; Van Dingenen, R.; Ervens, B.; Nenes, A.; Nielsen, C. J.; et al. Organic Aerosol and Global Climate Modelling: A Review. *Atmos. Chem. Phys.* **2005**, *5* (4), 1053–1123. https://doi.org/10.5194/acp-5-1053-2005.

(13) Mahowald, N. Supporting Online Material Aerosol Indirect Effect on Biogeochemical

Cycles and Climate Downloaded From. *Phys. Earth Planet. Inter* **1952**, *57* (B12), 63. https://doi.org/10.1126/science.1208265.

(14) Iavorivska, L.; Boyer, E. W.; DeWalle, D. R. Atmospheric Deposition of Organic Carbon via Precipitation. *Atmos. Environ.* **2016**, *146*, 153–163. https://doi.org/10.1016/j.atmosenv.2016.06.006.

(15) Allen, A. G.; Machado, C. M. D.; Cardoso, A. A. Measurements and Modeling of Reactive Nitrogen Deposition in Southeast Brazil. *Environ. Pollut.* **2011**, *159* (5), 1190–1197. https://doi.org/10.1016/j.envpol.2011.02.002.

(16) Likens, G. E.; Butler, T. J.; Claybrooke, R.; Vermeylen, F.; Larson, R. Long-Term Monitoring of Precipitation Chemistry in the U.S.: Insights into Changes and Condition. *Atmos. Environ.* **2020**, *245*, 118031. https://doi.org/10.1016/j.atmosenv.2020.118031.

(17) Lelieveld, J.; Haines, A.; Pozzer, A. Age-Dependent Health Risk from Ambient Air Pollution: A Modelling and Data Analysis of Childhood Mortality in Middle-Income and Low-Income Countries. *Lancet. Planet. Heal.* **2018**, *2* (7), e292–e300. https://doi.org/10.1016/S2542-5196(18)30147-5.

(18) Heft-Neal, S.; Burney, J.; Bendavid, E.; Burke, M. Robust Relationship between Air Quality and Infant Mortality in Africa. *Nature* **2018**, *559* (7713), 254–258. https://doi.org/10.1038/s41586-018-0263-3.

(19) Rager, J. E.; Lichtveld, K.; Ebersviller, S.; Smeester, L.; Jaspers, I.; Sexton, K. G.; Fry, R. C. A Toxicogenomic Comparison of Primary and Photochemically Altered Air Pollutant Mixtures. *Environ. Health Perspect.* **2011**, *119* (11), 1583–1589. https://doi.org/10.1289/ehp.1003323.

(20) Cohen, A. J.; Brauer, M.; Burnett, R.; Anderson, H. R.; Frostad, J.; Estep, K.;

Balakrishnan, K.; Brunekreef, B.; Dandona, L.; Dandona, R.; et al. Estimates and 25-Year Trends of the Global Burden of Disease Attributable to Ambient Air Pollution: An Analysis of Data from the Global Burden of Diseases Study 2015. *Lancet* **2017**, *389* (10082), 1907–1918. https://doi.org/10.1016/S0140-6736(17)30505-6.

(21) Landrigan, P. J.; Fuller, R.; Acosta, N. J. R.; Adeyi, O.; Arnold, R.; Basu, N. (Nil); Baldé, A. B.; Bertollini, R.; Bose-O'Reilly, S.; Boufford, J. I.; et al. The Lancet Commission on Pollution and Health. *Lancet* **2018**, *391* (10119), 462–512. https://doi.org/10.1016/S0140-6736(17)32345-0.

(22) Heft-Neal, S.; Burney, J.; Bendavid, E.; Burke, M. Robust Relationship between Air Quality and Infant Mortality in Africa. *Nature* **2018**, *559* (7713), 254–258. https://doi.org/10.1038/s41586-018-0263-3.

(23) Gordon, S. B.; Bruce, N. G.; Grigg, J.; Hibberd, P. L.; Kurmi, O. P.; Lam, K. H.; Mortimer, K.; Asante, K. P.; Balakrishnan, K.; Balmes, J.; et al. Respiratory Risks from Household Air Pollution in Low and Middle Income Countries. *Lancet Respir. Med.* **2014**, *2* (10), 823–860. https://doi.org/10.1016/S2213-2600(14)70168-7.

(24) Carter, W. P.; L Carter, W. P. Development of Ozone Reactivity Scales for Volatile Organic Compounds. *J. Air Waste Manag. Assoc* **1994**, *44* (7), 881–899. https://doi.org/10.1080/1073161X.1994.10467290.

(25) Barrefors, G.; Petersson, G. Volatile Hydrocarbons from Domestic Wood Burning. *Chemosphere* **1995**, *30* (8), 1551–1556. https://doi.org/10.1016/0045-6535(95)00048-D.

(26) Chang, D.; Wang, Z.; Guo, J.; Li, T.; Liang, Y.; Kang, L.; Xia, M.; Wang, Y.; Yu, C.; Yun, H.; et al. Characterization of Organic Aerosols and Their Precursors in Southern China during a Severe Haze Episode in January 2017. *Sci. Total Environ.* **2019**, *691*, 101–

111. https://doi.org/10.1016/j.scitotenv.2019.07.123.

(27) Kumar, M.; Burrell, E.; Hansen, J. C.; Francisco, J. S. Molecular Insights into Organic Particulate Formation. *Commun. Chem.* **2019**, *2* (1). https://doi.org/10.1038/s42004-019-0183-7.

(28) Steenhof, M.; Gosens, I.; Strak, M.; Godri, K. J.; Hoek, G.; Cassee, F. R.; Mudway, I. S.; Kelly, F. J.; Harrison, R. M.; Lebret, E.; et al. In Vitro Toxicity of Particulate Matter (PM) Collected at Different Sites in the Netherlands Is Associated with PM Composition, Size Fraction and Oxidative Potential - the RAPTES Project. *Part. Fibre Toxicol.* **2011**, *8* (1), 26. https://doi.org/10.1186/1743-8977-8-26.

(29) Reiss, R.; Anderson, E. L.; Cross, C. E.; Hidy, G.; Hoel, D.; McClellan, R.; Moolgavkar, S. Evidence of Health Impacts of Sulfate-and Nitrate-Containing Particles in Ambient Air. *Inhal. Toxicol.* **2007**, *19* (5), 419–449. https://doi.org/10.1080/08958370601174941.

(30) Twigg, M. V.; Phillips, P. R. Cleaning the Air We Breathe - Controlling Diesel Particulate Emissions from Passenger Cars. https://doi.org/10.1595/147106709X390977.

(31) *ENVIRONMENTAL PROTECTION AGENCY 40 CFR Part 50 Technical Correction to the National Ambient Air Quality Standards for Particulate Matter*.

(32) Valberg, P. A. Is PM More Toxic Than the Sum of Its Parts? Risk-Assessment Toxicity Factors vs. PM-Mortality "Effect Functions." *Inhal. Toxicol.* **2004**, *16* (sup1), 19–29. https://doi.org/10.1080/08958370490442935.

(33) Sotty, J.; Garçon, G.; Denayer, F.-O.; Alleman, L.-Y.; Saleh, Y.; Perdrix, E.; Riffault, V.; Dubot, P.; Lo-Guidice, J.-M.; Canivet, L. Toxicological Effects of Ambient Fine (PM2.5-0.18) and Ultrafine (PM0.18) Particles in Healthy and Diseased 3D Organo-Typic Mucocilary-Phenotype Models. *Environ. Res.* **2019**, *176*, 108538.

https://doi.org/10.1016/j.envres.2019.108538.

(34) Lichtveld, K. M.; Ebersviller, S. M.; Sexton, K. G.; Vizuete, W.; Jaspers, I.; Jeffries, H. E. In Vitro Exposures in Diesel Exhaust Atmospheres: Resuspension of PM from Filters versus Direct Deposition of PM from Air. *Environ. Sci. Technol.* **2012**, *46* (16), 9062–9070. https://doi.org/10.1021/es301431s.

(35) de Bruijne, K.; Ebersviller, S.; Sexton, K. G.; Lake, S.; Leith, D.; Goodman, R.; Jetters, J.; Walters, G. W.; Doyle-Eisele, M.; Woodside, R.; et al. Design and Testing of Electrostatic Aerosol *In Vitro* Exposure System (EAVES): An Alternative Exposure System for Particles. *Inhal. Toxicol.* **2009**, *21* (2), 91–101. https://doi.org/10.1080/08958370802166035.

(36) Lichtveld, K. M.; Ebersviller, S. M.; Sexton, K. G.; Vizuete, W.; Jaspers, I.; Jeffries, H. E. In Vitro Exposures in Diesel Exhaust Atmospheres: Resuspension of PM from Filters versus Direct Deposition of PM from Air. *Environ. Sci. Technol.* **2012**, *46* (16), 9062–9070. https://doi.org/10.1021/es301431s.

(37) Vizuete, W.; Sexton, K. G.; Nguyen, H.; Smeester, L.; Aagaard, K. M.; Shope, C.; Lefer, B.; Flynn, J. H.; Alvarez, S.; Erickson, M. H.; et al. From the Field to the Laboratory: Air Pollutant-Induced Genomic Effects in Lung Cells. *Environ. Health Insights* **2015**, *9s4*, EHI.S15656. https://doi.org/10.4137/EHI.S15656.

(38) Arashiro, M.; Lin, Y.-H.; Sexton, K. G.; Zhang, Z.; Jaspers, I.; Fry, R. C.; Vizuete, W. G.; Gold, A.; Surratt, J. D. In Vitro Exposure to Isoprene-Derived Secondary Organic Aerosol by Direct Deposition and Its Effects on COX-2 and IL-8 Gene Expression. *Atmos. Chem. Phys.* **2016**, *16* (22), 14079–14090. https://doi.org/10.5194/acp-16-14079-2016.

(39) Donahue, N. M.; Robinson, A. L.; Pandis, S. N. Atmospheric Organic Particulate Matter:

From Smoke to Secondary Organic Aerosol. *Atmos. Environ.* **2009**, *43* (1), 94–106. https://doi.org/10.1016/j.atmosenv.2008.09.055.

(40) De Gouw, J.; Jimenez, J. L. Organic Aerosols in the Earth's Atmosphere. *Environmental Science and Technology*. American Chemical Society October 15, 2009, pp 7614–7618. https://doi.org/10.1021/es9006004.

(41) Hallquist, M.; Wenger, J. C.; Baltensperger, U.; Rudich, Y.; Simpson, D.; Claeys, M.; Dommen, J.; Donahue, N. M.; George, C.; Goldstein, A. H.; et al. The Formation, Properties and Impact of Secondary Organic Aerosol: Current and Emerging Issues. *Atmos. Chem. Phys.* **2009**, *9* (14), 5155–5236. https://doi.org/10.5194/acp-9-5155-2009.

(42) Rudich, Y.; Donahue, N. M.; Mentel, T. F. Aging of Organic Aerosol: Bridging the Gap between Laboratory and Field Studies. *Annu. Rev. Phys. Chem.* **2007**, *58*, 321–352. https://doi.org/10.1146/annurev.physchem.58.032806.104432.

(43) Radke, L. F.; Hobbs, P. V.; Eltgroth, M. W. Scavenging of Aerosol Particles by Precipitation. *J. Appl. Meteorol.* **1980**, *19* (6), 715–722. https://doi.org/10.1175/1520-0450(1980)019<0715:SOAPBP>2.0.CO;2.

(44) Willoughby, A. S.; Wozniak, A. S.; Hatcher, P. G. Detailed Source-Specific Molecular Composition of Ambient Aerosol Organic Matter Using Ultrahigh Resolution Mass Spectrometry and 1H NMR. *Atmosphere (Basel).* **2016**, *7* (6), 1–7. https://doi.org/10.3390/atmos7060079.

(45) Altieri, K. E.; Hastings, M. G.; Peters, A. J.; Sigman, D. M. Molecular Characterization of Water Soluble Organic Nitrogen in Marine Rainwater by Ultra-High Resolution Electrospray Ionization Mass Spectrometry. *Atmos. Chem. Phys.* **2012**, *12* (7), 3557–3571. https://doi.org/10.5194/acp-12-3557-2012.

(46) Mead, R. N.; Felix, J. D.; Avery, G. B.; Kieber, R. J.; Willey, J. D.; Podgorski, D. C. Characterization of CHOS Compounds in Rainwater from Continental and Coastal Storms by Ultrahigh Resolution Mass Spectrometry. *Atmos. Environ.* **2015**, *105*, 162–168. https://doi.org/10.1016/j.atmosenv.2015.01.057.

(47) Mead, R. N.; Mullaugh, K. M.; Brooks Avery, G.; Kieber, R. J.; Willey, J. D.; Podgorski, D. C. Insights into Dissolved Organic Matter Complexity in Rainwater from Continental and Coastal Storms by Ultrahigh Resolution Fourier Transform Ion Cyclotron Resonance Mass Spectrometry. *Atmos. Chem. Phys.* **2013**, *13* (9), 4829–4838. https://doi.org/10.5194/acp-13-4829-2013.

(48) Li, L.; Fang, Z.; He, C.; Shi, Q. Separation and Characterization of Marine Dissolved Organic Matter (DOM) by Combination of Fe(OH) 3 Co-Precipitation and Solid Phase Extraction Followed by ESI FT-ICR MS. *Anal. Bioanal. Chem.* **2019**, *411* (10), 2201–2208. https://doi.org/10.1007/S00216-019-01663-Y/FIGURES/7.

(49) Reemtsma, T.; These, A.; Linscheid, M.; Leenheer, J.; Spitzy, A. Molecular and Structural Characterization of Dissolved Organic Matter from the Deep Ocean by FTICR-MS, Including Hydrophilic Nitrogenous Organic Molecules. *Environ. Sci. Technol.* **2008**, *42* (5), 1430–1437. https://doi.org/10.1021/es7021413.

(50) Sleighter, R. L.; Hatcher, P. G. Molecular Characterization of Dissolved Organic Matter (DOM) along a River to Ocean Transect of the Lower Chesapeake Bay by Ultrahigh Resolution Electrospray Ionization Fourier Transform Ion Cyclotron Resonance Mass Spectrometry. *Mar. Chem.* **2008**, *110* (3–4), 140–152. https://doi.org/10.1016/J.MARCHEM.2008.04.008.

(51) Martins, C. P. B.; Bromirski, M.; Prieto Conaway, M. C.; Makarov, A. A. Orbitrap Mass

Spectrometry: Evolution and Applicability. *Compr. Anal. Chem.* **2016**, *71*, 3–18. https://doi.org/10.1016/bs.coac.2016.01.001.

(52) Eliuk, S.; Makarov, A. Evolution of Orbitrap Mass Spectrometry Instrumentation. *Annu. Rev. Anal. Chem.* **2015**, *8* (1), 61–80. https://doi.org/10.1146/annurev-anchem-071114-040325.

(53) Laskin, A.; Smith, J. S.; Laskin, J. Molecular Characterization of Nitrogen-Containing Organic Compounds in Biomass Burning Aerosols Using High-Resolution Mass Spectrometry. *Environ. Sci. Technol.* **2009**, *43* (10), 3764–3771. https://doi.org/10.1021/es803456n.

(54) Remucal, C. K.; Cory, R. M.; Sander, M.; McNeill, K. Low Molecular Weight Components in an Aquatic Humic Substance as Characterized by Membrane Dialysis and Orbitrap Mass Spectrometry. *Environ. Sci. Technol.* **2012**, *46* (17), 9350–9359. https://doi.org/10.1021/es302468q.

(55) Nguyen, T. B.; Laskin, J.; Laskin, A.; Nizkorodov, S. A. Nitrogen-Containing Organic Compounds and Oligomers in Secondary Organic Aerosol Formed by Photooxidation of Isoprene. *Environ. Sci. Technol.* **2011**, *45* (16), 6908–6918. https://doi.org/10.1021/es201611n.

(56) Graham, B.; Mayol-Bracero, O. L.; Guyon, P.; Roberts, G. C.; Decesari, S.; Cristina Facchini, M.; Artaxo, P.; Maenhaut, W.; Köll, P.; Andreae, M. O.; et al. Water-Soluble Organic Compounds in Biomass Burning Aerosols over Amazonia 1. Characterization by NMR and GC-MS. *J. Geophys. Res* **2002**, *107* (20), 8047. https://doi.org/10.1029/2001JD000336.

(57) de Souza, P. A.; Ponette-González, A. G.; de Mello, W. Z.; Weathers, K. C.; Santos, I. A.

Atmospheric Organic and Inorganic Nitrogen Inputs to Coastal Urban and Montane Atlantic Forest Sites in Southeastern Brazil. *Atmos. Res.* **2015**, *160*, 126–137. https://doi.org/10.1016/j.atmosres.2015.03.011.

(58) Voiland, A. Reflecting on a Tumultuous Amazon Fire Season https://earthobservatory.nasa.gov/images/146355/reflecting-on-a-tumultuous-amazon-fire-season (accessed Oct 28, 2020).

(59) Deforestation of Amazon rainforest accelerates amid COVID-19 pandemic - ABC News https://abcnews.go.com/International/deforestation-amazon-rainforest-accelerates-amid-covid-19-pandemic/story?id=70526188 (accessed Oct 28, 2020).

(60) Deforestation of the Amazon has soared under cover of the coronavirus https://www.nbcnews.com/science/environment/deforestation-amazon-has-soared-under-cover-coronavirus-n1204451 (accessed Oct 28, 2020).

(61) Nakada, L. Y. K.; Urban, R. C. COVID-19 Pandemic: Impacts on the Air Quality during the Partial Lockdown in São Paulo State, Brazil. *Sci. Total Environ.* **2020**, *730*, 139087. https://doi.org/10.1016/j.scitotenv.2020.139087.

(62) Statistics), I. (Brazilian I. of G. and. Estimativas da População | IBGE https://www.ibge.gov.br/estatisticas/sociais/populacao/9103-estimativas-de-populacao.html?=&t=o-que-e (accessed Nov 2, 2020).

(63) Coronavírus Brasil https://covid.saude.gov.br/ (accessed Feb 14, 2022).

(64) COVID-19 Community Mobility Reports https://www.google.com/covid19/mobility/ (accessed Mar 6, 2022).

(65) Coelho, C. H.; Allen, A. G.; Fornaro, A.; Orlando, E. A.; Grigoletto, T. L. B.; Campos, M. L. A. M. Wet Deposition of Major Ions in a Rural Area Impacted by Biomass Burning

Emissions. *Atmos. Environ.* **2011**, *45* (30), 5260–5265. https://doi.org/10.1016/j.atmosenv.2011.06.063.

(66) Avery, G. B.; Willey, J. D.; Kieber, R. J. Carbon Isotopic Characterization of Dissolved Organic Carbon in Rainwater: Terrestrial and Marine Influences. *Atmos. Environ.* **2006**, *40* (39), 7539–7545. https://doi.org/10.1016/J.ATMOSENV.2006.07.014.

(67) Ribeiro, F. A. D. L.; Ferreira, M. M. C.; Morano, S. C.; Da Silva, L. R.; Schneider, R. P. Planilha de Validação: Uma Nova Ferramenta Para Estimar Figuras de Mérito Na Validação de Métodos Analíticos Univariados. *Quim. Nova* **2008**, *31* (1), 164–171. https://doi.org/10.1590/S0100-40422008000100029.

(68) Crispim, C. P.; Nogueira, R. F. P.; Ometto, J. P.; Campos, M. L. A. M. Photo-Fenton Approach for the Determination of Organic Nitrogen in Rainwater. *Atmos. Environ.* **2018**, *191* (April), 525–531. https://doi.org/10.1016/j.atmosenv.2018.08.029.

(69) Kourtchev, I.; O'Connor, I. P.; Giorio, C.; Fuller, S. J.; Kristensen, K.; Maenhaut, W.; Wenger, J. C.; Sodeau, J. R.; Glasius, M.; Kalberer, M. Effects of Anthropogenic Emissions on the Molecular Composition of Urban Organic Aerosols: An Ultrahigh Resolution Mass Spectrometry Study. *Atmos. Environ.* **2014**, *89*, 525–532. https://doi.org/10.1016/j.atmosenv.2014.02.051.

(70) Cui, X.; Churchill, G. A. Statistical Tests for Differential Expression in CDNA Microarray Experiments. *Genome Biology*. BioMed Central March 17, 2003, p 210. https://doi.org/10.1186/gb-2003-4-4-210.

(71) Jolliffe, I. T. Principal Component Analysis. **2002**. https://doi.org/10.1007/B98835.

(72) US-EPA. EPA Positive M Atrix Factorization (PM F) 5 . 0 Fundamentals And. *Environ. Prot. Agency Off. Researc Dev. Publushing House Whashington, DC 20460* **2014**, 136.

(73) Miyazaki, Y.; Kawamura, K.; Sawano, M. Size Distributions of Organic Nitrogen and Carbon in Remote Marine Aerosols: Evidence of Marine Biological Origin Based on Their Isotopic Ratios. *Geophys. Res. Lett.* **2010**, *37* (6). https://doi.org/10.1029/2010GL042483.

(74) Hunt, A. P.; Parry, J. D.; Hamilton-Taylor, J. Further Evidence of Elemental Composition as an Indicator of the Bioavailability of Humic Substances to Bacteria. *Limnol. Oceanogr.* **2000**, *45* (1), 237–241. https://doi.org/10.4319/LO.2000.45.1.0237.

(75) Seitzinger, S. P.; Sanders, R. W.; Styles, R. Bioavailability of DON from Natural and Anthropogenic Sources to Estuarine Plankton. *Limnol. Oceanogr.* **2002**, *47* (2), 353–366. https://doi.org/10.4319/LO.2002.47.2.0353.

(76) Bao, H.; Yi, Y.; Wang, C.; Spencer, R. G. M.; Deng, X.; Guo, W. Dissolved Organic Matter in Coastal Rainwater: Concentration, Bioavailability and Depositional Flux to Seawater in Southeastern China. *Mar. Chem.* **2018**, *205*, 48–55. https://doi.org/10.1016/J.MARCHEM.2018.07.008.

(77) Yang, L.; Chen, W.; Zhuang, W. E.; Cheng, Q.; Li, W.; Wang, H.; Guo, W.; Chen, C. T. A.; Liu, M. Characterization and Bioavailability of Rainwater Dissolved Organic Matter at the Southeast Coast of China Using Absorption Spectroscopy and Fluorescence EEM-PARAFAC. *Estuar. Coast. Shelf Sci.* **2019**, *217*, 45–55. https://doi.org/10.1016/j.ecss.2018.11.002.

(78) Avery, G. B.; Willey, J. D.; Kieber, R. J.; Shank, G. C.; Whitehead, R. F.; Willey, J. D.; Kieber, R. J.; Shank, G. C.; Whitehead, R. F. Flux and Bioavailability of Cape Fear River and Rainwater Dissolved Organic Carbon to Long Bay, Southeastern United States. *Global Biogeochem. Cycles* **2003**, *17* (2), 1042. https://doi.org/10.1029/2002GB001964.

(79) Strauss, E. A.; Lamberti, G. A. Effect of Dissolved Organic Carbon Quality on Microbial Decomposition and Nitri®cation Rates in Stream Sediments.

(80) Chen, M.; Jaffé, R. Quantitative Assessment of Photo- and Bio-Reactivity of Chromophoric and Fluorescent Dissolved Organic Matter from Biomass and Soil Leachates and from Surface Waters in a Subtropical Wetland. *Biogeochemistry* **2016**, *129* (3), 273–289. https://doi.org/10.1007/S10533-016-0231-7/FIGURES/5.

(81) Giorgio, P. A. del; Davis, J. Patterns in Dissolved Organic Matter Lability and Consumption across Aquatic Ecosystems. *Aquat. Ecosyst.* **2003**, 399–424. https://doi.org/10.1016/B978-012256371-3/50018-4.

(82) Spencer, R. G. M.; Guo, W.; Raymond, P. A.; Dittmar, T.; Hood, E.; Fellman, J.; Stubbins, A. Source and Biolability of Ancient Dissolved Organic Matter in Glacier and Lake Ecosystems on the Tibetan Plateau. *Geochim. Cosmochim. Acta* **2014**, *142*, 64–74. https://doi.org/10.1016/J.GCA.2014.08.006.

(83) Noziè, B.; Córdova, A. A Kinetic and Mechanistic Study of the Amino Acid Catalyzed Aldol Condensation of Acetaldehyde in Aqueous and Salt Solutions. **2008**. https://doi.org/10.1021/jp7096845.

(84) Gorzelska, K.; Galloway, J. N.; Watterson, K.; Keene, W. C. Water-Soluble Primary Amine Compounds in Rural Continental Precipitation. *Atmos. Environ. Part A, Gen. Top.* **1992**, *26* (6), 1005–1018. https://doi.org/10.1016/0960-1686(92)90032-G.

(85) Zhang, Q.; Anastasio, C. Chemistry of Fog Waters in California's Central ValleyFPart 3: Concentrations and Speciation of Organic and Inorganic Nitrogen. *Atmos. Environ.* **2001**, *35*, 5629–5643.

(86) Ervens, B.; Volkamer, R. Glyoxal Processing by Aerosol Multiphase Chemistry: Towards

a Kinetic Modeling Framework of Secondary Organic Aerosol Formation in Aqueous Particles. *Atmos. Chem. Phys.* **2010**, *10* (17), 8219–8244. https://doi.org/10.5194/ACP-10-8219-2010.

(87) Bateman, A. P.; Nizkorodov, S. A.; Laskin, J.; Laskin, A. Photolytic Processing of Secondary Organic Aerosols Dissolved in Cloud Droplets. *Phys. Chem. Chem. Phys.* **2011**, *13* (26), 12199–12212. https://doi.org/10.1039/c1cp20526a.

(88) Coelho, C. H.; Francisco, J. G.; Nogueira, R. F. P.; Campos, M. L. A. M. Dissolved Organic Carbon in Rainwater from Areas Heavily Impacted by Sugar Cane Burning. *Atmos. Environ.* **2008**, *42* (30), 7115–7121. https://doi.org/10.1016/j.atmosenv.2008.05.072.

(89) Chen, S.; Xie, Q.; Su, S.; Wu, L.; Zhong, S.; Zhang, Z.; Ma, C.; Qi, Y.; Hu, W.; Deng, J.; et al. Source and Formation Process Impact the Chemodiversity of Rainwater Dissolved Organic Matter along the Yangtze River Basin in Summer. *Water Res.* **2021**, 118024. https://doi.org/10.1016/j.watres.2021.118024.

(90) Chen, Y.; Takeuchi, M.; Nah, T.; Xu, L.; Canagaratna, M. R.; Stark, H.; Baumann, K.; Canonaco, F.; Prevot, A. S. H.; Gregory Huey, L.; et al. Chemical Characterization of Secondary Organic Aerosol at a Rural Site in the Southeastern US: Insights from Simultaneous High-Resolution Time-of-Flight Aerosol Mass Spectrometer (HR-ToF-AMS) and FIGAERO Chemical Ionization Mass Spectrometer (CIMS) Measurements. *Atmos. Chem. Phys.* **2020**, *20* (14), 8421–8440. https://doi.org/10.5194/ACP-20-8421-2020.

(91) Roberts, J. M. The Atmospheric Chemistry of Organic Nitrates. *Atmospheric Environment Part A, General Topics*. Elsevier January 1, 1990, pp 243–287.

https://doi.org/10.1016/0960-1686(90)90108-Y.

(92) Zeisel, S. H. A Brief History of Choline. *Ann. Nutr. Metab.* **2012**, *61* (3), 254–258. https://doi.org/10.1159/000343120.

(93) Cox, R. A.; Hoppel, C. L. Biosynthesis of Carnitine and 4-N-Trimethylaminobutyrate from 6-N-Trimethyl-Lysine. *Biochem. J.* **1973**, *136* (4), 1083. https://doi.org/10.1042/BJ1361083.

(94) Liu, J.; Chu, B.; Chen, T.; Zhong, C.; Liu, C.; Ma, Q.; Ma, J.; Zhang, P.; He, H. Secondary Organic Aerosol Formation Potential from Ambient Air in Beijing: Effects of Atmospheric Oxidation Capacity at Different Pollution Levels. *Cite This Environ. Sci. Technol* **2021**, *55*, 4572. https://doi.org/10.1021/acs.est.1c00890.

(95) Wang, W.; Zhang, Y.; Cao, G.; Song, Y.; Zhang, J.; Li, R.; Zhao, L.; Dong, C.; Cai, Z. Influence of COVID-19 Lockdown on the Variation of Organic Aerosols: Insight into Its Molecular Composition and Oxidative Potential. *Environ. Res.* **2021**, 112597. https://doi.org/10.1016/j.envres.2021.112597.

(96) Siciliano, B.; Dantas, G.; da Silva, C. M.; Arbilla, G. Increased Ozone Levels during the COVID-19 Lockdown: Analysis for the City of Rio de Janeiro, Brazil. *Sci. Total Environ.* **2020**, *737*, 139765. https://doi.org/10.1016/J.SCITOTENV.2020.139765.

(97) Wagner, S.; Dittmar, T.; Jaffé, R. Molecular Characterization of Dissolved Black Nitrogen via Electrospray Ionization Fourier Transform Ion Cyclotron Resonance Mass Spectrometry. *Org. Geochem.* **2015**, *79*, 21–30. https://doi.org/10.1016/j.orggeochem.2014.12.002.

(98) Decesari, S.; Facchini, M. C.; Matta, E.; Mircea, M.; Fuzzi, S.; Chughtai, A. R.; Smith, D. M. Water Soluble Organic Compounds Formed by Oxidation of Soot. *Atmos. Environ.*

2002, *36* (11), 1827–1832. https://doi.org/10.1016/S1352-2310(02)00141-3.

(99) Kamegawa, K.; Nishikubo, K.; Kodama, M.; Adachi, Y.; Yoshida, H. Oxidative Degradation of Carbon Blacks with Nitric Acid: II. Formation of Water-Soluble Polynuclear Aromatic Compounds. *Carbon N. Y.* **2002**, *40* (9), 1447–1455. https://doi.org/10.1016/S0008-6223(01)00310-4.

(100) Lundqvist, T.; Schneider, G. Crystal Structure of the Ternary Complex of Ribulose-1,5-Bisphosphate Carboxylase, Magnesium(II) and Activator Carbon Dioxide at 2.3-.ANG. Resolution. *Biochemistry* **2002**, *30* (4), 904–908. https://doi.org/10.1021/BI00218A004.

(101) Rutz, A.; Bisson, J.; Allard, P.-M. The LOTUS Initiative for Open Natural Products Research: Frozen Dataset Union Wikidata (with Metadata). **2022**. https://doi.org/10.5281/ZENODO.6378204.

(102) Purwanto, Y.; Munawaroh, E.; Penelitian, P.; Dan, B.-L.; Kebun, P.; Bogor-Lipi, R. ETNOBOTANI JENIS-JENIS PANDANACEAE SEBAGAI BAHAN PANGAN DI INDONESIA.

(103) Ebrahimpoor, M.; Goeman, J. J. Inflated False Discovery Rate Due to Volcano Plots: Problem and Solutions. *Brief. Bioinform.* **2021**, *22* (5), 1–12. https://doi.org/10.1093/BIB/BBAB053.

(104) Chebbi, A.; Carlier, P. Carboxylic Acids in the Troposphere, Occurrence, Sources, and Sinks: A Review. *Atmos. Environ.* **1996**, *30* (24), 4233–4249. https://doi.org/10.1016/1352-2310(96)00102-1.

(105) Fornaro, A.; Gutz, I. G. R. Wet Deposition and Related Atmospheric Chemistry in the São Paulo Metropolis, Brazil: Part 2—Contribution of Formic and Acetic Acids. *Atmos. Environ.* **2003**, *37* (1), 117–128. https://doi.org/10.1016/S1352-2310(02)00885-3.

APPENDIX A.

SUPPLEMENTAL FIGURES AND TABLES

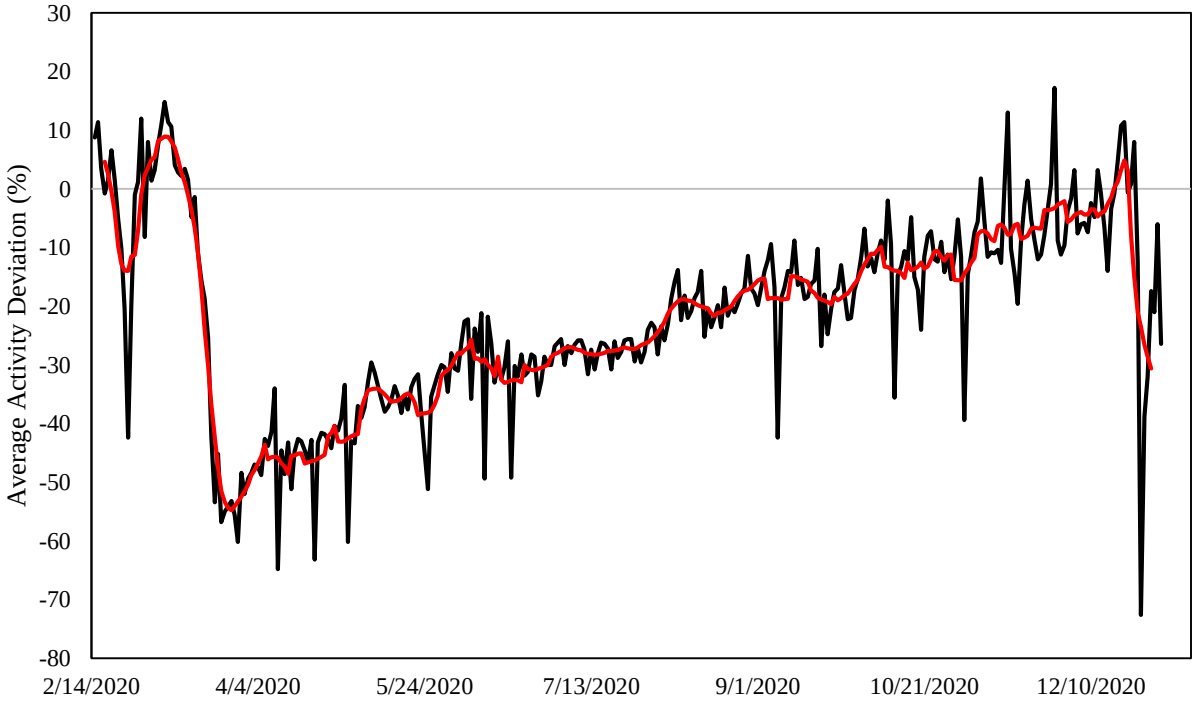

Figure A1. Average activity deviation of retail, transit, and workplace areas in Ribeirão Preto relative to the two months prior to February 16, 2020. Red line represents rolling seven-day average. Data retrieved from the Google COVID-19 Community Mobility Reports.[64]

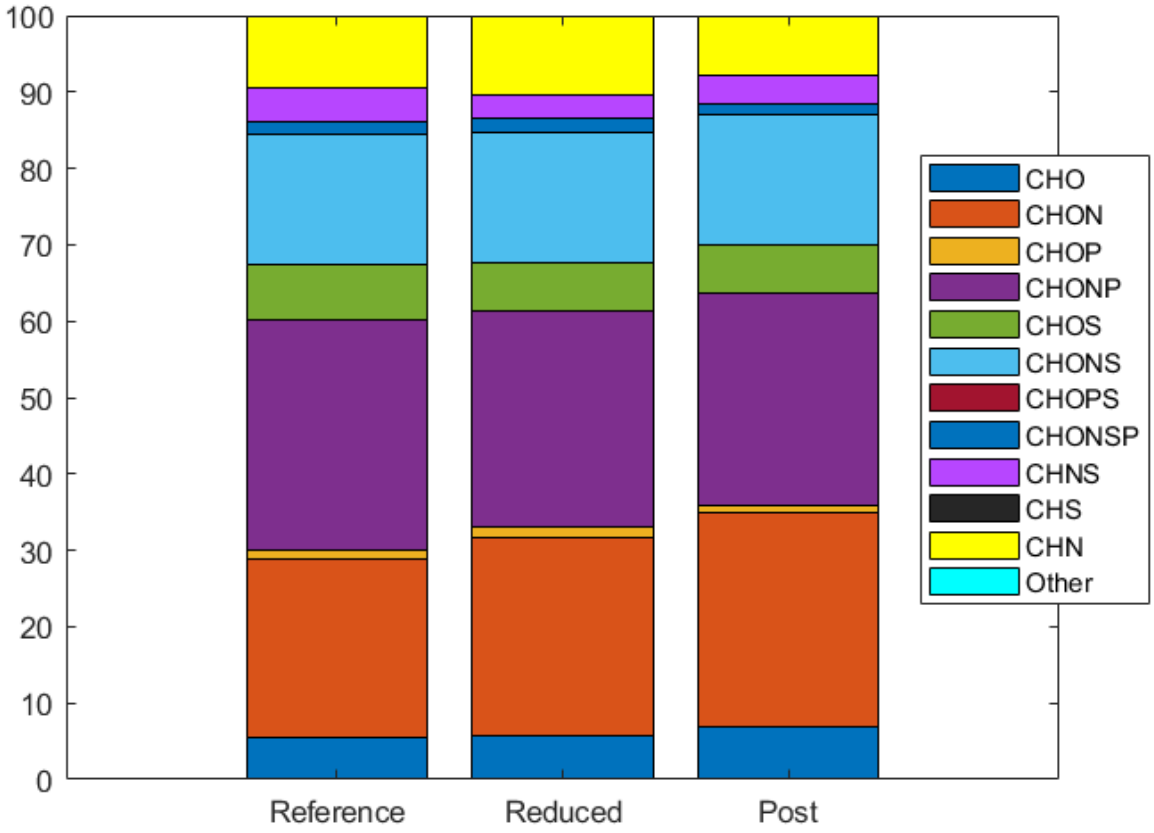

Figure A2. Percent composition of sample grouping

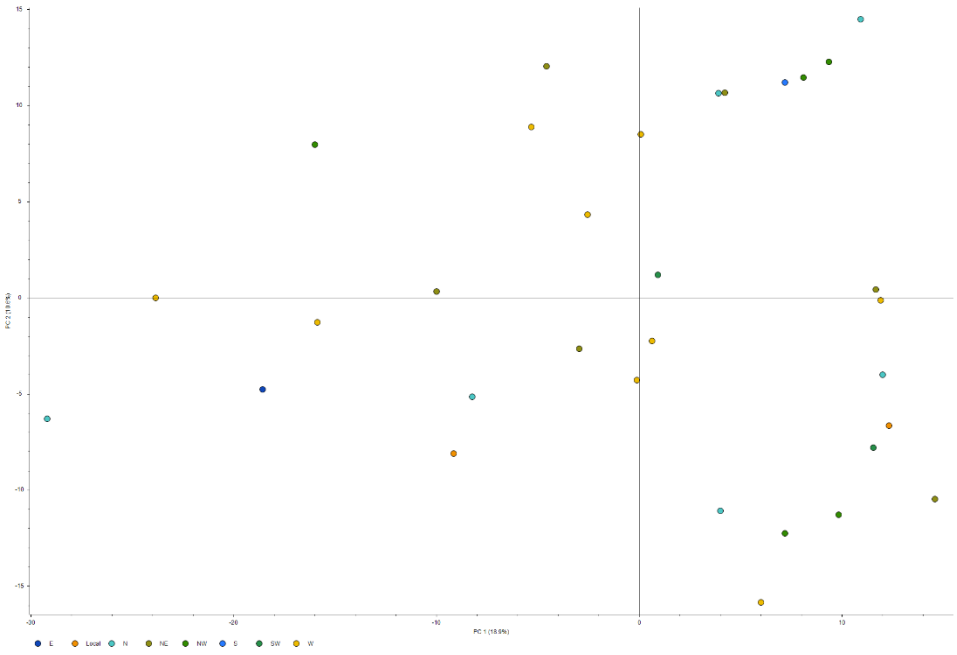

Figure A3. Organic Character PCA plot of all samples, labeled by HYSPLIT backtrajectory grouping.

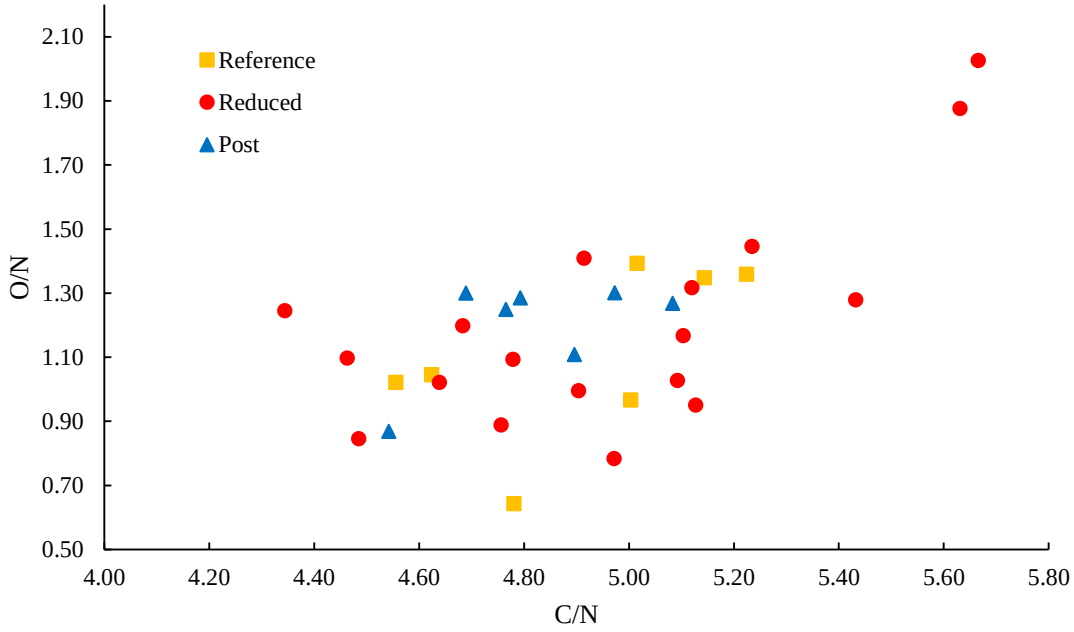

Figure A4. Atomic ratio analysis for nitrogen

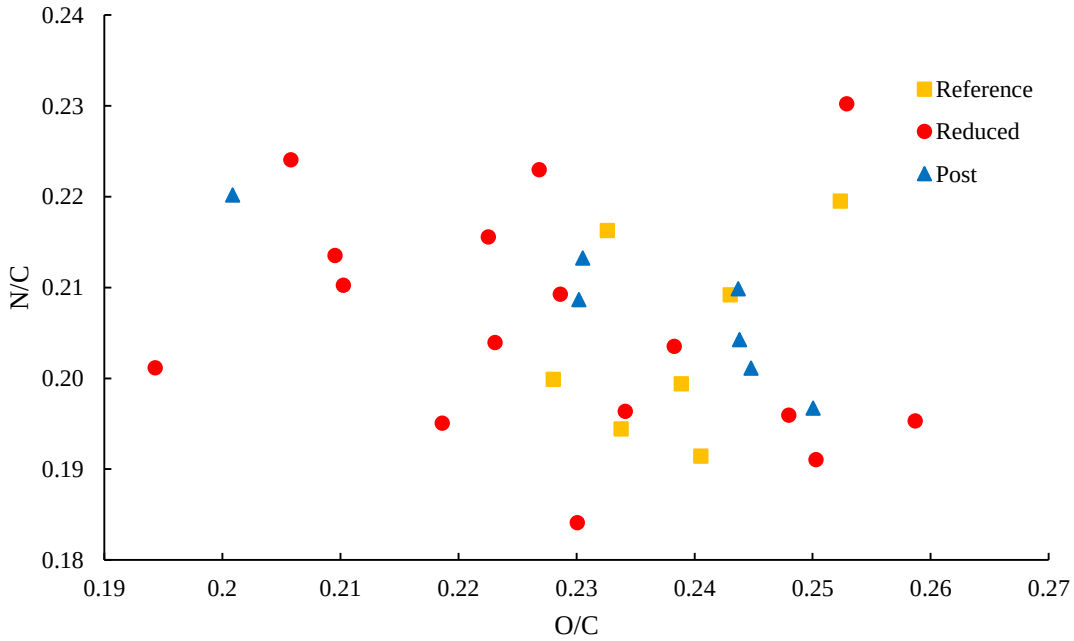

Figure A5.

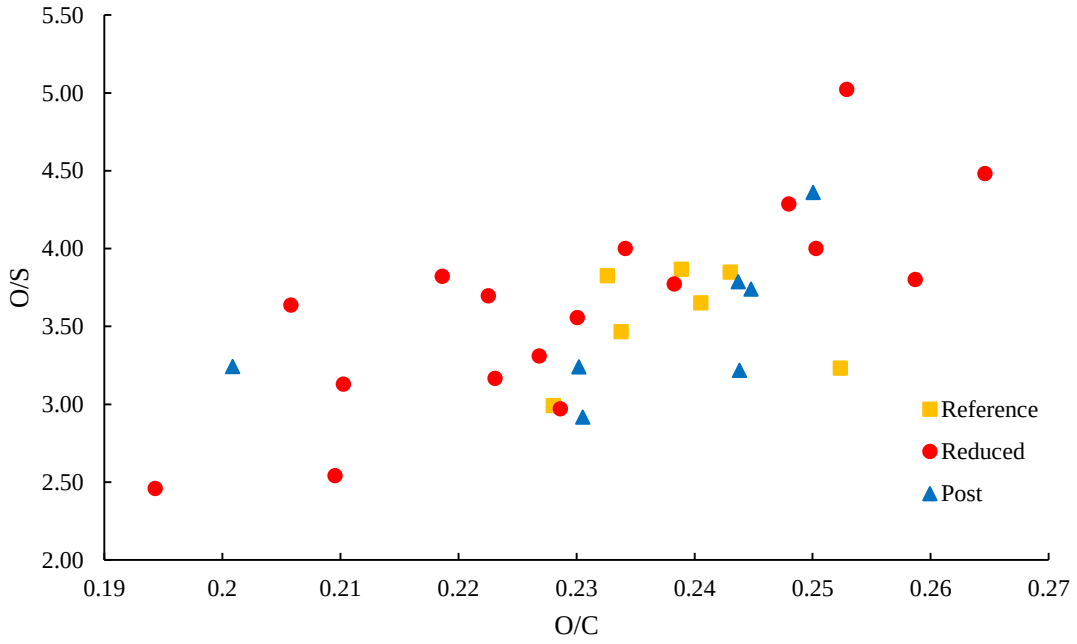

Figure A6.

Predicted Compound	**Predicted Formula**	**Calculated MW**	**m/z**
L-Phenylalanine	C9 H11 N O2	165.0789	166.0862
		217.9427	109.9786
	C20 H39 N O7	405.2724	406.2797
THIOQUINOX	C9 H4 N2 S3	235.9532	118.9839
	C10 H N3 O4 S	258.9691	130.4918
O-ureido-D-serine	C4 H9 N3 O4	163.0597	82.53715
		145.0225	146.0298
		176.9679	159.9646
		181.895	223.9288
Phenethylamine	C8 H11 N	121.0891	122.0964
		145.0225	128.0192
	C8 H7 O4 P	198.0079	100.0112
N-{4-[(2R,3R)-3-(Hydroxymethyl)-4-isobutyl-5-oxo-2-morpholinyl]phenyl}cyclobutanecarboxamide	C20 H28 N2 O4	382.1965	383.2038
toluidine	C7 H9 N	107.0735	108.0808
SJ4950000	C6 H7 N O	109.0528	110.0601
		253.9418	254.9491
		117.9765	118.9839

	C9 H7 N O2 S2	224.9917	225.999
	C8 H7 O4 P	198.0079	100.0112
	C4 H5 N O	83.03715	101.071
AE4025000	C8 H9 N O2	151.0632	152.0706
(2E)-2-Bromo-4-oxo-2-hexenedioic acid	C6 H5 Br O5	235.9312	236.9385
		147.3233	148.3306
		303.8884	304.8957
phendimetrazine	C12 H17 N O	191.1309	192.1382
		100.977	101.9842
	C3 H4 N3 O9 P	256.9686	129.4915
		227.9368	135.489
		153.9001	154.9074
		141.9691	184.0029
MFCD00130070	C10 H21 N O	171.1622	172.1695
		172.0243	87.01944
adrenaline	C9 H13 N O3	183.0895	166.0862
		233.9526	117.9836
(3E)-4-(4-Hydroxy-3,5-dimethoxyphenyl)-3-buten-2-one	C12 H14 O4	222.0891	205.0858
	C16 H37 N8 P	372.2873	373.2945
		333.9074	334.9147
		208.9696	105.4921
	C10 H22 N2	170.1782	171.1855
		108.4717	109.4789
		180.1225	181.1298
	C10 H N O3	182.9956	184.0029
	C3 H2 O9 S	213.942	107.9783
		106.4687	89.46536
	C7 H2 N3 O6 P	254.9683	128.4914
		268.9634	135.489
		200.9683	201.9756
		97.46336	98.47065
		381.197	382.2042
L-threo-3-Phenylserine	C9 H11 N O3	181.0738	182.0811
		212.9373	107.4759
2-((4-Nitrophenoxy)methyl)oxirane	C9 H9 N O4	195.053	196.0603
		179.8943	180.9016
		344.838	173.4263
2-Methylhippuric Acid	C10 H11 N O3	193.0738	194.0811
5-acetyl-2,6-dimethyl-1,2,3,4-tetrahydropyridin-4-one	C9 H13 N O2	167.0945	168.1018
Tyramine	C8 H11 N O	137.084	138.0913
	C12 H27 N	185.2143	186.2216

Umbelliferone	C9 H6 O3	162.0316	163.0389
		126.9818	127.9891
	C4 H9 N8 O5 P	280.0436	281.0508
		255.9696	128.9921
Phenethylamine	C8 H11 N	121.0891	122.0964
	C17 H31 N O6	345.2149	346.2221
2-Cyclopenten-1-one, 4-hydroxy-3-methyl-2-(2-pentenyl)-	C11 H16 O2	180.115	181.1222
		356.1398	357.1471
	C3 H4 O10 S	231.9526	116.9836
		232.9537	117.4841
		220.9209	221.9282
Thymine	C5 H6 N2 O2	126.0429	127.0502
		344.84	173.4273
Pyridoxal	C8 H9 N O3	167.0581	168.0654
		113.4901	114.4974
		257.892	258.8993
	C17 H31 N O6	345.2148	346.2221
	C10 H23 N7 O6	337.1714	338.1786
		92.97685	93.98413
SJ6078000	C7 H9 N O	123.0684	124.0757
(4S)-6-Methyl-2-oxa-6-azatricyclo[3.3.1.0~3,7~]nonan-4-ol	C8 H13 N O2	155.0946	138.0913
		218.9211	219.9284
		122.9331	263.8993
		177.8942	178.9015
		262.8921	263.8994
	C16 H24 N P	261.1647	262.172
Propoxur	C11 H15 N O3	209.1051	210.1123
N-acetyldopamine	C10 H13 N O3	195.0894	196.0967
(+/-)-Metanephrine	C10 H15 N O3	197.1051	198.1124
		390.101	391.1083
	C16 H33 N O2	271.251	272.2582
5-Imino-L-norvaline	C5 H10 N2 O2	130.0742	131.0815
O-propenoyl-D-carnitine	C10 H17 N O4	215.1157	216.1229
		178.8954	220.9293
		258.9082	259.9154
		235.901	236.9083
		311.8527	312.86
		236.9173	237.9246
		104.4848	105.4921
		151.8996	152.9067

Clomazone	C12 H14 Cl N O2	239.0712	240.0785
		231.0181	116.5163
Furfural	C5 H4 O2	96.02117	97.02844
		279.9382	280.9455
		180.8957	222.9295
propionylcarnitine	C10 H19 N O4	217.1313	218.1386
	C2 H5 N3 O6	167.0181	168.0253
		240.932	241.9393
		253.9638	127.9892
		159.9796	160.9869
		153.1113	154.1186
		134.4817	135.4889
QV1MVO1R	C10 H11 N O4	209.0687	210.0759
		261.9055	262.9128
Methyldopa	C10 H13 N O4	211.0844	212.0917
		294.1425	295.1498
		121.9172	122.9245
	C21 H42 N3 O P S	415.2778	416.2851
		255.8913	256.8985
		138.4899	139.4971
		207.9543	208.9616
1-Indolizidinone	C8 H13 N O	139.0996	140.1069
		221.9221	222.9293
		196.9936	198.0009
		127.4843	128.4916
		333.8681	334.8754
methyprylon	C10 H17 N O2	183.1258	184.1331
		128.9854	129.9922
1640340	C10 H17 N O3	199.1208	200.1281

Table A1. Down-regulated species from Figure 10, i.e. species significant to Reduced activity samples against Reference period samples

Predicted Compound	Predicted Formula	Calculated MW	m/z
Phosphoric acid	H3 O4 P	97.97694	98.98421
		466.7934	467.8007
Choline	C5 H13 N O	103.0997	104.107
		466.7937	467.8009
		511.8148	494.8113
		448.783	490.8168

	C7 H10 N3 O P	183.0565	184.0637
		489.8096	490.8169
		494.7884	495.7956
SL3675000	C18 H30 O	262.2295	280.2634
	C6 H4 N10	216.0623	217.0695
	C11 H2 N O8 P S	338.9239	170.4693
Linoleamide	C18 H33 N O	279.2561	280.2633
		219.8583	220.8656
		203.9595	204.9667
		227.9243	494.8113
		293.8585	316.8477
		493.8041	494.8114
		466.7938	467.8011
		493.804	494.8113
		494.7885	495.7958
		235.1603	236.1676
Chloropicrin	C Cl3 N O2	162.8998	163.9071
		119.0946	120.1019
		466.7935	467.8008
cyclohexenone	C6 H8 O	96.05754	138.0913
		222.0788	223.086
		297.8974	149.956
		466.7936	467.8009
		466.7935	467.8008
		288.1613	289.1686
		493.8037	494.811
		466.7934	467.8007
		414.8249	208.4197
		489.8095	490.8167
		265.8754	266.8835
		466.7935	467.8008
		466.794	467.8013
		464.7985	465.8058
		509.8057	510.813
		489.8097	490.817
BX2625000	C6 H5 Cl2 N	160.9798	161.9871
		347.9385	174.9765
		93.49661	94.50394
		193.9306	194.9379
		136.0115	178.0453
		200.9853	201.9926
		494.7885	495.7958
		494.7884	495.7957

		489.8093	490.8166
		120.9507	121.9579
		494.7884	495.7957
		493.8039	494.8111
		494.7882	495.7954
D-PANTOTHENIC ACID	C9 H17 N O5	219.1106	220.1178
		126.0924	127.0997
		296.9562	297.9634

Table A2. Up-regulated species from Figure 10, i.e. species significant to Reference activity samples against Reduced period samples

Predicted Compound	**Predicted Formula**	**Calculated MW**	**m/z**
Phosphoric acid	H3 O4 P	97.97694	98.98421
		466.7934	467.8007
		466.7936	467.8009
	C5 H2 N2 O4 S	185.9736	186.9808
		538.1212	561.1104
		120.9589	121.9662
		466.7933	467.8006
Choline	C5 H13 N O	103.0997	104.107
		466.7937	467.8009
		511.8148	494.8113
		448.783	490.8168
	C7 H10 N3 O P	183.0565	184.0637
4,5-dihydroxy-6-(hydroxymethyl)-2-[2,4,6-trihydroxy-3-(4-hydroxybenzoyl)phenyl]oxan-3-yl 3,4,5-trihydroxybenzoate	C26 H24 O14	560.1031	561.1104
		489.8099	490.8172
		489.8096	490.8169
	C24 H31 N O2 S	397.2074	398.2147
		200.9853	201.9926
		494.7887	495.796
		494.7884	495.7956
D-Carnitine	C7 H15 N O3	161.1051	162.1124
	C10 H21 N O5	235.1418	236.1491
		473.3409	474.3482
	C11 H2 N O8 P S	338.9239	170.4693
		219.8583	220.8656
		203.9595	204.9667
		227.9243	494.8113

		293.8585	316.8477
	C11 H2 N O8 P S	338.924	170.4693
		466.7938	467.8011
		493.804	494.8113
		494.7885	495.7958
		235.1603	236.1676
		564.7262	283.3704
	C8 H5 N6 O3 P	264.0157	265.023
		635.1226	636.1298
	C7 H15 N O4 S	209.0721	210.0793
Chloropicrin	C Cl3 N O2	162.8998	163.9071
	C4 H N3 O7 S	234.954	235.9613
		119.0946	120.1019
		466.7935	467.8008
cyclohexenone	C6 H8 O	96.05754	138.0913
		297.8974	149.956
		466.7936	467.8009
		466.7935	467.8008
	C7 H7 N3 O6 S	261.006	262.0133
		466.7934	467.8007
		414.8249	208.4197
L-alpha-Glycerylphosphorylcholine	C8 H20 N O6 P	257.1027	258.11
		489.8095	490.8167
		265.8754	266.8835
		466.7935	467.8008
		466.794	467.8013
	C8 H2 N3 O P	186.9933	94.50393
L-(+)-Leucine	C6 H13 N O2	131.0946	132.1019
		464.7985	465.8058
		489.8097	490.817
2-(4-Methylthiazol-5-yl)ethyl butyrate	C10 H15 N O2 S	213.0822	214.0895
		93.49661	94.50394
	C5 H7 N6 O9 P	326.0006	327.0078
		136.0115	178.0453
		184.9932	93.50388
Hopantenic acid	C10 H19 N O5	233.1262	234.1335
		200.9853	201.9926
		466.7935	467.8008
		494.7885	495.7958
Benzophenone	C13 H10 O	182.0731	183.0803
		494.7884	495.7957
		489.8093	490.8166
		175.9996	177.0069

		149.4489	150.4562
		120.9507	121.9579
		494.7884	495.7957
		493.8039	494.8111
		371.2516	372.2588
		207.9825	208.9897
		234.954	235.9612
g-Butyrobetaine	C7 H15 N O2	145.1102	146.1175
		355.2568	356.264
		494.7882	495.7954
D-PANTOTHENIC ACID	C9 H17 N O5	219.1106	220.1178
		341.2411	342.2483
		297.2149	298.2222
		102.9483	103.9556
		296.9562	297.9634
4-Nitrosobiphenyl	C12 H9 N O	183.0683	184.0756
		236.1452	237.1525

Table A3. Up-regulated species from Figure 11, i.e. species significant to Reference activity samples against Post-baseline period samples

Predicted Compound	**Predicted Formula**	**Calculated MW**	**m/z**
	C44 H70 N O4 P	707.504	708.5113
	C9 H19 N O	157.1466	158.1539
	C39 H61 N2 O6 P	684.428	685.4353
		217.9427	109.9786
	C20 H39 N O7	405.2724	406.2797
THIOQUINOX	C9 H4 N2 S3	235.9532	118.9839
	C10 H N3 O4 S	258.9691	130.4918
	C36 H63 N5 S	597.4815	598.4887
	C18 H32 O7	360.2146	361.222
	C40 H65 N2 O P S2	684.4282	685.4354
5-(1,4-Dihydroxycyclohexyl)-1,2-dihydroxy-3-[(2E,4E,6E,8R,10R)-6,8,10-trimethyl-2,4,6-dodecatrienoyl]-4(1H)-pyridinone	C26 H37 N O6	459.2618	460.269
		176.9679	159.9646
		181.895	223.9288
Phenethylamine	C8 H11 N	121.0891	122.0964
	C8 H7 O4 P	198.0079	100.0112

7-(1-Ethoxyethoxy)-4,10-dimethyl-3,5,9,11-tetraoxatridecane	C15 H32 O6	308.2196	309.2269
	C8 H7 O4 P	198.0079	100.0112
N-{4-[(2R,3R)-3-(Hydroxymethyl)-4-isobutyl-5-oxo-2-morpholinyl]phenyl}cyclobutanecarboxamide	C20 H28 N2 O4	382.1965	383.2038
Methyl palmitate	C17 H34 O2	287.2822	288.2895
	C19 H45 N8 O3 P	464.3345	465.3418
		253.9418	254.9491
	C21 H44 O8	424.3033	447.2925
	C21 H42 O7	406.2927	424.3266
		117.9765	118.9839
		172.421	173.4282
	C28 H66 N9 O6 P	655.4868	656.4941
	C5 H2 N5 O P	178.9995	90.50701
	C8 H7 O4 P	198.0079	100.0112
	C30 H58 N3 O P S	539.4029	540.4102
	C24 H51 N O8	481.3611	482.3684
(2E)-2-Bromo-4-oxo-2-hexenedioic acid	C6 H5 Br O5	235.9312	236.9385
		441.3297	442.337
	C12 H26 O5	250.1779	251.1852
	C32 H76 N10 O11	776.5689	777.5762
	C22 H51 N8 O4 P	522.3763	523.3836
		169.9503	170.9576
	C24 H50 O9	482.3451	500.3789
		89.49972	90.507
		353.2775	354.2848
	C18 H38 O7	366.2615	367.2687
Bis(4-ethylbenzylidene)sorbitol	C24 H30 O6	414.2039	415.2112
	C39 H64 O6 S	660.4421	661.4494
		156.9812	100.0112
Methyl palmitate	C17 H34 O2	287.2822	288.2895
	C30 H66 N6 O4 S2	638.4598	656.4937
	C22 H53 N8 O5 P	540.3868	541.3942
	C3 H4 N3 O9 P	256.9686	129.4915
		227.9368	135.489
		147.0201	185.9833
		115.9546	116.9619
		157.0606	158.0679
	C27 H52 N10 O4	580.4181	598.4519
		153.9001	154.9074
	C16 H37 N8 P	372.2873	373.2945
Glycerol 5-hydroxydodecanoate	C15 H30 O5	290.2092	291.2164

	C8 H5 O3 P	179.9973	91.00593
	C30 H60 N3 O2 P S	557.4134	558.4207
		171.0597	172.067
		143.9495	185.9833
tranexamic acid	C8 H15 N O2	157.1102	158.1175
		208.9696	105.4921
		295.2357	296.2429
		108.4717	109.4789
		588.3844	589.3917
		115.9547	116.962
		143.9495	185.9833
		383.2881	384.2954
	C19 H38 N6 O6	446.2851	447.2924
	C25 H48 N6 O7	544.3584	545.3657
	C3 H2 O9 S	213.942	107.9783
		554.4587	555.4659
	C15 H33 N O	243.2561	244.2634
	C30 H46 O3 S	486.3165	487.3237
	C18 H36 O6	348.251	349.2582
		106.4687	89.46536
		598.4847	599.4919
	C15 H33 N O	243.2561	244.2634
	C7 H2 N3 O6 P	254.9683	128.4914
	C28 H58 N10 S2	598.4286	599.4359
		268.9634	135.489
		411.3192	412.3265
		200.9683	201.9756
benzyl N-(1-{[(3,4-dimethoxyphenethyl)amino]carbonyl}-2-methylpropyl)carbamate	C23 H30 N2 O5	431.2304	432.2377
NP-020014	C15 H26 O3	254.188	255.1953
		97.46336	98.47065
		381.197	382.2042
	C21 H43 N4 O2 P S	446.2852	447.2925
	C16 H30 N6 O4	370.2329	371.2402
	C25 H60 N9 O5 P	597.4445	598.4518
AJ4900000	C2 H4 O5 S	139.9782	162.9673
13-oxotrideca-9,11-dienoic acid	C13 H20 O3	224.1411	225.1484
Methyl palmitate	C17 H34 O2	287.2823	288.2895
		212.9373	107.4759
	C25 H62 N9 O6 P	615.4553	616.4625
		275.8894	276.8966
		339.9244	340.9317

		117.4769	118.4842
	C18 H39 N O6	365.2775	366.2848
		179.8943	180.9016
		344.838	173.4263
	C17 H37 N O5	335.267	336.2742
	C21 H45 N O8	439.3142	440.3215
		184.976	185.9833
		98.52392	99.53119
		482.3645	483.3718
		383.288	384.2953
	C12 H27 N	185.2143	186.2216
		126.9818	127.9891
	C4 H9 N8 O5 P	280.0436	281.0508
	C26 H52 N3 P S	469.361	470.3683
		255.9696	128.9921
		356.1398	357.1471
	C3 H4 O10 S	231.9526	116.9836
		232.9537	117.4841
Diethanolamine	C4 H11 N O2	105.079	106.0863
		133.9652	116.9619
dihydromethanophenazine	C37 H52 N2 O	540.4061	541.4133
	C28 H49 N6 P	500.375	501.3822
		220.9209	221.9282
	C28 H51 N8 P S	562.3689	563.3762
	C38 H67 N5 O3 S	673.4967	674.504
		344.84	173.4273
	C14 H28 N8 O6 S	436.1859	437.1932
	C23 H49 N O7	451.3508	452.3581
		113.4901	114.4974
		482.3645	483.3718
		598.4479	599.4552
	C10 H23 N7 O6	337.1714	338.1786
	C17 H35 N O2	285.2666	286.2739
		206.9779	207.9851
	C18 H39 N O7	381.2724	382.2797
		218.9211	219.9284
		122.9331	263.8993
		177.8942	178.9015
		262.8921	263.8994
	C16 H24 N P	261.1647	262.172
	C30 H59 N2 O5 P	558.4169	559.4242
	C24 H34 O2 S	386.2278	387.2351
	C5 H7 N9 O9	337.0373	338.0446

	C27 H58 N2 O12	602.3998	603.4071
	C29 H47 N5 S	497.3561	498.3634
	C16 H33 N O2	271.251	272.2582
	C13 H24 N6 O4	328.186	329.1932
		178.8954	220.9293
		161.96	144.9568
		266.9627	134.4886
		311.8527	312.86
		236.9173	237.9246
	C14 H31 N O4	277.2252	278.2324
	C24 H60 N10 O8	616.4584	617.4657
	C22 H54 N9 O5 P	555.3977	556.405
	C17 H37 N O6	351.2619	352.2692
		104.4848	105.4921
		151.8996	152.9067
	C28 H56 N6 O9	620.4103	621.4176
		380.8618	381.869
		309.9054	310.9127
		233.9526	117.9836
		231.0181	116.5163
		189.9914	116.5163
		279.9382	280.9455
		174.9472	175.9545
	C39 H61 N5 O2 S	663.4551	664.4623
		367.265	368.2723
		180.8957	222.9295
		393.3088	394.316
		240.932	241.9393
		253.9638	127.9892
	C29 H58 N3 O P S	527.4028	528.4101
		429.2782	430.2855
		407.9118	408.919
		94.99574	96.00304
6,8-Dimethyl-6,7,8,9-tetradehydroergoline	C16 H17 N2	237.1382	238.1455
		153.1113	154.1186
		134.4817	135.4889
	C28 H45 N5 S	483.3403	484.3476
4232620	C14 H28 O6	292.1884	293.1956
	C21 H40 N10 O2	464.3342	465.3415
	C30 H61 N O10	595.4292	596.4365
		354.2808	355.2881
		122.9737	123.981

	C42 H69 N9 S	731.5391	732.5464
		367.2649	368.2722
		312.8744	313.8817
	C21 H44 O8	424.3034	425.3107
	C13 H29 N4 O2 P S	336.1749	337.1822
	C20 H50 N9 O3 P	495.3763	496.3836
	C19 H36 N6 O6	444.2696	445.2769
	C23 H44 N3 P S	425.2987	426.306
	C34 H47 N3 O3	545.3618	546.3691
	C10 H20 N6 O3	272.16	273.1672
	C15 H33 N O6	323.2306	324.2379
	C22 H47 N O9	469.3246	470.3319
		138.4899	139.4971
		354.2809	355.2882
		207.9543	208.9616
1-Indolizidinone	C8 H13 N O	139.0996	140.1069
		221.9221	222.9293
		196.9936	198.0009
		127.4843	128.4916
	C24 H47 N4 O3 P S	502.3116	503.3189
	C32 H64 N3 O2 P S	585.4447	586.452
	C41 H70 N3 O3 P	683.5167	684.5239
	C29 H58 N4 O4 S	558.4169	559.4242
	C10 H18 N6 O2	254.1493	255.1566
	C41 H63 N2 O4 P	678.4528	679.46
(2E,6Z)-N-Cyclopropyl-2,6-nonadienamide	C12 H19 N O	193.1465	194.1538
	C31 H62 N6 O10	678.4519	679.4592
	C21 H52 N9 O3 P	509.3927	510.4
		500.3749	501.3822
		128.9854	129.9922
	C19 H41 N O8	411.2828	412.2901
	C16 H35 N O6	337.2462	338.2535
	C27 H55 N O9	537.3873	538.3946
		383.2882	384.2954
		479.3454	480.3527
	C23 H49 N O8	467.3454	468.3527
	C38 H67 N5 O3 S	673.4971	674.5043
	C21 H43 N O7	421.3038	422.311
	C10 H18 N6 O3	270.1443	271.1516
		527.3669	528.3742

Table A4. Down-regulated species from Figure 11, i.e. species significant to Post-baseline activity samples against Reference period samples

Predicted Compound	Predicted Formula	Calculated MW	m/z
	C44 H70 N O4 P	707.504	708.5113
	C9 H19 N O	157.1466	158.1539
	C39 H61 N2 O6 P	684.428	685.4353
5-Methoxybenzimidazole	C8 H8 N2 O	148.0632	149.0704
Medronic Acid	C H6 O6 P2	175.9645	176.9718
		158.9617	159.969
	C40 H65 N2 O P S2	684.4282	685.4354
	C42 H66 N O4 P	679.4727	680.4799
5-(1,4-Dihydroxycyclohexyl)-1,2-dihydroxy-3-[(2E,4E,6E,8R,10R)-6,8,10-trimethyl-2,4,6-dodecatrienoyl]-4(1H)-pyridinone	C26 H37 N O6	459.2618	460.269
		99.05589	100.0632
7-(1-Ethoxyethoxy)-4,10-dimethyl-3,5,9,11-tetraoxatridecane	C15 H32 O6	308.2196	309.2269
Medronic Acid	C H6 O6 P2	175.9645	176.9718
	C8 H7 O4 P	198.0079	100.0112
Methyl palmitate	C17 H34 O2	287.2822	288.2895
	C19 H45 N8 O3 P	464.3345	465.3418
		253.9418	254.9491
	C21 H44 O8	424.3033	447.2925
	C21 H42 O7	406.2927	424.3266
		172.421	173.4282
	C28 H66 N9 O6 P	655.4868	656.4941
	C30 H58 N3 O P S	539.4029	540.4102
	C24 H51 N O8	481.3611	482.3684
		441.3297	442.337
	C12 H26 O5	250.1779	251.1852
	C22 H51 N8 O4 P	522.3763	523.3836
	C24 H50 O9	482.3451	500.3789
		353.2775	354.2848
	C18 H38 O7	366.2615	367.2687
		136.98	159.969
Bis(4-ethylbenzylidene)sorbitol	C24 H30 O6	414.2039	415.2112
	C39 H64 O6 S	660.4421	661.4494
		156.9812	100.0112
Methyl palmitate	C17 H34 O2	287.2822	288.2895
	C30 H66 N6 O4 S2	638.4598	656.4937
	C22 H53 N8 O5 P	540.3868	541.3942

Linoleamide	C18 H33 N O	279.2561	280.2633
		157.0606	158.0679
	C27 H52 N10 O4	580.4181	598.4519
Glycerol 5-hydroxydodecanoate	C15 H30 O5	290.2092	291.2164
	C3 H N2 O3 P S	175.9448	176.9521
	C30 H60 N3 O2 P S	557.4134	558.4207
		295.2357	296.2429
		143.9495	185.9833
		383.2881	384.2954
	C19 H38 N6 O6	446.2851	447.2924
	C25 H48 N6 O7	544.3584	545.3657
	C15 H33 N O	243.2561	244.2634
	C30 H46 O3 S	486.3165	487.3237
	C18 H36 O6	348.251	349.2582
	C15 H33 N O	243.2561	244.2634
	C28 H58 N10 S2	598.4286	599.4359
		411.3192	412.3265
benzyl N-(1-{[(3,4-dimethoxyphenethyl)amino]carbonyl}-2-methylpropyl)carbamate	C23 H30 N2 O5	431.2304	432.2377
	C21 H43 N4 O2 P S	446.2852	447.2925
	C16 H30 N6 O4	370.2329	371.2402
	C25 H60 N9 O5 P	597.4445	598.4518
AJ4900000	C2 H4 O5 S	139.9782	162.9673
13-oxotrideca-9,11-dienoic acid	C13 H20 O3	224.1411	225.1484
Methyl palmitate	C17 H34 O2	287.2823	288.2895
	C25 H62 N9 O6 P	615.4553	616.4625
		275.8894	276.8966
		119.0162	161.05
	C18 H39 N O6	365.2775	366.2848
	C17 H37 N O5	335.267	336.2742
	C33 H66 N O2 P S	571.4556	572.4629
	C21 H45 N O8	439.3142	440.3215
		482.3645	483.3718
		383.288	384.2953
	C26 H52 N3 P S	469.361	470.3683
Diethanolamine	C4 H11 N O2	105.079	106.0863
dihydromethanophenazine	C37 H52 N2 O	540.4061	541.4133
	C28 H49 N6 P	500.375	501.3822
	C28 H51 N8 P S	562.3689	563.3762
	C38 H67 N5 O3 S	673.4967	674.504
	C14 H28 N8 O6 S	436.1859	437.1932
	C23 H49 N O7	451.3508	452.3581

		482.3645	483.3718
		598.4479	599.4552
	C17 H35 N O2	285.2666	286.2739
	C18 H39 N O7	381.2724	382.2797
	C14 H31 N O5	293.2201	294.2273
	C30 H59 N2 O5 P	558.4169	559.4242
	C24 H34 O2 S	386.2278	387.2351
	C27 H58 N2 O12	602.3998	603.4071
	C29 H47 N5 S	497.3561	498.3634
	C13 H24 N6 O4	328.186	329.1932
		161.96	144.9568
	C14 H31 N O4	277.2252	278.2324
	C24 H60 N10 O8	616.4584	617.4657
	C22 H54 N9 O5 P	555.3977	556.405
	C17 H37 N O6	351.2619	352.2692
	C28 H56 N6 O9	620.4103	621.4176
		233.9526	117.9836
		189.9914	116.5163
		174.9472	175.9545
		367.265	368.2723
		393.3088	394.316
	C29 H58 N3 O P S	527.4028	528.4101
		429.2782	430.2855
		94.99574	96.00304
6,8-Dimethyl-6,7,8,9-tetradehydroergoline	C16 H17 N2	237.1382	238.1455
	C28 H45 N5 S	483.3403	484.3476
4232620	C14 H28 O6	292.1884	293.1956
	C21 H40 N10 O2	464.3342	465.3415
	C30 H61 N O10	595.4292	596.4365
		354.2808	355.2881
	C42 H69 N9 S	731.5391	732.5464
		367.2649	368.2722
	C21 H44 O8	424.3034	425.3107
	C13 H29 N4 O2 P S	336.1749	337.1822
	C20 H50 N9 O3 P	495.3763	496.3836
	C19 H36 N6 O6	444.2696	445.2769
	C23 H44 N3 P S	425.2987	426.306
	C34 H47 N3 O3	545.3618	546.3691
	C10 H20 N6 O3	272.16	273.1672
	C15 H33 N O6	323.2306	324.2379
	C22 H47 N O9	469.3246	470.3319
		354.2809	355.2882

	C24 H47 N4 O3 P S	502.3116	503.3189
	C32 H64 N3 O2 P S	585.4447	586.452
	C29 H58 N4 O4 S	558.4169	559.4242
	C41 H63 N2 O4 P	678.4528	679.46
	C31 H62 N6 O10	678.4519	679.4592
	C21 H52 N9 O3 P	509.3927	510.4
		500.3749	501.3822
	C19 H41 N O8	411.2828	412.2901
	C16 H35 N O6	337.2462	338.2535
	C27 H55 N O9	537.3873	538.3946
		383.2882	384.2954
		479.3454	480.3527
	C23 H49 N O8	467.3454	468.3527
	C38 H67 N5 O3 S	673.4971	674.5043
	C21 H43 N O7	421.3038	422.311
	C10 H18 N6 O3	270.1443	271.1516
		527.3669	528.3742

Table A5. Up-regulated species from Figure 12, i.e. species significant to Post-baseline activity samples against Reduced period samples

Predicted Compound	**Predicted Formula**	**Calculated MW**	**m/z**
Farnesylacetone	C18 H30 O	262.2296	280.2634
	C5 H2 N2 O4 S	185.9736	186.9808
Acetyl-L-carnitine	C9 H17 N O4	203.1157	204.1229
4,5-dihydroxy-6-(hydroxymethyl)-2-[2,4,6-trihydroxy-3-(4-hydroxybenzoyl)phenyl]oxan-3-yl 3,4,5-trihydroxybenzoate	C26 H24 O14	560.1031	561.1104
D-Carnitine	C7 H15 N O3	161.1051	162.1124
Amide C18	C18 H37 N O	283.2874	284.2947
Acetyl-L-carnitine	C9 H17 N O4	203.1156	204.1229
	C7 H15 N O4 S	209.0721	210.0793
Hydroxynorleucine	C6 H13 N O3	147.0895	148.0968
L-threo-3-Phenylserine	C9 H11 N O3	181.0738	182.0811
norfenefrine	C8 H11 N O2	153.0789	154.0862
2-((4-Nitrophenoxy)methyl)oxirane	C9 H9 N O4	195.053	196.0603
L-(+)-Leucine	C6 H13 N O2	131.0946	132.1019
5-Imino-L-norvaline	C5 H10 N2 O2	130.0742	131.0815
4-Aminophenol	C6 H7 N O	109.0528	142.0862
propionylcarnitine	C10 H19 N O4	217.1313	218.1386
Benzophenone	C13 H10 O	182.0731	183.0803

		371.2516	372.2588
		601.7593	301.8869
	C21 H42 N3 O P S	415.2778	416.2851
g-Butyrobetaine	C7 H15 N O2	145.1102	146.1175
		355.2568	356.264
		341.2411	342.2483
		297.2149	298.2222

Table A6. Down-regulated species from Figure 11, i.e. species significant to Reduced activity samples against Post-baseline period samples

	NH_4^+	NO_2^-	NO_3^-	DON	Na^+	K^+	Ca^{2+}	Mg^{2+}	F^-	$C_2H_3O_3^-$	H_3CCOO^-	$HCOO^-$	Cl^-	PO_4^{3-}	SO_4^{2-}	$C_2O_4^{2-}$	DOC	H/C	O/C	O/N	O/S	N/C	DBE	AI
NH_4^+	1.000																							
NO_2^-	0.475	1.000																						
NO_3^-	0.425	0.000	1.000																					
DON	0.488	0.248	0.432	1.000																				
Na^+	-0.088	-0.046	0.079	-0.035	1.000																			
K^+	0.412	0.197	0.615	0.352	0.702	1.000																		
Ca^{2+}	0.204	0.174	0.120	0.144	0.823	0.768	1.000																	
Mg^{2+}	0.510	0.137	0.387	0.252	0.618	0.858	0.845	1.000																
F^-	0.108	-0.195	0.883	0.315	0.057	0.482	-0.019	0.192	1.000															
$C_2H_3O_3^-$	0.510	0.025	0.902	0.326	0.023	0.636	0.154	0.519	0.749	1.000														
H_3CCOO^-	0.236	0.149	0.867	0.457	-0.029	0.487	-0.030	0.135	0.852	0.718	1.000													
$HCOO^-$	0.382	-0.113	0.922	0.359	0.063	0.637	0.114	0.482	0.836	0.963	0.769	1.000												
Cl^-	0.396	0.016	0.878	0.345	0.425	0.819	0.483	0.623	0.732	0.830	0.690	0.811	1.000											
PO_4^{3-}	0.152	0.060	0.641	0.382	0.121	0.519	0.034	0.232	0.710	0.532	0.654	0.622	0.565	1.000										
SO_4^{2-}	0.657	0.138	0.664	0.327	0.049	0.629	0.269	0.695	0.446	0.880	0.427	0.825	0.640	0.334	1.000									
$C_2O_4^{2-}$	0.168	-0.157	0.854	0.395	0.068	0.530	0.016	0.234	0.969	0.739	0.838	0.829	0.724	0.781	0.463	1.000								
DOC	0.595	0.181	0.546	0.537	-0.268	0.162	-0.099	0.040	0.332	0.453	0.550	0.372	0.385	0.190	0.292	0.332	1.000							
H/C	-0.433	-0.261	-0.703	-0.511	-0.368	-0.694	-0.436	-0.513	-0.566	-0.599	-0.632	-0.582	-0.817	-0.500	-0.477	-0.580	-0.399	1.000						
O/C	0.048	0.272	-0.376	-0.230	0.043	-0.160	0.008	0.006	-0.468	-0.251	-0.377	-0.316	-0.226	-0.365	-0.024	-0.457	-0.402	0.058	1.000					
O/N	0.141	0.091	-0.177	-0.150	0.054	-0.100	-0.059	0.020	-0.308	-0.175	-0.216	-0.178	-0.117	-0.075	-0.024	-0.274	-0.191	0.015	0.686	1.000				
O/S	0.256	0.400	-0.242	0.017	-0.249	-0.278	-0.138	-0.188	-0.362	-0.203	-0.236	-0.336	-0.165	-0.243	-0.135	-0.330	0.024	-0.054	0.709	0.496	1.000			
N/C	-0.237	0.033	-0.079	-0.033	-0.186	-0.117	-0.121	-0.253	0.005	-0.064	0.007	-0.085	-0.108	-0.031	-0.178	-0.029	0.023	0.214	-0.424	-0.618	-0.186	1.000		
DBE	0.254	0.282	0.648	0.350	0.359	0.661	0.349	0.396	0.577	0.524	0.654	0.545	0.737	0.618	0.367	0.574	0.220	-0.896	-0.122	0.002	-0.058	-0.118	1.000	
AI	0.122	-0.122	-0.192	-0.247	-0.129	-0.275	-0.123	-0.114	-0.252	-0.152	-0.295	-0.212	-0.103	-0.303	-0.110	-0.247	-0.031	-0.043	0.491	0.504	0.684	-0.442	-0.065	1.000

Table A7. Pearson Correlation Coefficients

n	Ion PMF Contributors		Ion PMF Contributors (Outliers Removed)		Combined PMF Contributors	
	Dominant	Secondary	Dominant	Secondary	Dominant	Secondary
1	3		2	3	5	
2	1	5	1		1	4
3	5		3		1	
4	3		REMOVED		5	
5	2	1	3		3	4
6	2	5	3		3	
7	1	2	5		3	4
8	3		2		5	
9	3		1		5	
10	1		1	2	4	
11	1		REMOVED		4	
12	4				2	
13	4				2	
14	2		4	2	3	
15	2	5	4		3	
16	5		4		1	
17	1		5		4	
18	1		5		4	
19	1		5		4	
20	1		5		4	3
21	2	1	5		3	4
22	2		3		3	
23	5		4		1	
24	3		2		5	
25	3		2		5	
26	No Ion Data					
27						
28						
29						
30						
31						
32						

Table A8. Primary and Secondary Contributing Factors

Sample n	Date (d/m/yyyy)	NH_4^+ (µM)	NO_2^- (µM)	NO_3^- (µM)	DON (µM)	TDN (µM)	Na^+ (µM)	K^+ (µM)	Ca^{2+} (µM)
1	26-27/02/2020	14.1	0.55	3.6	15.94	34.2	3.7	2.8	1.9
2	27-28/02/2020	27.7	0.58	15.7	13.66	57.6	1.5	1.6	3.7
3	01-02/03/2020	10.9	0.51	3.8	5.99	21.2	1.5	1.1	1.2
4	19-20/03/2020	19	0.55	15.7	21.81	57.1	18.8	15.3	41
5	20-21/03/2020	22.6	0.52	9.2	24.51	56.8	1.7	1.8	3.2
6	29/03/2020	2	0.51	2	9.45	13.9	0.7	0.9	1.3
7	3/4/2020	53	0.59	15.4	13.34	82.3	2.4	3.5	3.6
8	14/4/2020	16.1	0.54	5.7	10.61	33	9	5.4	2.4
9	23/5/2020	12.9	0.55	4.5	7.78	25.8	5.6	4.1	4.7
10	7/6/2020	59.1	0.53	17.2	30.55	107.3	4.7	4.5	5.5
11	22/9/2020	84.4	1.38	27	62.78	175.6	3.3	6	6.7
12	28/9/2020	119.5	1.02	37.3	24.52	182.3	4	10.9	18.1
13	18/10/2020	53	0.27	127.8	46.89	227.9	5	14.9	6.3
14	19-20/10/2020	45.9	0.309	20.8	29.7	96.7	2.6	4.7	5.9
15	20/10/2020	9.6	0.125	7.4	38.25	55.4	0.8	1.1	1.7
16	24/10/2020	29.1	0.125	10.3	31.49	71	1.4	1.4	2.4
17	29-30/10/2020	69	0.352	31.7	36.55	137.5	2.7	2.8	4.5
18	12/11/2020	53.1	0.319	18.4	17.59	89.4	1.7	3.9	4
19	13-14/11/2020	70.4	1.658	29.2	47.11	148.4	2.3	6.4	6.9
20	18/11/2020	61.9	1.106	24.8	10.28	98.1	1	3.8	4
21	18/11/2020	38.5	1.233	20.5	13.97	74.1	1.2	2.4	3.3
22	18-19/11/2020	34	1.257	22.6	12.33	70.1	4	5.2	7.6
23	04-05/12/2020	33.4	0.161	54.7	11.72	100.1	4.4	2.6	3.8
24	6/12/2020	42.9	0.213	15.8	0.65	59.6	4.8	4	1.7
25	12-13/12/2020	7.4	0.2	0.4	9.81	17.9	1.8	1	0.4
26	13-14/01/2021	16.9	<LD	6.2	NA	23.1	1	0.7	1.2
27	18-19/01/2021	37.9	<LD	14.9	NA	52.8	6.5	2.9	4.1
28	21/2/2021	36.6	<LD	11.7	NA	48.3	3.6	3.1	6
29	06-07/03/2021	6.2	<LD	2.4	NA	8.6	1	6.2	1.2
30	18/4/2021	25.9	0.3	13.6	NA	39.8	5.3	2.2	7.9
31	18/4/2021	10.4	<LD	7.3	NA	17.7	1.8	1.8	0.7
32	10/6/2021	27.6	<LD	10.9	NA	38.5	3.1	4.6	3.9

Sample n	Mg^{2+} (µM)	F^- (µM)	$C_2H_3O_3^-$ (µM)	H_3CCOO^- (µM)	$HCOO^-$ (µM)	Cl^- (µM)	PO_4^{3-} (µM)	SO_4^{2-} (µM)	$C_2O_4^{2-}$ (µM)	DOC (µM)
1	0.66	0.2	0.2	4.1	3.1	3.6	<LQ	1.2	0.28	119
2	0.94	0.25	0.51	3.6	8.1	3.2	0.13	4.8	0.65	208
3	0.31	0.27	0.36	0.4	2.4	2.5	0.11	1.6	0.35	89
4	6.48	0.21	0.53	2.1	0.8	9.9	0.12	1.9	0.51	146
5	1.06	0.26	0.38	1.6	3.1	2.6	0.15	1.5	0.28	145
6	0.31	0.18	0.35	0.7	2.2	1.7	0.11	0.4	0.25	92
7	1.43	0.24	2.02	1.3	28.8	4.8	0.38	4.5	0.55	257
8	0.76	0.25	0.36	0.4	7.3	2.4	0.33	2.2	0.31	152
9	1.56	0.28	0.38	3.8	5.4	4.4	0.39	5.4	0.44	167
10	2.07	0.12	0.85	1.3	36.1	4.5	0.39	5.3	1.03	322
11	2.05	<LD	0.95	9.2	40.5	4.1	0.4	10.4	0.12	1073
12	6.95	<LD	10.35	<LD	301.3	8.4	<LD	60.4	<LD	585
13	3.68	2.685	16.03	31	695.4	16.6	1.321	44.2	6.522	964
14	2.38	0.608	1.54	3.6	47.6	4.4	0.699	3.7	1.572	710
15	0.26	0.184	0.55	2.3	20.5	1.8	<LD	1.4	0.539	599
16	0.22	<LD	2.35	2.4	13.7	5.4	<LD	3.3	<LD	833
17	1.35	0.857	2.58	3.7	51.1	5.9	<LD	7.6	1.9	878
18	1.54	0.225	1.89	4.4	47.8	4.3	0.294	4.2	0.488	863
19	0.89	0.355	2.52	10.3	19.3	6.8	0.323	6.6	0.919	752
20	0.99	0.35	1.93	8.6	12.7	4.1	<LD	4.9	0.532	877
21	0.75	0.301	2.91	10.3	20.6	3.4	<LD	3.2	0.441	807
22	1.03	0.222	2.61	3.8	3.6	6.8	0.612	2.2	0.788	571
23	1.03	0.551	4.09	6	129.3	8.7	<LD	5.6	0.211	795
24	0.55	0.196	1.69	3	29.5	5.1	<LD	1.7	0.626	648
25	0.14	<LD	0.07	2.2	0.4	1.5	<LD	0.7	<LD	433
26	0.2	<LD	<LD	4.9	6.5	1.6	<LD	0.5	0.2	843
27	0.9	<LD	1.8	11.7	12.6	5.9	<LD	1.8	0.8	918
28	1.6	<LD	3.5	9.3	8.5	3.7	0.4	5.7	0.9	217
29	0.3	0.1	0.5	0.4	0.6	2.6	0.1	0.2	<LD	165
30	2.1	<LD	1.5	8.1	6.9	4.8	<LD	2.7	0.4	255
31	0.1	<LD	1.6	3.8	3.7	7.8	<LD	1.9	0.2	211
32	1.24	0.2	1.9	8.2	12.6	4.5	<LD	5	0.1	282

Table A9. Inorganic and Organic Species concentrations for all Samples